Vrije Universiteit Brussel

Faculty of Engineering
Department of Mechanical Engineering

Design of an actuated orthosis for support of the sound leg of transfemoral dysvascular amputees

Thesis submitted in fulfillment of the requirements for the degree of Master in Engineering: Electro-Mechanical Engineering (Master Ingenieurswetenschappen: Werktuigkunde - elektrotechniek)

Karen Junius
Tom Verstraten

Promotor: Prof. Dr. ir. Dirk Lefeber

Academic year: 2011 – 2012

Contents

Acknowledgments

Now the last pages of this thesis are written, we can take the time to write the first one. What better way to start than by giving thanks to the persons that made this thesis possible?

First of all, we would like to thank our promotor, prof. Dirk Lefeber, who gave us the opportunity of going our own way, but who was also there to assist us when needed. Of course, we also want to thank all the persons of MECH for their advice and guidance when we called upon them.

Second, we would like to thank our parents. Without their support and love, the past five years would have been even more challenging.

Third, we would like to thank Veerle for lending her computer when it was most needed. One word of advice for future last year students: do not run Inventor on a five year old HP laptop! Or perhaps the crash could have been caused by Vitani and Noet, the housecats, but we find it hard to blame these lovable creatures.

Last but not least, we could not have made it to the end of this thesis without each other's constant support and hard work. Even though there were some disagreements from time to time, we enjoyed working together. Throughout this turbulent year our friendship has grown only stronger and 't Complex has certainly benefitted from that.

We look back on our studies with a happy spirit and look forward to the years to come, hoping that they will be at least as enjoyable.

Karen Junius and Tom Verstraten
Brussels, June 2012

Abstract

Transfemoral amputees consume much more energy during walking than non-amputees, despite their decreased gait velocity. This gets even worse if the amputation is caused by a vascular disease. Because the remaining leg is also affected by the disease, it has a hard time bearing the increased load. An actuated ortho-prosthesis can help the transfemoral dysvascular amputee by restoring the ankle and knee function of the amputated leg and by providing assistance to the sound leg. Creating such an ortho-prosthesis is the ultimate goal of the CYBERLEGs project.

In this thesis, a design for the orthosis part of the ortho-prosthesis is presented. A design with six degrees of freedom is proposed to maximize wearability, comfort and safety. The orthosis will assist flexion and extension of the joints by delivering about 50% of the biological joint torque for an average 75kg person. Based on Winter's gait data for normal cadence walking, the design was optimized to meet these demands in an energy-efficient way. On the sound leg, it will do so by means of two biarticular MACCEPA actuators, which consist of a motor (one at the ankle, one at the hip) and a spring that connects it to the knee, so that two joints are spanned. Actuation of the hip joint of the amputated leg is achieved by means of a conventional MACCEPA. To further increase energy-efficiency and to reduce the size of the motors, parallel springs are used at all joints for storage and release of elastic energy. The parallel spring at the knee is engaged only during stance, which is accomplished by means of a ratchet locking mechanism. All secondary (i.e. non-flexion/extension) orthosis degrees of freedom are left free, except for hip abduction/adduction, where a spring is designed to deliver 50% of the abductor torque.

Simulations have shown that this system can transfer 19% of the absorbed energy at the knee to the energy-demanding ankle and hip joints. It succeeds reasonably well in delivering the required torques, with a limited power consumption of 36J per step. All this is achieved with only a 40W motor at the ankle and 15W motors at both hips, and a 2,015kg battery pack.

Samenvatting

Bovenbeengeamputeerden verbruiken veel meer energie tijdens het stappen dan niet-geamputeerden, ook al is hun stapsnelheid lager. Deze situatie is nog ernstiger indien de amputatie door een vaatziekte werd veroorzaakt. Omdat het overblijvende been ook getroffen is door de ziekte, kan het de bijkomende belasting maar moeilijk aan. Een geactueerde ortho-prothese kan de dysvasculaire bovenbeengeamputeerde helpen door de knie- en enkelfunctie van het geamputeerde been over te nemen en door het gezonde been te assisteren. Het vervaardigen van zo'n ortho-prothese is het ultieme doel van het CYBERLEGs-project, waarin deze thesis kadert.

Dit afstudeerwerk beschrijft het ontwerp van het orthesegedeelte van de ortho-prothese. Een ontwerp met zes vrijheidsgraden wordt voorgesteld om draagbaarheid, comfort en veiligheid te maximaliseren. De orthese zal het buigen en strekken van de gewrichten vergemakkelijken door ongeveer 50% van het koppel te leveren dat normaal door de biologische gewrichten van een gemiddelde persoon van 75kg wordt geleverd. Op basis van Winters data voor het stappen op normale snelheid werd het ontwerp geoptimaliseerd, zodat op een zo energie-efficiënt mogelijke manier aan deze eisen voldaan wordt. Dit wordt verwezenlijkt door aan het intacte been twee biarticulaire MACCEPA-actuatoren te plaatsen, die bestaan uit een motor (een aan de enkel, een aan de heup) en een veer die de motor verbindt met de knie, zodat de twee gewrichten overbrugd worden. De actuatie van de heup aan de kant van het geamputeerde been wordt verzorgd door een conventionele MACCEPA. Om energie-efficiëntie verder te bevorderen en om de grootte van de motoren zoveel mogelijk te verkleinen, worden aan alle gewrichten parallelle veren gebruikt om elastische energie op te slaan en vrij te geven. De parallelle veer aan de knie is enkel actief gedurende de standfase. Dit wordt verwezenlijkt door een ratelmechanisme. Alle secundaire vrijheidsgraden (m.a.w. niet buigen/strekken) worden vrijgelaten, behalve abductie/adductie van de heup, waar een veer ontworpen werd om 50% van het abductiekoppel te leveren.

Uit simulaties bleek dat dit systeem 19% van de geabsorbeerde energie uit de knie kan overbrengen naar de energieverbruikende enkel- en heupgewrichten. Het slaagt er redelijk goed in om de vereiste koppels te leveren, met een beperkt energieverbruik van 36J per stap. Dit alles wordt verwezenlijkt door motoren van niet meer dan 40W aan de enkel en 15W aan de heupen, en door een batterij van 2.015kg.

Résumé

Les amputés transfémoraux consomment beaucoup plus d'énergie en marchant que des personnes non-amputés, même si leur vitesse de déplacement est réduite. Cette situation est encore aggravée si cette amputation est causée par une maladie vasculaire. Puisque la jambe contralatérale est aussi affectée par la maladie, elle a du mal à supporter la charge supplémentaire. Une ortho-prothèse actionnée peut aider l'amputé transfémoral en restituant la fonctionnement de la cheville et du genou de la jambe amputée et en assistant la jambe saine. La création d'une telle ortho-prothése est le but ultime du projet CYBERLEGs.

Dans cette thèse, une réalisation de la partie orthèse de l'ortho-prothèse est présenté. Une orthèse à six degrés de liberté est proposé afin de maximiser la portabilité, le confort et la sécurité. L'orthèse aidera la flexion et l'extension des articulations en fournissant environ 50% du couple biologique pour une personne moyenne de 75kg. Basé sur les données de la marche de Winter pour la cadence normale, l'orthèse a été optimisée afin de satisfaire à ces demandes d'une manière efficace en énergie. Ceci sera accompli à l'aide de deux actionneurs MACCEPA bi-articulaires, qui se composent d'un moteur (un à la cheville, un à la hanche) et un ressort qui le relie au genou, tant que les deux articulations sont enjambées. L'actionnement de l'articulation de la hanche de la jambe amputée est réalisé à l'aide d'une MACCEPA classique. Afin d'augmenter encore l'efficacité énergétique et de réduire la taille des moteurs, des ressorts parallèles sont utilisés à toutes les articulations pour le stockage et la récupération d'énergie. Le ressort parallèle au niveau du genou est actif seulement pendant la phase d'appui, ce qui est réalisé à l'aide d'un mécanisme de verrouillage à cliquet. Tous les degrés de liberté secondaires de l'orthèse (c'est à dire autres que flexion/extension) sont laissées libres, sauf pour l'abduction et l'adduction de la hanche, où un ressort est conçu qui fournit 50% du couple d'abduction.

Des simulations ont montré que ce système permet de transférer 19% de l'énergie absorbée au niveau du genou aux articulations de la cheville et de la hanche, où il y a un besoin d'énergie. Il réussit assez bien à délivrer les couples requis, avec une consommation d'énergie limitée de 36J par pas. Tout ceci est réalisé avec seulement un moteur 40W à la cheville et des moteurs 15W aux deux hanches, et une batterie de 2,015 kg.

1. Introduction

1.1. Motivation

When the Department of Mechanical Engineering gave us the opportunity of making a thesis in the field of robotics we were both interested. Being able to create something with social importance, convinced us to accept the challenge. Walking is one of those things people often take for granted. It is only when that ability is suddenly taken away, that we truly understand how it affects us not only physically but mentally as well. Mobility is especially important for the elderly because it is their link to society. With this thesis we made an attempt to improve the quality of life of the less mobile.

1.2. CYBERLEGs

This February (2012) a three year project will be started. It is named CYBERLEGs or **CYBER**netic **L**ow**E**r Limb Co**G**nitive Ortho-Prosthesi**s**. It is a cooperation between five European universities: two in Italy, one in Slovenia and two in Belgium. One of the latter is the Vrije Universiteit Brussel. The objective of the CYBERLEGs project is the development of an active ortho-prosthesis for transfemoral dysvascular amputees.

The human leg can be amputated at different levels. When the leg is severed at the shank the amputation is called *transtibial*. When it is severed at thigh-level we denote it as *transfemoral*. It is clear that a transtibial amputation poses less challenges for the patient than a transfemoral one since the normal knee function is conserved. When both knee and ankle function are lost the patient deals with following issues:

- They consume up to 1.3 times the energy non-amputees consume for walking the same distance.
- They walk slower than non-amputees (about 60% of non-amputee gait speed).
- They take steps and stairs step-by-step, one step at a time, rather then step-over-step meaning that they step up with the sound leg first, then bring the prosthetic side up to the same step.

- They face more problems with stumbling and falling, so a much greater concentration is needed.

All the above challenges are not overcome by the passive prostheses in the current state of the art. As a result, patients often opt not to wear the prosthesis and to use other means to remain mobile such as crutches or a wheelchair.

The arguments presented above clearly show that transfemoral amputation complicates daily life activities such as walking or climbing stairs. The dysvascular nature of the amputation brings along even more challenges. An amputation is called *dysvascular* when it is caused by a vascular disease. This is in most cases caused by diabetes, with people over 70 years old being the highest risk group. Since in dysvascular amputees the remaining leg is also affected by the disease, their energy use is higher and their walking speed lower. Dysvascular amputees walk at about 40% of the non-amputee gait speed and expend 2.5 times more energy. Additionally, the doctor often prohibits the use of a prosthesis because of the extra load put on the remaining leg which would cause it to rapidly deteriorate.

Some of these issues have already been addressed by state-of-the-art semi-active and active prostheses but

- the sound limb is still loaded excessively
- it takes a long time to learn how to walk wearing the prosthesis
- existing prostheses have a limited autonomy; they have to be recharged very often

The goal of this project is to resolve these issues by building an active ortho-prosthesis. It should comprise an active artificial leg and a wearable active orthosis. The orthosis will assist the sound leg in such a way that it relieves the extra load. Prosthesis and orthosis will be mechanically connected by a pelvis module which allows a partial weight transfer to the floor via the leg in stance. It will have hip joints and house a battery pack as well as a computational unit. Amputee motor intention will be derived from sensor input and the ortho-prosthesis will automatically act and assist the user. When it detects stumbling it will help the wearer to execute the appropriate response to remain standing. The ultimate goal is to make it energy efficient allowing the user to use the ortho-prosthesis for one full day before it needs to be recharged.

1.3. State of the art

An exoskeleton is defined as an active mechanical device that is essentially anthropomorphic in nature. It is “worn” by an operator, fits closely to his or her body and works in concert with the operator’s movements [19]. In the nearly six decades since researchers began to explore the use of exoskeletons, they have progressed from an idea in science fiction to commercialized products. While there are still

many challenges associated with exoskeleton design that are yet to be perfected, the advances in the field have been enormous. In this paragraph, we review the history and discuss the state of the art of lower limb exoskeletons and active orthoses. Note that because of the rapid evolution of exoskeletons, this review cannot be exhaustive nor is it meant to be.

1.3.1. Exoskeletons

Research in powered human exoskeletons began in the late 1960s [19]. There are three main types of powered exoskeletons for humans: rehabilitation exoskeletons, assistive exoskeletons and performance augmenting exoskeletons. Their common goal is the assistance of human gait. Therefore these exoskeletons are not easily categorized.

1.3.1.1. Rehabilitation exoskeletons

In this section we look at the evolution of exoskeletons used to aid in rehabilitation of the lower limbs.

(a) AutoAmbulator **(b)** Lokomat **(c)** LOPES **(d)** ALEX

Figure 1.1.: Rehabilitation exoskeletons

Two commercially available devices are the AutoAmbulator (HealthSouth, USA) and the Lokomat (Hocoma, Switzerland) (Figure 1.1a, Figure 1.1b). Not much is reported in literature about the AutoAmbulator. The Lokomat rehabilitation device consists of a treadmill, a body weight support (BWS) system and a robotic orthosis connected to the patient's lower limbs. Hip and knee flexion/extension is actuated by linear ball screw assemblies driven by DC motors. The device is extensively tested, with adults as well as with children. Research is done to establish completely patient-driven cooperative robotic training [20] but it has not yet been implemented in the device that is currently on the market.

In the above devices the generated walking motion is not completely as it is in healthy subjects. This results from the limited degrees of freedom (DOF) incorporated in the devices. In order to make walking less forced, the number of DOFs has been increased in the following exoskeletons.

LOPES (Figure 1.1c), designed by the University of Twente, combines a freely translatable and 2D-actuated pelvis segment with a leg exoskeleton containing three actuated rotational joints: two at the hip and one at the knee. Besides flexion/extension of the hip and knee, hip ab- and adduction is also assisted [50]. Remote actuation was used to power the joints through bowden-cable based series actuators.

Unlike aforementioned devices, ALEX (Figure 1.1d) is a unilateral rehabilitation device. It consists of a right leg orthosis which is attached to a walker via a harness on the trunk. This connection supports the device and keeps the patient stable on the treadmill during training [9]. The motorized orthosis, of which both hip and knee are actuated by linear drives, is architecturally similar to the GBO (Gravity Balancing Orthosis, [8]).

1.3.1.2. Assistive exoskeletons

In general, the term "exoskeleton" is used to describe a device designed to augment the capabilities of an able-bodied wearer. The devices described in this section are built to increase the ambulatory ability of a person suffering from a leg pathology. They are often denoted with the term "active orthosis". Occasionally however the term "exoskeleton" is used for certain assistive devices, particularly when they comprise most of the lower limbs.

(a) Pupin Institute exoskeleton **(b)** ReWalk **(c)** EXPOS **(d)** AAFO

Figure 1.2.: Assistive exoskeletons or active orthoses

As mentioned above, the research in powered human exoskeletons started in the 1960s. Pioneering work was done amongst others by Miomir Vukobratović and his

associates at the Mihailo Pupin Institute in Belgrade [19]. In 1990 they finally developed a full lower limb exoskeleton (Figure 1.2a) to aid walking for paraplegics [52]. They assisted patients in walking by commanding the exoskeleton to track pre-defined trajectories. A more recent development is the ReWalk (Figure 1.2b), a commercially available assistive exoskeleton by the Israelian company Argo Medical Technologies. It is a bilateral robotic suit for the mobility impaired. Utilizing sophisticated algorithms, body movements are analyzed and used to trigger and maintain different modes of operation such as walking, stair-climbing and shifting from sit to stand. User stability and safety during ambulation is secured by concurrent use of safety means such as crutches for walking and railing for stairs [31].

Even more recent is the arise of EXPOS (Figure 1.2c), an exoskeleton designed specifically to assist the elderly [25]. It consists of a full lower limb orthosis paired with a specially designed walker that houses the battery, DC motors and the control computer. A cable drive transmits mechanical power to the joints of the exoskeleton from the actuators in the walker. This design greatly reduces the weight of the orthosis but constrains the wearer to a fixed distance from the walker.

As one could expect not all assistive devices comprise the whole lower limbs. Several single joint active orthoses have arisen in the past decades. One of the most widely known is the Active Ankle-Foot Orthosis (AAFO, Figure 1.2d), by the MIT Biomechatronics Group, developed to assist in dropfoot gait. The device consists of a modified passive AFO with the addition of a linear series elastic actuator (SEA). Using the SEA, the device assists with dorsiflexion during swing [10].

1.3.1.3. Performance augmenting exoskeletons

One of the first known performance augmenting exoskeletons that were actually built is the Hardiman (Figure 1.3a) in the late 1960s by General Electrics Research. Hardiman (Human Augmentation Research and Development Investigation) was an enormous hydraulically powered machine equipped with components to amplify the strength of the arms and the legs of the wearer. Although satisfactory results were gained with the arms, problems with the lower limb components were never resolved [19].

Most performance augmenting exoskeletons focus on load-carrying augmentation with military applications in mind. Three of the most important exoskeletons (BLEEX, the Sarcos exoskeleton and the MIT exoskeleton) were commissioned by the Defense Advanced Research Projects Agency (DARPA). They started a program called Exoskeletons for Human Performance Augmentation (EHPA) to "increase the capabilities of ground soldiers beyond that of a human".

The Berkeley Lower Extremity EXoskeleton (BLEEX, Figure 1.3b) was created to augment human load-carrying capabilities. It features seven DOFs (three at the hip, one at the knee and three at the ankle) of which four are actuated: hip, knee and ankle flexion/extension and hip abduction/adduction. It is, as claimed by its

(a) Hardiman **(b)** BLEEX **(c)** MIT exoskeleton **(d)** Nurse-assist **(e)** HAL-5

Figure 1.3.: Performance augmenting exoskeletons

developers [24], the first functional load-carrying and energetically autonomous exoskeleton. The Sarcos Research Company worked on a full body robot. It was named "Wearable Energetically Autonomous Robot (WEAR)". As the name suggests it is also energetically autonomous. The exoskeleton had reportedly been successful demonstrating a number of impressive feats: wearer standing on one leg while carrying another person on the back, structure supporting an entire load of 84 kg, squatting, kneeling,... Unfortunately after the project ended, the technology was transitioned to the Army and very little further information regarding the design and performance of the exoskeleton has been made public [19]. A quasi-passive leg exoskeleton using a fraction of the power consumed by the two aforementioned devices is the MIT exoskeleton (Figure 1.3c) [54]. The design relies completely on the controlled release of energy in springs during the negative power phases of the gait cycle. The hip employs a spring-loaded joint that stores energy during extension which is released during flexion. At the hip a cam design was incorporated to adjust the exoskeletal leg length during hip abduction/adduction. The knee consists of a variable damper. For the ankle separate springs for dorsi- and plantarflexion were implemented.

Japan has also been an important player in the evolution of the exoskeleton. The nurse assisting exoskeleton (Figure 1.3d) is a full body suit designed to aid nurses in patient transfer. It is completely powered by pneumatic actuators. One of the interesting aspects of the mechanical design of the suit is that there are no mechanical components in front of the wearer, allowing the nurse to have direct physical contact with the person he/she is carrying. The robot suit HAL (by Cyberdyne, Figure 1.3e) is targeted for both performance-augmenting and rehabilitative purposes. The control relies on muscle EMG measurements. It is now available for use in Japan.

1.3.2. Pelvis module

Although the development of exoskeletons has been intensively investigated, the domain of pelvic assistance has been somewhat neglected. However, the last few years more and more researchers have become interested in this area. Two known devices immediately come to mind: PAM and NaTUre-gaits.

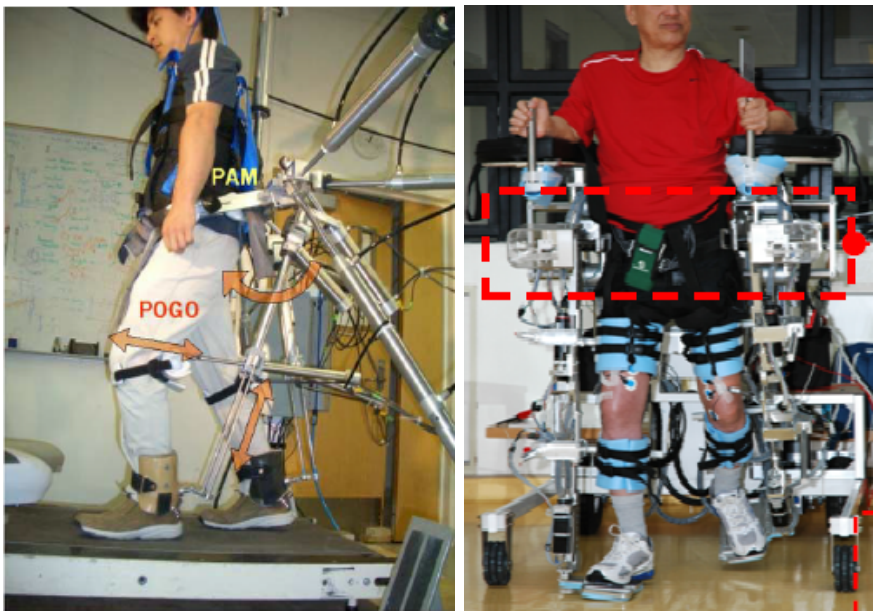

(a) PAM/POGO **(b)** NaTUre-gaits

Figure 1.4.: Pelvic assistance modules

PAM (Figure 1.4a), or the Pelvic Assist Manipulator, actuates five DOFs of which three are translational (side-to-side, forward-and-back, up-and-down) and the remaining two are rotational (pelvic rotation and obliquity) [7]. Although pelvic tilt remains unactuated, it is stabilized by the overhead BWS system. Actuation is provided by two 'subrobots' each consisting of three pneumatic cylinders. The pelvic module is used in combination with POGO, pneumatically operated gait orthosis, actuating hip and knee flexion/extension. The whole is placed on a treadmill and is designed for rehabilitation purposes.

NaTUre-gaits (Figure 1.4b), or Natural and TUrnable rehabilitation gait system, consists of three major components: the pelvis assistance (PA), the robotic orthosis (RO) and the mobile platform (MP) [30]. It is unique in the sense that the patient walks over-ground rather than on a treadmill. The PA has two functions, BWS and pelvic control, and it consists of two robotic arms holding the subject at both sides of the pelvis via a harness. Each of the robotic arms holds three actuators composed of a linear sliding mechanism and a DC-motor. Interaction of these actuators makes it possible to assist five pelvic motions, all except pelvic tilt.

1.3.3. Prostheses

Because the prosthesis is an important element in the CYBERLEGs project, we thought it was necessary to inform the reader about recent evolutions in prosthesis design. We therefore refer to following overviews of the state-of-the-art in powered lower limb prosthetics: [32], [51].

1.4. Goal

As seen in section 1.3, there are a lot of researchers developing orthoses for a variety of goals. Most of those however are not portable, meaning that they are attached to a treadmill or some sort of mobile unit. If our orthosis is to be used for every day activities, it is important not to be dependent of such a structure. The key is to design a lightweight structure with a portable energy supply, without undermining the autonomy of the device. To accomplish just that, we will look into the possibility of harvesting energy from the knee joint and deploying it at the other joints. Studies like [29] have shown that there is in fact energy available at the knee and that it is possible to extract it and use it in other applications. Rather than converting the mechanical energy to an electrical form and back to be deployed at the other joint, we will transfer the energy mechanically, bypassing the small efficiencies of the energy conversion.

1.5. Overview

In the coming chapters the design of the orthosis will be described. It will be based on several findings coming from a detailed review of the human gait pattern and factors influencing it (chapter 2: Human biomechanics). Based on the requirements of the orthosis an initial design concept will be elaborated, each time eliminating conflicts that come up, leading to the final design (chapter 3: Design). Basic control strategies will be discussed in chapter 4: Control aspects, after which the mechanical design is developed in chapter 5: Mechanical implementation. A thorough explanation of all design choices will be offered together with a stress analysis of the key parts. Finally the orthosis will be critically reviewed, mentioning possible flaws and points of improvement (chapter 6: Future work).

2. Human biomechanics

After a brief overview of basic gait-related definitions and nomenclature used in this thesis, the different phases of human gait are closely studied. Joint kinematics and kinetics will be brought into focus further on in this chapter. Winter's gait data for normal cadence walking will be used as a reference [57]. A good comprehension of gait is of the utmost importance since the design requirements of the actuator system (chapter 3) as well as the controller system (chapter 4) rely on it.

Since the orthosis is meant for a specific target group, the effects of age on human gait is discussed as well.

2.1. Definitions and nomenclature

The human body can be characterized by three planes: the *sagittal plane*, the *frontal (coronal) plane* and the *transverse plane* (Figure 2.1).

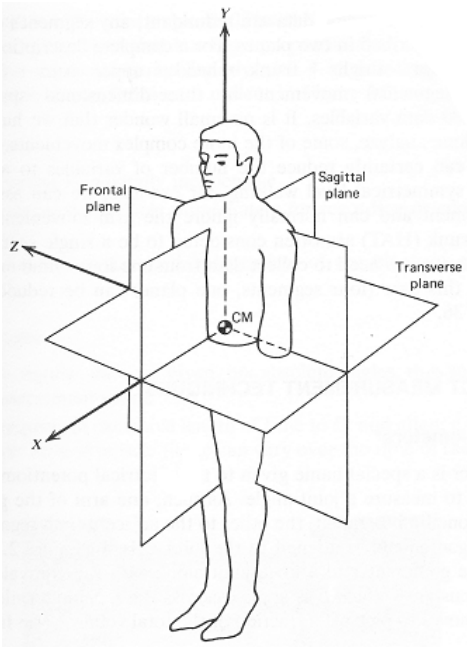

Figure 2.1.: Spatial coordinate system [56]

Movement of the hip and knee in the sagittal plane is called *flexion* (rotation around z-axis, positive for hip, negative for knee) or *extension* (negative rotation for hip,

positive for knee). For the ankle, the terms *plantarflexion* (foot pointed towards ground) and *dorsiflexion* (foot pointed towards trunk) are used. Rotation around the x-axis is called *abduction* (away from other leg) or *adduction* (towards other leg) or in case of the ankle *eversion/inversion* (Figure 2.2). Finally, rotations of the leg around the y-axis are called *internal* (inward) and *external* (outward) rotation.

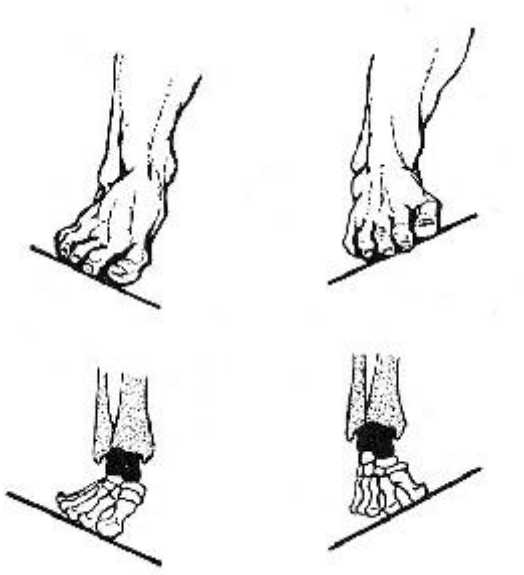

(a) Eversion **(b)** Inversion

Figure 2.2.: Frontal plane ankle motion [39]

Joint angles are defined in Figure 2.3.

Joint power P is equal to $M \cdot \omega$ and joint work W to

$$W = \int Pdt = \int M\omega dt \tag{2.1}$$

Positive work is done by *concentrically* contracting muscles, i.e. the muscles shorten under tension. *Negative work* is done on *eccentrically* contracting muscles, i.e. the muscles lengthen under tension. In biomechanics literature, negative joint power is often referred to as "power absorbed". This term may however be misleading, since the eccentric contraction of the muscles during power absorption comes at a metabolic cost [15].

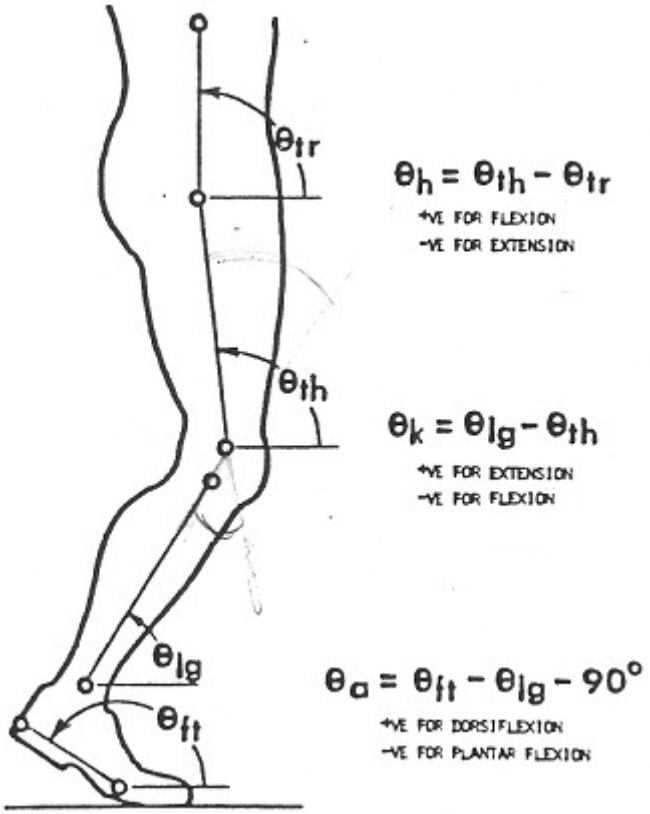

Figure 2.3.: Joint angle definition (adapted from [57]). θ_h = hip angle, θ_k = knee angle, θ_a = ankle angle.

2.2. Human gait

2.2.1. Introduction

Gait - both human and animal - has been studied thoroughly for decades [55]. However, many aspects are still not very well understood or debated among physiologists. Exoskeletons can provide a better understanding of human physiology. Still, limited data is available on the human physiological response to exoskeleton use [21].

It has been shown that changes in gait increase the physiological energy expended in locomotion [35]. Therefore, it is clear that mimicking human gait is a key issue in the design of exoskeletons. This explains why most exoskeleton prototypes are based on gait analysis data.

Several data sets exist comprising hip, knee and ankle angles and torque during one gait cycle. Initial studies often only investigated movement in the sagittal plane. However, recently a growing number of studies also consider the frontal and transverse plane. These studies show that some kinetic and kinematic variables in these planes are significant as well [15]. We will therefore not only discuss sagittal plane

DOFs (Degree Of Freedom), but also abduction/adduction and internal/external rotation DOFs.

Note that care is to be taken when interpreting these measurements, because of the many assumptions made in the collection and analysis. These assumptions and their possible effects, as well as other sources of error, are discussed extensively in [15]. It is also important to note that the work observed at a joint does not directly relate to the work performed by muscles acting around the joint. Two important methods of energy transfer exist in the human leg. Biarticular muscles, which act across two joints, can transfer power between joints. Additionally, stretched tendons may contribute to joint power [21]. This feature is discussed in subsection 2.3.2.

We will first introduce some general concepts regarding gait.

2.2.2. Gait cycle

As the body moves forward during walking, one leg acts as a support while the other moves itself to a new support site. Weight is shifted from one leg to the other during two leg contact. These events are repeated over and over again. One sequence of these functions is defined as a *gait cycle* (GC). Since there is no specific start or end point, one could select a random event as the onset of the gait cycle. Floor contact of one of the legs is generally accepted as the start event of the gait cycle and is denoted as *initial contact* (IC). This is also the convention used in [41]. In what follows, all terms and definitions describing the human gait cycle and its phases are in accordance with this reference work.

As mentioned before, human gait has been extensively investigated in the past decades. Researchers have attempted to divide the gait cycle in different phases in order to identify the important gait events. This subdivision can be made following three different approaches. The first is based on variations in reciprocal foot contact. Another option is to divide the gait cycle based on the different functional phases of human gait, which will be discussed extensively in subsection 2.2.3. The third and last method uses time and distance of stride as a marker. The latter is not used in the following dissertation, however the notion *stride* is. It is defined as the interval between two ICs of the same leg and consists of two steps, a step being the interval between two sequential ICs. Note that with the chosen definition of the gait cycle, one GC coincides with one stride.

Following the first approach, the gait cycle is split up in two periods: *stance* and *swing*. As shown in Figure 2.4, the stance period starts at IC. In normal gait, IC is the placement of the heel on the floor. This is typically referred to as *heel contact* (HC). During this period, the regarded leg - often referred to as *stance leg* - supports the body weight. The stance period ends as the foot loses contact with the floor, at which point the swing period begins. The end of stance is referred to as *toe-off* (TO) since the toes are the last to lose contact with the floor. During the swing

period the leg repositions itself swinging to an onward support site. The leg is called *swing leg* during this phase.

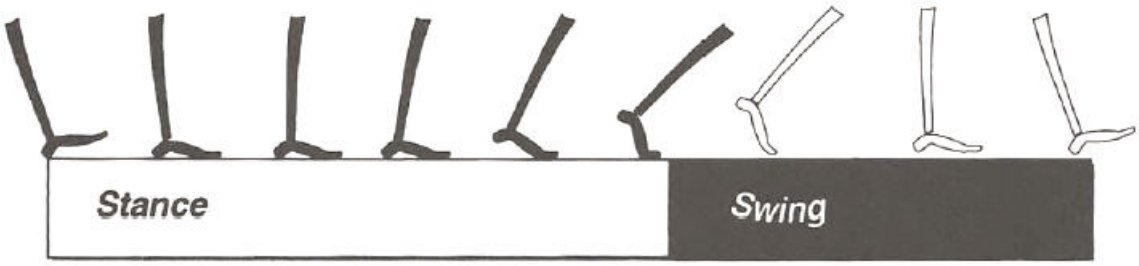

Figure 2.4.: Division of the gait cycle in stance and swing period

The gross normal distribution of the floor contact periods is 60% for stance and 40% for swing. One can distinguish three subdivisions in the stance period: initial double stance, single limb stance and terminal double stance (Figure 2.5). *Initial double stance* takes place at the beginning of the gait cycle. Both feet are on the floor after IC. *Single limb stance* begins when the opposite foot is lifted for swing. An alternate term is *single limb support*. This term is preferred since it emphasizes the importance of floor contact by just one foot as the entire body weight is resting on that one extremity. Note that right single limb support occurs in the same time interval as left swing. *Terminal double stance* is the third subdivision. It begins with floor contact of the other foot and continues until the original stance limb is lifted for swing. The third vertical bar (double limb stance) initiates the next gait cycle.

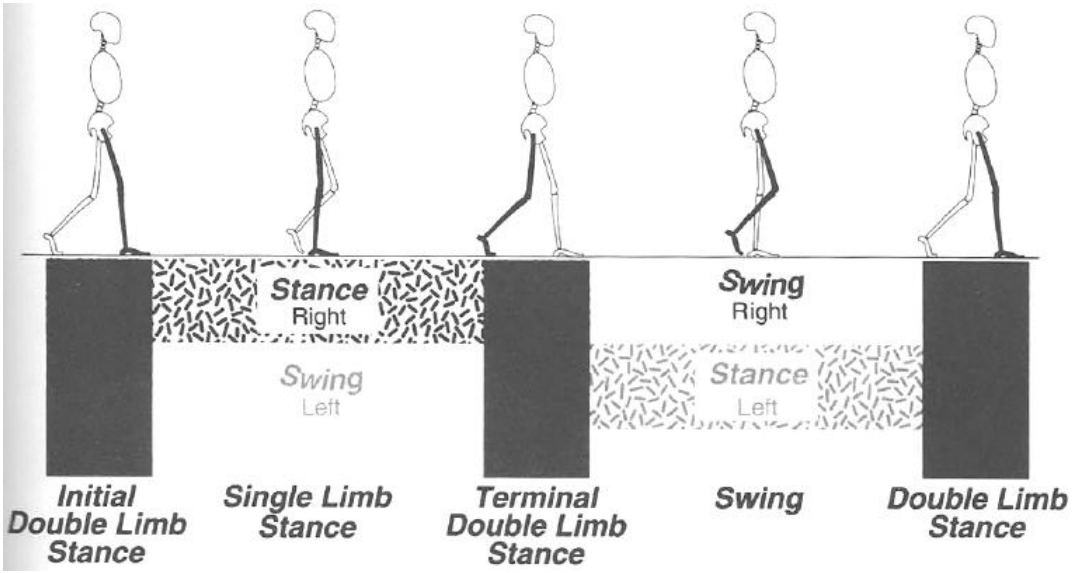

Figure 2.5.: Subdivisions of stance and their relationship to the contralateral leg.

The timing of these subdivisions is as follows: each double stance period spans 10%

GC, the single stance period spans 40% GC. Note that this timing is dependent of the walking velocity. As the velocity increases, the double stance periods shorten to disappear completely when the person enters the running mode of locomotion.

2.2.3. Phases of gait

By choosing IC as the start point of the gait cycle, the different events follow each other in a sequence that allows us to define three major tasks: *weight acceptance*, *single limb support* and *limb advancement* (Figure 2.6). There are eight functional gait phases in total. All of these phases can be classified under one of the defined tasks. In the following description we review all the gait phases encountered by one limb.

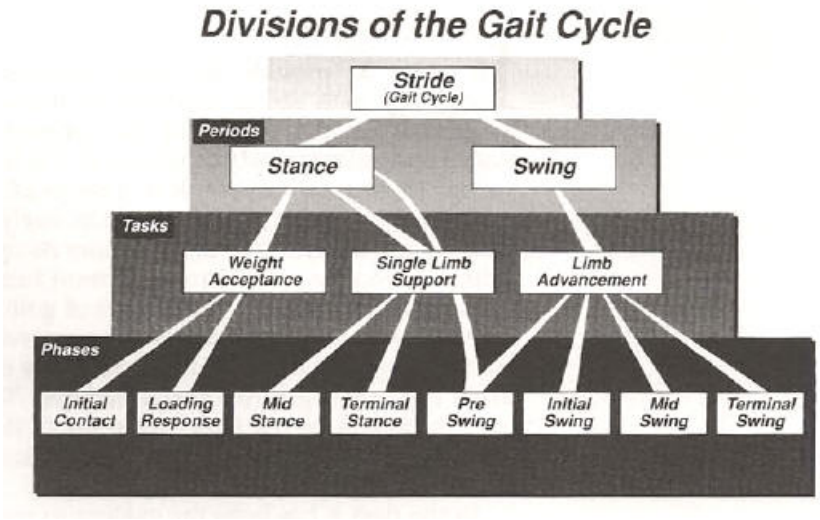

Figure 2.6.: Divisions of the gait cycle

Task A: Weight acceptance

Phase 1: Initial Contact

This phase extends from 0-2% GC. The foot touches the floor heel first. This is often referred to as heel contact (HC). The limb is preparing itself to start the *heel rocker*. This denotes the rolling motion over the heel which is depicted in Figure 2.7a.

Phase 2: Loading Response (LR)

This phase comprises the entire initial double stance period and extends from 0-10% GC. It begins with IC and ends when the contralateral leg is lifted for swing. Body weight is transferred onto the limb. Using the heel as a rocker, the knee is flexed for shock absorption. Note that the heel rocker is limited by forefoot contact with the floor.

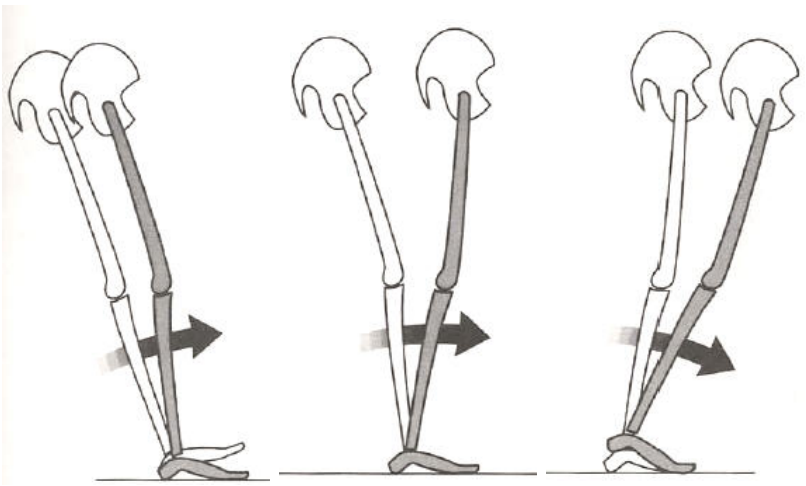

(a) Heel rocker **(b)** Ankle rocker **(c)** Forefoot rocker

Figure 2.7.: Three leg rockers

Task B: Single limb support

Phase 3: Mid Stance (MSt)

The first half of the single limb support period is denoted as mid-stance and spans 10-30% GC. It lasts until the body weight is aligned over the forefoot. The main objectives are progression of the body over the stationary foot and stability of the limbs as well as the trunk. During progression of the body the foot remains flat on the floor and the ankle acts as a rocker (Figure 2.7b).

Phase 4: Terminal Stance (TSt)

This phase completes the single limb support period ranging 30-50% GC. It begins with heel rise. The limb moves forward over the forefoot rocker (Figure 2.7c), progressing the body weight beyond the supporting foot. Terminal stance lasts until the contralateral leg strikes the ground.

Task C: Limb advancement

Phase 5: Pre-Swing (PSw)

Floor contact of the contralateral limb has started the terminal double stance. Body weight shifts from the ipsilateral to the contralateral limb. The unloaded limb prepares itself for swing. Pre-Swing can thus be interpreted as the transition between stance and swing and extends from 50-60% GC.

Phase 6, 7, 8: Initial Swing (ISw), Mid Swing (MSw), Terminal Swing (TSw)

The actual swing is divided into three phases: initial, mid and terminal swing. They extend respectively from 60-73% GC, 73-87% GC and 87-100% GC. The main

objectives of the swing phase are limb advancement, foot clearance from the floor and preparation of the limb for stance. Swing initiates with toe-off. Initial swing lasts until the swinging limb is opposite of the supporting limb, at which point mid swing begins. Mid swing ends when the swinging limb is forward and the tibia is vertical. Limb advancement is complete as the shank moves ahead of the thigh at which point heel strike initiates stance.

An overview of the different phases of the gait cycle is depicted in Figure 2.8. Note that at each phase both the described limb (shaded) as the contralateral one (clear) are depicted.

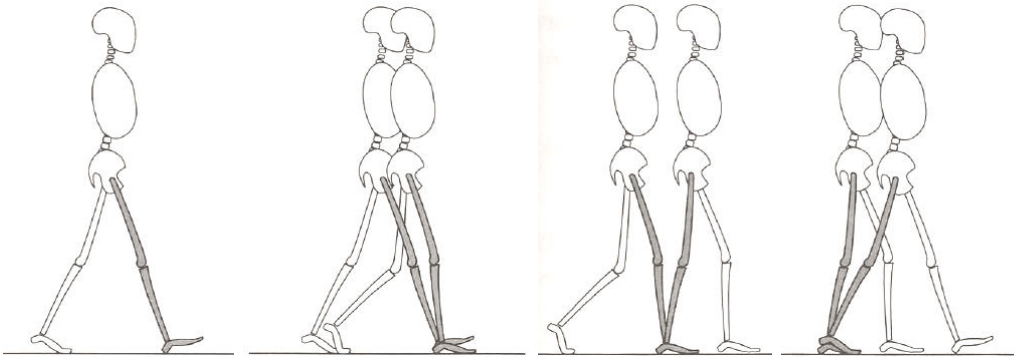

(a) Initial Contact **(b)** Loading Response **(c)** Mid Stance **(d)** Terminal Stance

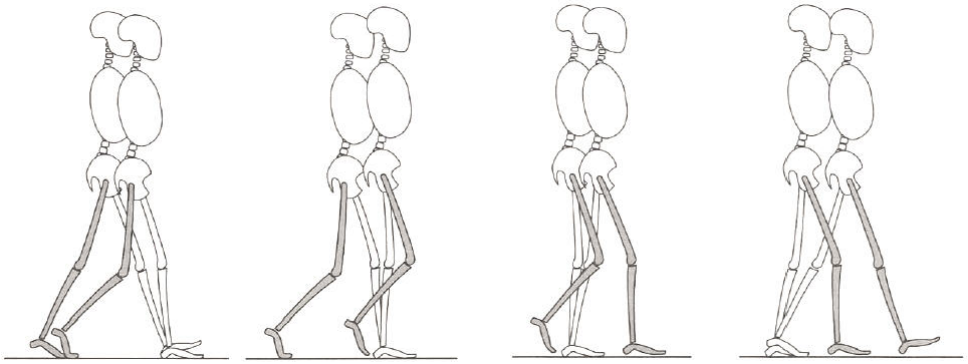

(e) Pre-Swing **(f)** Initial Swing **(g)** Mid Swing **(h)** Terminal Swing

Figure 2.8.: Functional phases of gait

2.2.4. Energy conservation: reducing COM work

The efficiency of doing any activity is the ratio between the work accomplished and the energy expended. During walking, preservation of stance stability and advancing the swinging limb as the body progresses, constitutes the work being performed. The amount of muscular effort required in these actions determines the energy cost. To maintain a “low “ effort level, the normal stride includes two mechanisms to conserve

energy. One of these is COM (Center Of Mass) alignment modulation in which the pelvis plays an important role.

Minimizing the amount that the body's COM is displaced from the line of progression is the most important mechanism to conserve energy. The least energy would be used if the weight being carried, in this case the entire body weight represented by the COM, remained at a constant height and followed a single central path. Then no additional lifting effort would be needed to recover from the intermittent falls downward or laterally.

Reciprocal, bipedal locomotion presents two potentially costly situations during one stride. As the body weight is carried alternately by the left and right limb, the body must shift from one side to the other resulting in a horizontal movement of the body's COM. The limbs also change their vertical alignment during gait causing a change in the height of the pelvis, leading to the COM moving up and down. During stance the COM rotates around the foot. This motion is often modeled as an inverted pendulum (Figure 2.9a). Looking at the complete gait cycle, one sees that the body is at its lowest position in double support stance when both feet are flat on the floor (Figure 2.10). The highest position occurs in single support stance when the supporting limb is vertical. The difference between both can be up to 9.5 cm if no modifying action would be performed [41]. Both extreme situations occur one after the other, resulting in a vertical movement of the COM which is approximately sinusoidal (Figure 2.9b).

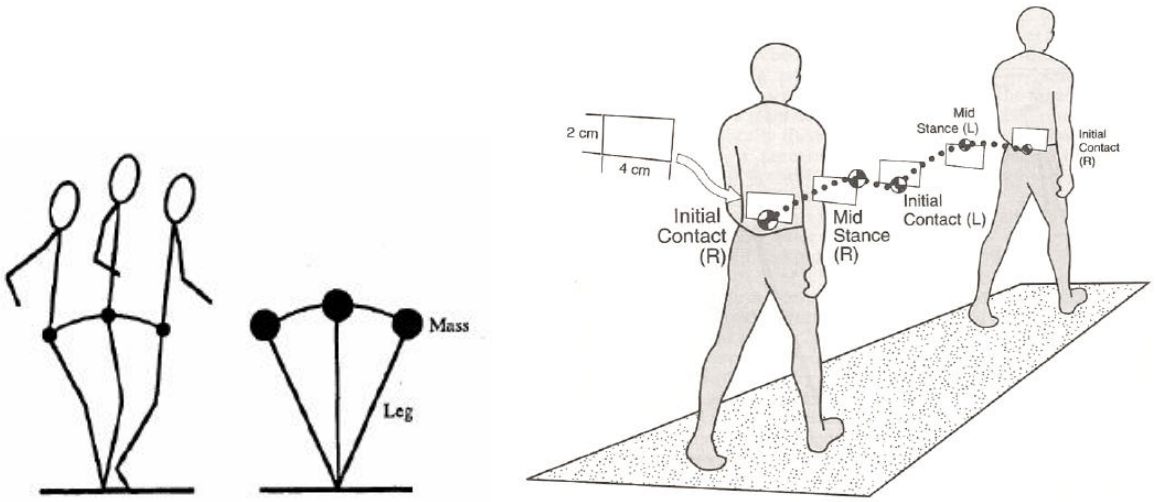

(a) Inverted pendulum model [53] **(b)** Sinusoidal movement of COM

Figure 2.9.: COM movement

Three types of changes in pelvic alignment reduce these costly horizontal and vertical displacements. In addition, abrupt changes in direction are avoided which is an energy-conserving maneuver as well. The three pelvic alignment changes are called *contralateral drop*, *horizontal rotation* and *lateral displacement*. Each motion spans

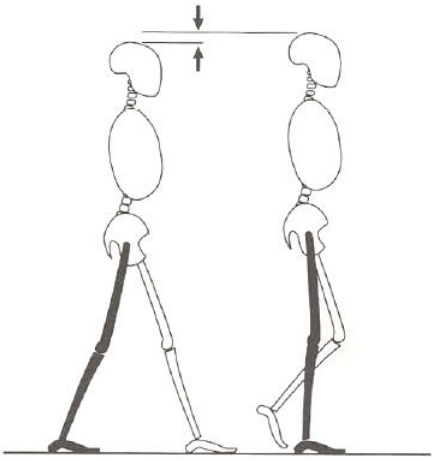

Figure 2.10.: Maximal vertical displacement

approximately 4 degrees. The first two actions occur passively. Lateral displacement of the pelvis relates to the transfer of body weight onto the limb.

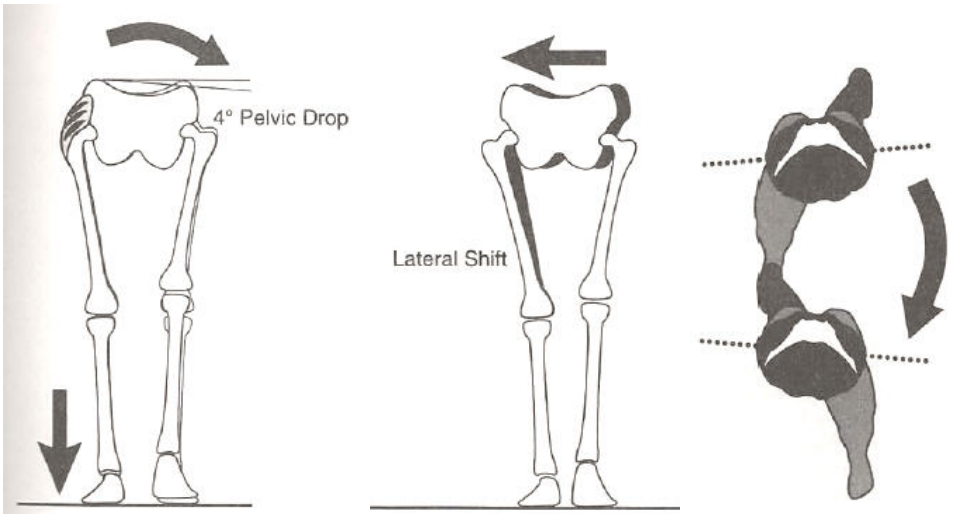

(a) Contralateral pelvic drop **(b)** Lateral shift **(c)** Horizontal rotation

Figure 2.11.: Changes in pelvic alignment as an energy conservation mechanism

During loading response and early mid stance both vertical and lateral realignment of the body's COM occurs. Lifting one limb for a step removes the support for that side. Gravity causes a moment around the hip joint which results in a contralateral pelvic drop depicted in Figure 2.11a. Half of this drop is experienced by the body's COM as it lies at the midpoint of the pelvic width between the two hip joints. Thus a vertical lowering of the COM has taken place.

The minimizations of lateral displacement of the pelvis consists of 2 factors. First is the natural angle between tibia and femur. The knees are positioned closer to each

other than a vertical line down from the hip joint could offer. This limits the step width to 30-40% of the actual hip width thus limiting the displacement needed to bring the COM exactly above the supporting limb.[1] The second contribution takes place at the knee joint. As the limb is loaded a slight increase in knee abduction moves the body's COM nearer to the supporting foot (Figure 2.11b).

The third pelvic motion is horizontal rotation and results in a decrease of the COM drop during double support. As the swinging limb moves forward, the hip joint is moved in front of the joint of the stance limb (Figure 2.12). This movement functionally lengthens the limbs by increasing the distance between the two points of floor contact. To accomplish the desired step length, the limbs do not need to be spread as much as would be necessary without pelvic rotation thus resulting in a decrease of COM lowering. The effect is greatest in terminal stance. Note that horizontal pelvic rotation also brings the hip joints (and thus the supporting feet) closer to the midline lowering lateral displacement.

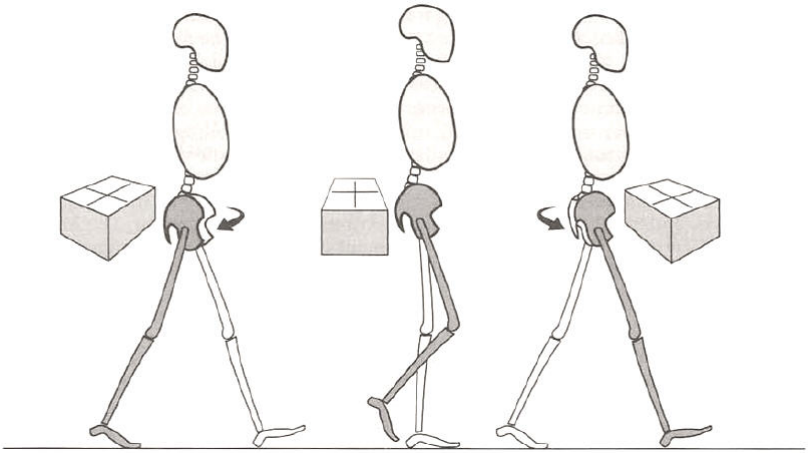

Figure 2.12.: Pelvis rotation in gait

Limb motion also smoothens the path of vertical COM motion. The mechanics vary with the phase of gait. During double stance intervals ankle control is critical. Heel rise in terminal stance and initial contact by heel strike simultaneously lift the COM (Figure 2.13a). The interchange of ankle and knee motion in stance is a second means of reducing COM displacement. As depicted in Figure 2.13b, a combination of knee and ankle movement "flattens" the locus of the body's COM (black) in comparison to the inverted pendulum model (red).

In summary, vertical lift of the COM during single limb support is decreased by contralateral tilt of the pelvis (pelvic drop) combined with stance limb ankle and

[1] In static single limb support, the body's COM is placed above the supporting limb thus attaining a stable position. This represents the maximal lateral displacement since in walking less stability is sought. The potential imbalance is controlled by inertia. By the time the body loses balance and would fall to the unsupported side, the swinging limb is prepared accept the load at the onset of stance. Therefore the COM does not need to be positioned exactly above the supporting leg.

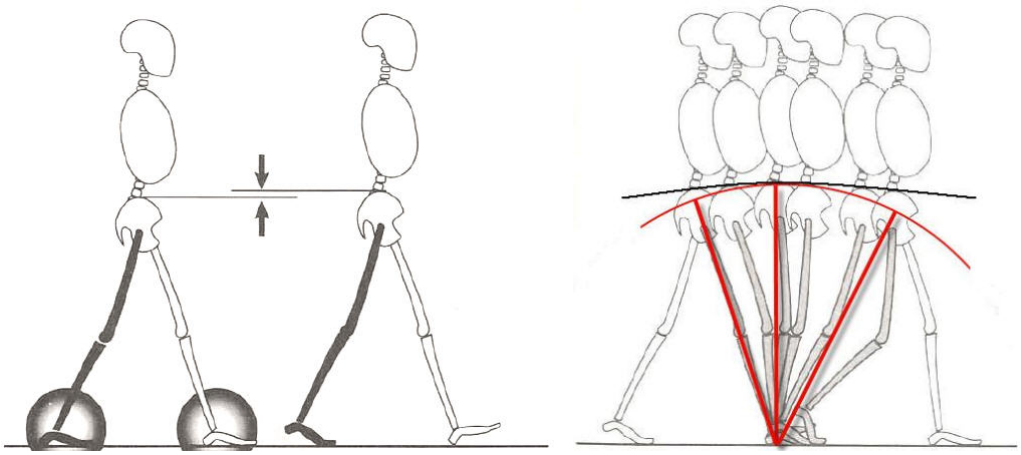

(a) Ankle control in double stance **(b)** Combined knee and ankle motion

Figure 2.13.: Effect of limb motion in vertical COM displacement

knee motion. Lowering of the body center by double limb support is reduced by terminal stance heel rise, initial heel strike and horizontal rotation of the pelvis. Lateral displacement is similarly minimized by pelvic rotation, angulation between femur and tibia and substitution of inertia for dynamic balance (footnote 1).

2.2.5. Ankle kinematics and kinetics

2.2.5.1. Plantarflexion/dorsiflexion

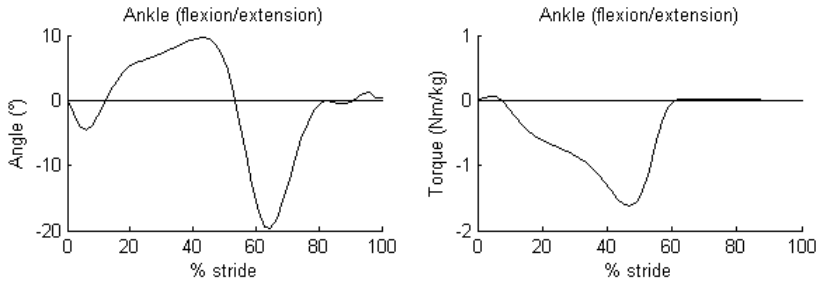

Figure 2.14.: Ankle kinetics and kinematics in the sagittal plane. Data from [57]

- During LR, the foot plantarflexes under control of a small dorsiflexor torque (Figure 2.14), demanding absorption of a small quantity of energy. This is known as the heel rocker (subsection 2.2.3).
- At 10% stride, the foot is flat on the ground and the leg rotates over the foot, causing the ankle to dorsiflex. This action is controlled by an increasing plantarflexor torque, requiring energy absorption by the ankle (A1 region in Figure 2.15). This continues until the first half of terminal stance (42% stride).

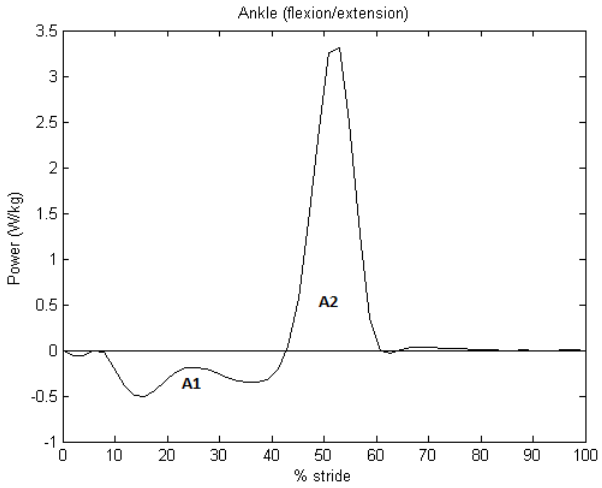

Figure 2.15.: Ankle power in the sagittal plane, derived from Winter's data [57]

- A burst of positive power (A2) is applied from 42% to 60% stride, causing the ankle to rapidly and powerfully plantarflex. This provides the trailing leg with the necessary push-off to propel it into swing. The energy generated during the A2 phase constitutes about 80-85% of the total energy that is generated during the entire gait cycle [57]. The importance of ankle push-off is further discussed in subsection 2.3.4.
- During swing, the position of the foot is carefully controlled to avoid stumbling and to prepare the foot for initial contact. The ankle is dorsiflexed to assure foot clearance. Ankle moments required for this action are small because of the low mass and inertia of the foot.

The most common way of visualizing the ankle kinetics and kinematics is by means of an angle-torque graph as shown in Figure 2.16. The different phases of gait are marked on the graph as well.

2.2.5.2. Inversion/eversion

Inversion and eversion of the ankle are mechanisms to fine-tune placement of the support site of the foot, which is essential for dynamic stability (subsection 2.3.1). As a result, a large variability in especially the angle and power characteristic is observed (Figure 2.17).

Eversion begins as part of the loading response immediately after HC. Peak eversion is reached by early mid-stance (14% stride). The ankle then inverts throughout stance, as the weight is shifted towards the hallux (big toe). In swing, eversion is started once again until a second eversion peak is reached at about 80% stride, followed by inversion during the last 20% of the cycle. The torque remains invertor throughout almost the entire gait cycle. Average energy absorption and generation is

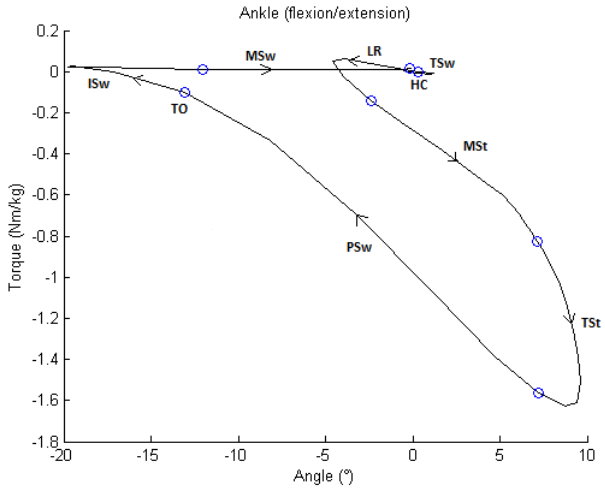

Figure 2.16.: Ankle angle-torque plot in the sagittal plane. Data from [57]

negligible, although the large variability indicates that bursts of power are sometimes applied during stance to correct foot placement.

From this discussion, it is evident that inversion/eversion should be a passive DOF of the orthosis if it is incorporated in the design.

2.2.5.3. Internal/external rotation

Data for ankle internal/external rotation is not available. However since the motion is strongly coupled with inversion/eversion we can come to the same conclusions. Incorporation of this DOF in the orthosis design will again be passive.

2.2.6. Knee kinematics and kinetics

2.2.6.1. Flexion/extension

The knee has three important functions during walking [41]: shock absorption as the limb is loaded, extensor stability during stance and rapidly flexing during swing. The plane associated with these functions is the sagittal plane. Flexion/extension is therefore the main DOF of the knee, with a ROM of 65 degrees. Knee kinematics and kinetics are shown in Figure 2.18.

- From 0 to 5% stride the knee shows an internal flexor moment to prevent hyperextension at the end of the swing phase [55]. This results in a short-lived power generation zone (unnamed peak in Figure 2.19).
- From 5 to 15% stride, the knee flexes under the control of an extensor torque, preventing it from buckling under the weight which is transferred onto the leg. This is the first major absorption phase, often referred to as K1 (Figure 2.19).

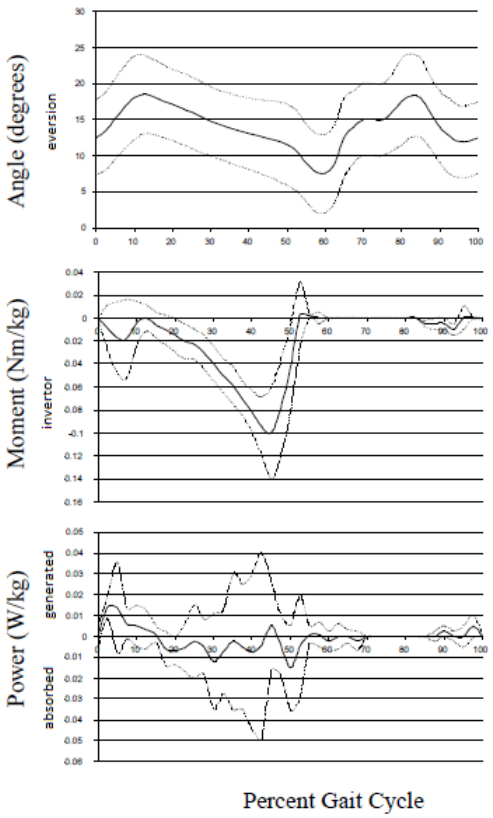

Figure 2.17.: Ankle kinematics, kinetics and energetics for the inversion/eversion DOF. Adapted from [15].

- From 15% stride, the knee extends under control of an extensor torque. In this phase (K2), the knee does its largest amount of positive work, which nevertheless represents only about 10-15% of the total energy generation in level walking. At 40% stride, which is about midway in terminal stance, minimum stance phase flexion is attained. Note that the knee angle remains fairly constant throughout mid stance.
- From 40% stride, the knee slowly starts to flex again under a small extensor moment, preparing toe-off. Right after toe-off (62% stride), the angular velocity decreases again, maintaining a small extensor moment to decelerate the backward swinging leg. This is the K3 phase in which energy is absorbed. At 70% stride, maximum flexion (65°) is attained, assuring toe clearance.
- From 70% stride (end of initial swing), the knee again extends under a nearly zero torque until about 80% stride. The energy in this phase is not provided by the knee joint, but by the conversion of potential energy to kinetic energy.
- From 80% stride, a flexor torque provides a burst of negative energy (K4) to decelerate the rapidly extending leg and to prevent overextension of the knee.
- At 97% stride, the knee has reached its maximum extension and starts to flex

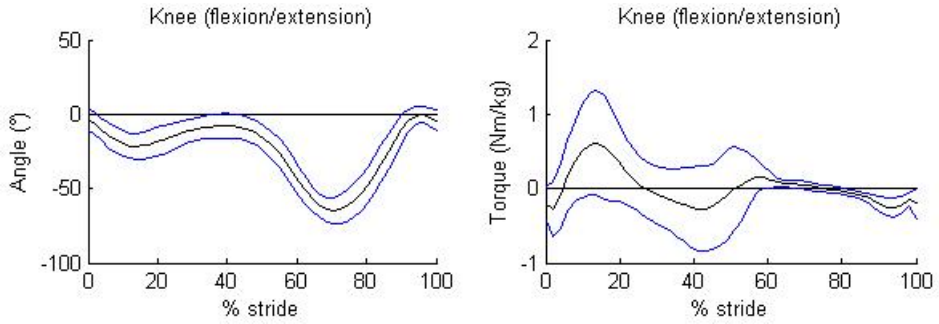

Figure 2.18.: Knee kinetics and kinematics in the sagittal plane. Blue curves denote the boundaries of the 95% confidence interval. Data from [57]

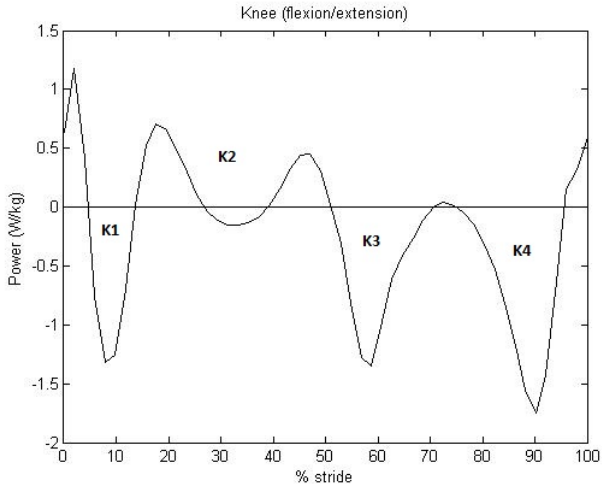

Figure 2.19.: Knee power in the sagittal plane, derived from Winter's data [57]

again, controlled by a flexor torque.

In conclusion, the knee joint mainly serves to absorb energy during normal walking (Figure 2.19). It would be tempting to use only a damper at the orthosis knee joint, neglecting the region of positive power (K2). However this is not a good idea, since generating power is metabolically more costly than absorbing power [17]. Interestingly, Figure 2.20 reveals a quasi-linear relationship between knee angle and torque during loading response and mid-stance (equivalent to the K1 and K2 phases). This can be exploited by placing a passive elastic element in the knee joint, storing the K1 phase energy and releasing it during K2, providing the necessary positive power.

2.2.6.2. Abduction/adduction

Knee abduction and adduction facilitates vertical balance over the limb, particularly during the single support phase of gait, and helps reduce horizontal COM work

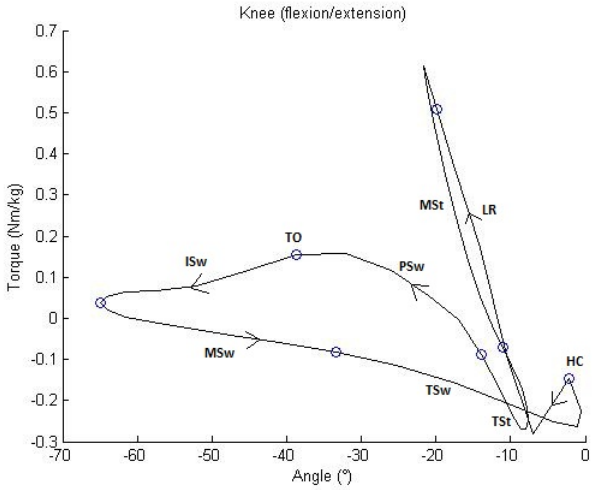

Figure 2.20.: Knee angle-torque plot in the sagittal plane. Data from [57]

(subsection 2.2.4). Knee abduction/adduction ROM (Range Of Motion) during gait is only about 6° (Figure 2.21). During terminal stance, the adduction angle remains constant at about 1°. The deviation from this angle remains small throughout stance (ROM about 2°). Knee adduction contributes to reduced lateral shift of the COM during this phase (Figure 2.11b). Peak adduction is attained at 80% stride, when the leg is closest to the contralateral leg.

Fairly large abductor torques are generated throughout stance. An abductor moment of no less than 1,1 Nm/kg is observed at the beginning of mid-stance. A second peak (0.7 Nm/kg) is found at the end of terminal stance. The magnitude of these torques is comparable to those observed in the sagittal plane. Nevertheless, power generated and absorbed is much smaller due to the limited ROM of this DOF. This DOF will therefore be constrained in our orthosis design. A constant adduction angle of 1° seems a sensible choice, since this is the angle maintained throughout most of stance.

2.2.6.3. Internal/external rotation

Internal/external rotation accommodates the changes in alignment as the body swings from behind to ahead of the supporting limb [41]. This DOF is also linked to the flexion/extension DOF through the so-called *screw-home mechanism* [37]: during knee extension, the tibia rotates externally and vice versa. At the end of loading response (10% stride), a peak of negative power is observed when the knee is at its maximum internal rotation under the maximum occurring external rotator torque. A maximum external rotation angle of 5° occurs at 85% stride, helping the foot not to coincide with the stance leg.

This DOF will not be implemented in our orthosis design. It is safe to assume that the wearer will be able to generate and absorb the required power.

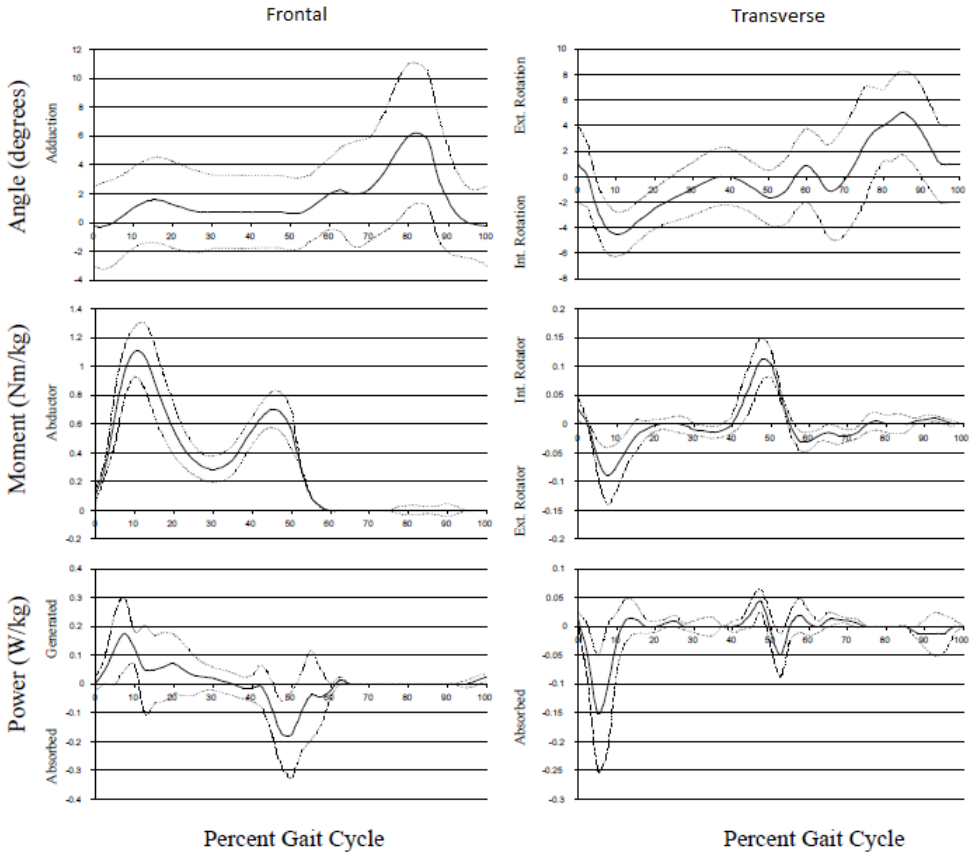

Figure 2.21.: Knee kinematics, kinetics and energetics in the frontal (abduction/adduction) and transverse (internal/external rotation) plane. Adapted from [15].

2.2.7. Hip kinematics and kinetics

2.2.7.1. Flexion/extension

Flexion/extension is the hip DOF with the largest ROM (33°). The movement of the hip in the sagittal plane can roughly be summarized as extension during stance and flexion during swing. Joint kinematics and kinetics are shown in Figure 2.22.

- At HC, the hip is almost at its maximum flexion angle. An extensor torque is applied to initiate extension of the hip, lifting the body's COM. This requires positive power (H1 region).
- Hip power shifts from positive (i.e. lifting COM) to negative (i.e. decelerating the falling COM) at about 20% stride, when COM is at its highest position. During most of mid-stance, hip torque is no larger than 0.1 Nm/kg. This highlights the passive nature of the motion, which can be modeled as an inverted pendulum subsection 2.2.4.

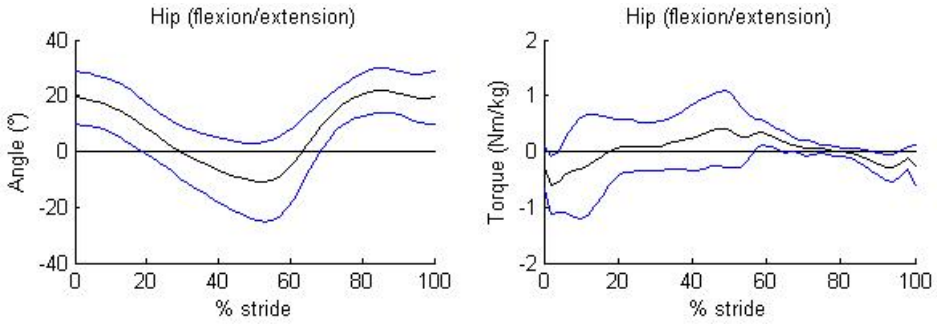

Figure 2.22.: Hip kinetics and kinematics in the sagittal plane. Blue curves denote the boundaries of the 95% confidence interval. Data from [57]

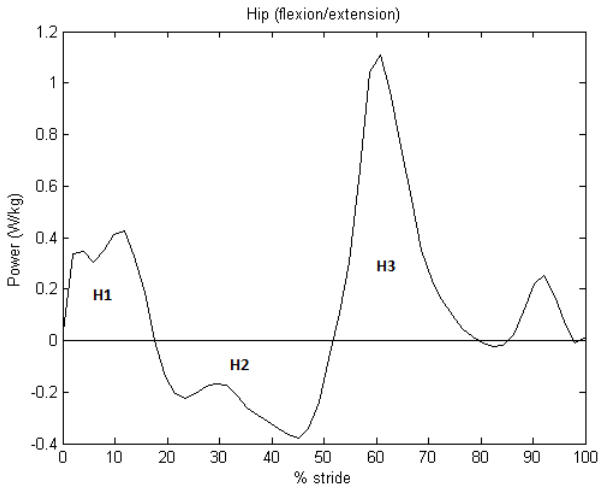

Figure 2.23.: Hip power in the sagittal plane, derived from Winter's data [57]

- Terminal stance is marked by a flexor moment, while the hip is still extending. This means that part of the potential energy released from the falling COM is absorbed in the hip (H2) to decelerate the thigh and prevent the hip from overextending.
- At pre-swing, the hip starts to flex. The torque remains flexor, resulting in a positive burst of power (H3), helping to lift the foot and initiate swing. The power level increases rapidly as the inertial load of the swinging limb becomes important.
- Just like at the knee joint, torques observed at the hip are low (smaller than 0.1 Nm/kg) during mid-swing, which once again proves the passive nature of leg swing. Maximum flexion is attained during this phase.
- Terminal swing prepares the leg for stance. An extensor torque slightly extends the hip to allow for an optimal positioning for initial contact. This requires a small burst of positive power.

Because the hip provides substantial amounts of power, actuation at this joint is advised. Figure 2.24 shows the complex relationship between hip angle and torque. The possibility of using passive elastic devices for actuation of the hip is not easily assessed from this figure.

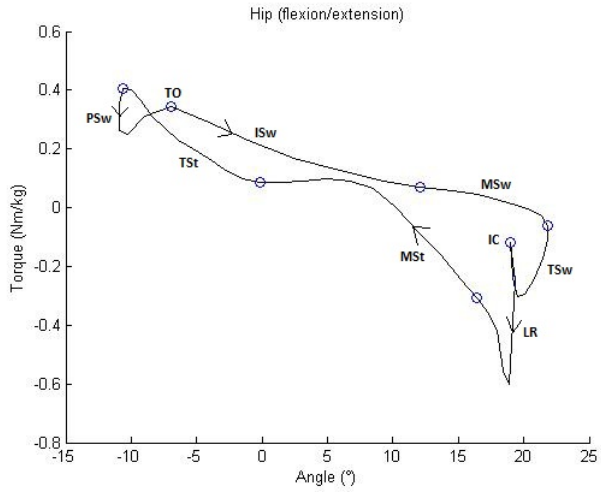

Figure 2.24.: Hip angle-torque plot in the sagittal plane. Data from Winter [57].

It is important to note that hip powers are seen to be quite variable across subjects. Inter-subject variability for the knee and ankle joint is lower than it is for the hip [57].

2.2.7.2. Abduction/adduction

During the single-support stance phase, the hip is adducted and a significant abductor torque is applied to the hip joint (Figure 2.26). This can easily be understood by looking at Figure 2.25. As mentioned before (subsection 2.2.4), lifting one limb for a step removes the support for that side. Gravity, represented by the weight suspended in the COM, causes a moment around the hip joint which would force it to adduct. This moment is reacted on by a shift of the body towards the stance limb and a strong contraction of the hip abductors. These actions do not completely counter the gravitational moment, allowing some contralateral pelvic drop (subsection 2.2.4). This is reflected in Figure 2.26 as the hip abduction angle during initial swing. During the double-support phase of gait, the abductor torque disappears and the hip displays a small adduction angle again. Note that the counteraction of gravity requires negative joint power.

From this discussion, it is clear that the hip abduction/adduction DOF plays a crucial role in allowing pelvic motion. Actuation of this DOF is necessary to allow the body to maintain its balance when the weight is carried by one only leg. Looking at

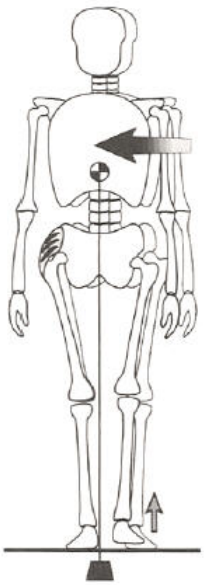

Figure 2.25.: Abductor torque is needed to counter the moment caused by gravity. [41]

Figure 2.26, some similarity can be noted between the angle and torque characteristics for this DOF. The use of a passive elastic element (torsion spring) to provide the necessary torques is therefore an interesting option.

2.2.7.3. Internal/external rotation

At HC, the ipsilateral side of the pelvis is rotated forward (subsection 2.2.4). The hip is rotated externally to keep the leg (and more importantly the foot) from moving inward, achieving a correct placement of the foot. As we move into stance, the ipsilateral side of the pelvis rotates backward. Because the foot is fixed to the floor, this causes the leg to rotate internally. As can be seen in Figure 2.26, this movement is controlled by an external rotator torque from about 5 to 25% stride, meaning that power is absorbed. A second peak of power absorption occurs at late terminal stance, when the pelvis almost reaches its maximum rotation and internal rotation is halted. Rotation of the pelvis also explains why the hip moves from an internally to an externally rotated position during swing. A positive torque is applied during terminal swing to place the leg in the correct position for HC. This torque is however small compared to the torques observed during swing in the sagittal plane, since the leg's moment of inertia for movement in the frontal and transverse plane is substantially smaller.

From this discussion we can conclude that, just like the abduction/adduction DOF, internal/external rotation is very important to allow pelvic movement. The need for actuation is nevertheless a lot lower. Peak power is only -0.15W/kg and almost

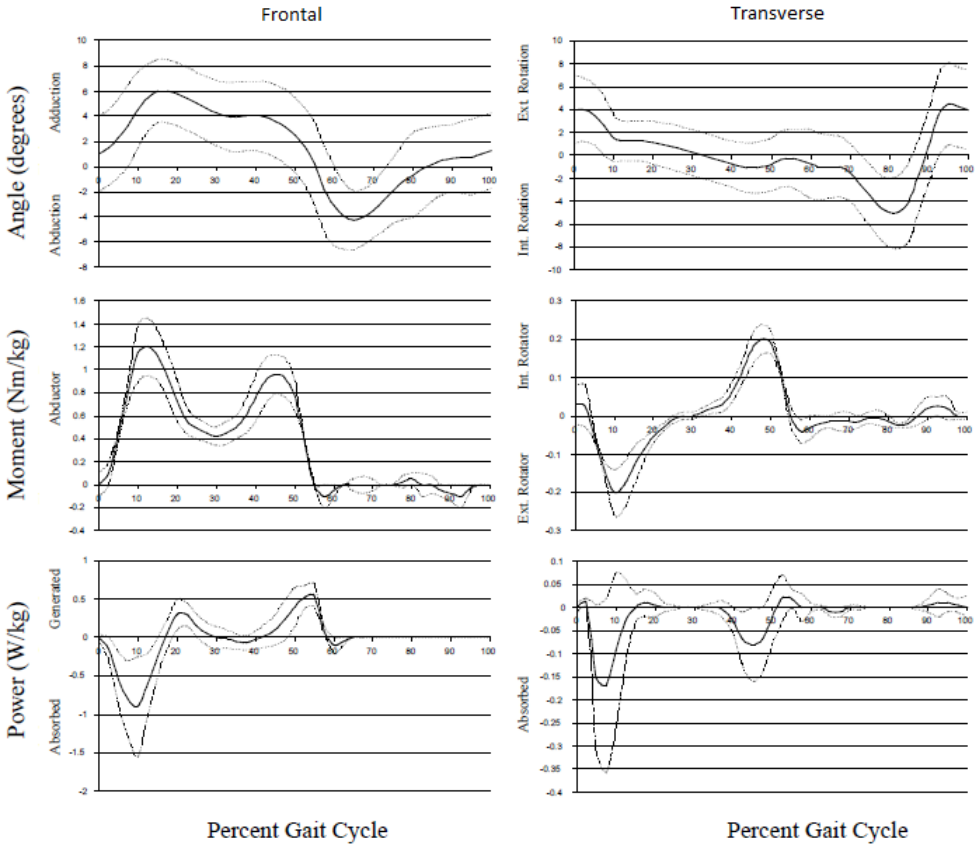

Figure 2.26.: Hip kinematics, kinetics and energetics in the frontal (abduction/adduction) and transverse (internal/external rotation) plane. Adapted from [15].

all power is to be absorbed, which is metabolically least costly. It seems safe to assume that the wearer of the exoskeleton can absorb this power without the aid of the orthosis. The internal/external rotation DOF will therefore be left free.

2.2.8. Ground reaction forces

The stance leg transmits the body weight to the ground. This must of course be accompanied by reaction forces on the foot. These reaction forces, exerted by the ground, are termed *ground reaction forces* (GRF). They are measured by means of a force platform during gait trials. Results obtained by Winter are plotted in Figure 2.27. As the stance leg accepts weight, the vertical GRF increase towards 100% body weight (BW). A first peak GRF of about 110% B.W. is observed. Here, the GRF not only supports body weight, but also reacts to the upward acceleration of the body's center of mass, which is necessary to decrease the downward velocity of the body. The second peak is due to push-off, which once again accelerates the body's center of mass upwards. The horizontal force is negative during the first half of stance, meaning that the body is decelerated, whereas the positive force during

pre- and terminal swing indicates that the body is pushed forward. Notice that the horizontal GRF are about 1/5th of the vertical GRF.

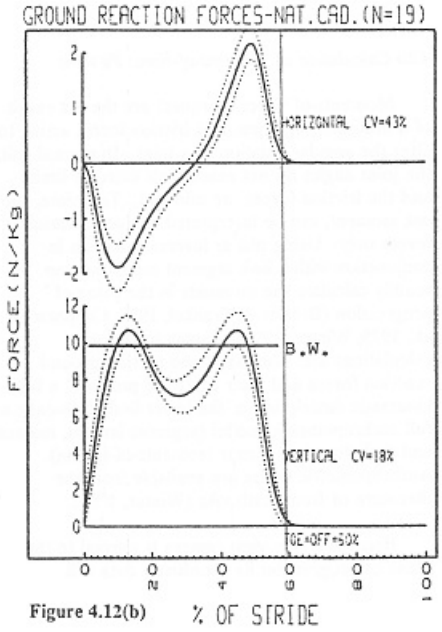

Figure 2.27.: Ground reaction forces [57]. Dotted lines denote the boundaries the 95% confidence interval.

2.3. Factors affecting lower limb kinematics and kinetics

In this paragraph we will focus on several factors that influence lower limb kinetics and kinematics during locomotion. Special attention will be paid to their effect on the orthosis design.

2.3.1. Keeping balance

A particularly challenging task, especially during gait, is to keep the body balanced. Static balance (i.e. while standing) is dominated by action of the ankle muscles (plantarflexors/dorsiflexors and invertors/evertors), keeping the body's center of gravity within the base of support. In walking, which is a dynamic task, the center of gravity is accelerated forward in an inverted-pendulum fashion, leaving its position within the base of support. The potential imbalance is controlled by inertia. By the time the body loses balance and would fall to the unsupported side, the swinging

limb is prepared to accept the load at the onset of stance. As a result, the role of the ankle muscles in dynamic balance is more limited: they cannot avert a fall, but they still serve to fine-tune the acceleration of the center of gravity in the transverse plane. The key to balance during walking is a safe placement of the swing foot.

The upper body, which comprises 2/3 of body mass, poses an additional balancing challenge due to its inertia and the large gravitational moment that occurs when the body is not aligned directly above the support foot. Maintaining an erect position is a strategy to keep this gravitational moment small. Hip flexors and extensors provide the necessary torque to counter the remaining moment.

It is evident that hip abductors and adductors and foot invertors and evertors are the primary contributors to frontal plane stability. The role of the hip abductors/adductors was already explained in subsubsection 2.2.7.2. Ankle invertors/evertors fine-tune the medial-lateral position of the foot during stance, thus controlling the position of the foot support site relative to the body's center of gravity.

Finally, a well-planned trajectory of the foot during swing is essential to prevent stumbling. Sufficient toe clearance is needed to avoid bumping into low obstacles. The control of the foot during swing is essentially a ballistic and positional task. A relatively small change in a number of joint angles can strongly influence the end-point trajectory of the heel and toe. Therefore it is clear that a good orthosis design does not restrict movement of the limb in any way and has a minimal effect on limb kinematics, especially during swing.

A more detailed discussion of balance and posture in human gait can be found in [57], the work on which this subsection was based.

2.3.2. Tendons

As already noted in subsection 2.2.1, some of the work done on joints during gait can be attributed to elastic energy storage and release in the series-elastic element of a muscle-tendon complex. Tendons are tissues that connect the muscles to the bones. They are thus placed in series with the muscles. The tendons have elastic properties, allowing them to store and release energy. This mechanism is believed to contribute to metabolic energy economy. For example, the Achilles tendon executes a stretch-recoil cycle in each gait cycle, storing and releasing strain energy. As a result, the gastrocnemius medialis (an ankle plantarflexor muscle) maintains a near-constant length, i.e. generating a minimal amount of power [22].

Based on this idea, Van den Bogert studied the use of elastic cords (called "exotendons") in exoskeleton design [46]. Note that these exotendons are used in parallel with the human muscle, unlike human tendons which act in series with the muscle. In numerical simulation, reductions of joint power up to 74% were obtained. An actual exoskeleton was built to verify these findings experimentally [48]. Results were rather disappointing: an increase in energy expenditure was observed compared to

normal walking, most likely due to factors such as increased mass and inertia and restriction of movement in some DOFs.

2.3.3. Mass and inertia

When equipping a person with an orthosis, one must take into consideration that total leg mass is increased. This has an effect on ground reaction forces and leg inertia, which would logically affect joint torques and kinematics. Studies [12, 42] have shown that metabolic energy consumption is higher when mass is added to the legs, an effect which is amplified if the mass is placed at more distal locations. Kinematics however remain largely unchanged. Loads can be attached to the hips with a relatively low metabolic cost [12]. This makes the hips the preferred location for the placement of e.g. batteries. Furthermore, these studies show that increasing leg inertia also increases stride frequency and the relative duration of swing.

An additional problem is that, if more mass is added to one leg than to the other, the inertial asymmetry will cause a more asymmetrical gait pattern [44]. This is relevant for the CYBERLEGs project, since the combined mass of limb and orthosis is likely to be larger than the mass of the prosthesis. The question is whether this should be resolved by increasing prosthesis weight accordingly. A study by Mattes et al. [33] investigated this issue by matching the mass and inertia of the prosthetic limb of people with transtibial amputations with that of the sound limb. As mass and moment of inertia of the prosthetic limb became more closely matched to the intact limb, step length, swing time, and stance time became less symmetrical. Energy cost was also significantly greater (6% to 7%). These results suggest that matching prosthesis and orthosis weight is not necessarily the best option, although it does not rule out that a prosthesis which completely restores ankle function could benefit from such an approach. Either way, the decision lies with the prosthesis designer, since the orthosis leg will likely be the heaviest.

In conclusion, the orthosis design needs to be lightweight and favour a more proximal placement of heavier parts.

2.3.4. Ankle push-off

When the leading leg collides with the ground, energy is lost. In order to keep a constant speed on a horizontal surface (i.e. total energy remains constant), this energy loss must somehow be compensated by positive work provided by the muscles. Minimizing collision losses is therefore an interesting strategy for energy-efficient walking. Simulation has shown that push-off of the trailing leg, can reduce collision losses, as well as taking shorter steps [26]. However, the latter option increases energy needed for leg swing, since the leg is forced to swing faster in order to maintain the same walking speed. Step length is considered a trade-off between collision and leg swinging costs, and is therefore strongly dependent on swing leg

inertia properties - as previously noted in subsection 2.3.3 - and push-off of the trailing leg.

Experiments comparing the CESR foot (actuated ankle) to a conventional SACH foot (unactuated ankle) also provide valuable insight into the role of ankle push-off [14]. Subjects walked with slower strides (i.e. larger steps) with the CESR foot than with the SACH foot, confirming the above theory. Metabolic rate was also lower with the CESR foot. These results were confirmed in a similar study where subjects walked with powered ankle-foot orthoses (PAFO's) [38]. Several studies also suggest that decreased ankle push-off leads to increased hip moments [38, 18] and vice-versa. Simulation [27] shows that providing active hip actuation throughout stance requires four times more mechanical energy than pre-emptive push-off, making the latter strategy the preferred one.

In conclusion, compensating decreased ankle push-off should be one of the design priorities for the orthosis.

2.3.5. Age

As noted in section 1.2, the CYBERLEGs exoskeleton is expected to be worn primarily by elderly people. This raises the question whether the orthosis should be designed using standard gait data or data originating from studies on the elderly. A good understanding of gait adaptations with age is the key to making a well-considered choice.

2.3.5.1. Gait kinematics and kinetics

Studies have shown that gait of elderly subjects is significantly different from that of younger subjects. A study by DeVita and Hortobagyi [18] compared gait for elderly and young subjects walking at identical velocities. Elderly subjects exhibited a shorter step length and thus a higher stride frequency, while swing time was relatively shorter. Joint angles and torques revealed a completely different walking strategy. Ankle plantarflexor torque was significantly lower for elderly people, whereas hip extensor torque was exerted longer into stance phase and hip flexor torque was somewhat lower. The ankle ROM was also smaller, whereas the hip flexed more. Knee extensor torques were lower throughout stance, flexor torques higher. In short, it seems like lower plantarflexor torque is compensated for by a larger hip extensor torque during early and mid-stance, while step length is decreased. This is consistent with the findings presented in subsection 2.3.4.

A decrease in muscle power production with age is a likely explanation for the decrease in ankle plantarflexor torque. However, the authors of [18] point out that plantarflexor torque exerted during walking is far less (40%) than the maximum amount that can be produced. Elderly people would still be able to produce this

torque. However, they seem to prefer making less use of their ankle plantarflexor muscles. A likely explanation is that providing the same torque with degenerated muscles comes at a higher metabolic cost.

The same differences in gait were observed in a study by Winter [57]. Variability in gait of the elderly compared to gait of young adults was found to be lower. This may be interpreted by a loss of neural plasticity, forcing the elderly to choose a more cautious and more consistent motor pattern. Winter also noted that reduced ankle push-off may be the consequence of decreased step length rather than the cause. Since balance is maintained dynamically during gait (subsection 2.3.1), he suggested that elderly may choose to reduce step length to increase double support time, which would give them a larger period to re-establish stability.

Older people have also been observed to prefer a larger step width. The reason for this may be an increase in lateral stability. However, it was found that young adults stabilize their gait by increasing lateral foot placement variability, not step width [14]. A possible explanation is that step width is only adjusted over a long time.

Note that the change in joint kinematics possibly influences tendon work. Increased flexion of the hip may stretch the hip extensors more, such that work is done in a passive elastic way, which is energetically favorable. This would be a possible incentive for the forward leaning trunk observed with elderly people. This hypothesis was however rejected in a study by Silder et al. [43], which attributed increased hip work to active power production rather than passive contributions.

In conclusion, gait adaptations in the elderly are well-documented but the causes are still poorly understood. Improved security is generally considered the main reason for most adaptations, although reduced ankle plantarflexor muscle strength may be an important factor as well. Even though conclusive evidence is still lacking, we will assume that patients will again adopt a normal posture if ankle plantarflexor torque is restored. Therefore, we will base our orthosis design on standard gait data and scale it down to account for muscle degeneration.

2.3.5.2. Muscle degeneration

The most common way to evaluate muscle degeneration with age is to compare *isometric* (limb not moving) and *isokinetic* (moving limb) torque data. Because walking is a dynamic task, the latter were used. Isokinetic data is always specified at a certain angular velocity. To be able to choose the right data, average angular velocities were derived from Winter's gait data [57]. Results are shown in Table 2.1.

We compared isokinetic joint torque data from Danneskiold-Samsøe [16] for groups of subjects aged 20-29 and 70-79. Data was provided for both genders separately; we chose to average the values obtained from male and female subjects. Isokinetic torque measurements were conducted at 3 angular velocities, all of which were smaller than the values found in Table 2.1. We used data for the largest angular

Joint	Average angular velocity (°/s)
Ankle	61.3
Knee	135.7
Hip	57.5

Table 2.1.: Average angular velocities for humain joints during gait

velocities, being 45°/s for the ankle and 90°/s for the knee and hip. This will lead to an underestimation of muscle degeneration, since the ability to produce torque at higher angular velocity declines at a faster rate (e.g. [28]). Results are shown in Table 2.2. Columns labelled "20-29" and "70-79" give the average torque in Nm for subjects aged 20-29 and 70-79. Columns labelled "retained" give the ratio of the torques for subjects aged 70-79 w.r.t. the torques for subjects aged 20-29, expressed as a percentage. Finally, the column "Average" gives the average of the values obtained from men and women.

	Women			**Men**			**Average**
	20-29	**70-79**	**retained**	**20-29**	**70-79**	**retained**	**retained**
Ankle DF (Nm)	20,4	15,3	75,0%	29,7	19,6	66,0%	70,5%
Ankle PF (Nm)	71,6	39	54,5%	106	74,4	70,2%	62,3%
Knee ext. (Nm)	120	69,8	58,2%	193	120	62,2%	60,2%
Knee flex. (Nm)	67,2	44,4	66,1%	106	68,7	64,8%	65,4%
Hip ext. (Nm)	165	92,5	56,1%	250	185	74,0%	65,0%
Hip flex. (Nm)	103	58,2	56,5%	171	115	67,3%	61,9%

Table 2.2.: Reduction with age in isokinetic torque for the ankle, knee and hip joint [16].

We will apply these constant scaling factors to the gait torque data used for the orthosis design. In fact, because of the dependence of isokinetic torques on angular velocity, this scaling factor would have to be dependent on angular velocity as well. We opted for a constant scaling factor for simplicity.

2.4. Conclusions

Although sagittal plane DOFs are the most crucial in walking, the importance of the secondary DOFs cannot be overlooked. Especially hip rotation and abduction/adduction and ankle inversion/eversion are of the utmost importance because they play a key role in energy conservation resp. balance. Incorporating these movements in the orthosis is thus strongly recommended.

3. Design

Given the specifications of the project, in which this thesis fits, in the introductory section (section 1.2) and the basic aspects of gait in chapter 2, the orthosis requirements are first set out.

In designing the orthosis several assumptions were made which are listed in section 3.2. The design process started with an initial concept discussed in subsection 3.6.1, which was then continuously improved in the following subsections.

3.1. Requirements

In short, the orthosis must make daily activities of transfemoral amputees easier by assisting their leg motion. This would reflect in lower joint torques and ultimately a metabolic rate comparable to that of healthy persons. Most issues which should be taken into consideration to achieve this goal are covered in chapter 2. We will summarise these principles and their consequences for orthosis design in this section.

- It must be possible to wear the orthosis during *all daily activities*. The orthosis must have the same ROM as the human leg and may never impede the desired movement of its user, i.e. a good detection of user intent is needed and actuation should be adjusted accordingly.
- The orthosis must *assist the main motions of the human leg*. For this thesis, the motion in need of assistance is level walking.
- The orthosis must *not conflict with human motion*, and should therefore accommodate most (and preferably all) of the human DOFs.
- The orthosis must be *energy efficient*. Minimizing battery power keeps the orthosis weight low and reduces recharge time. This is achieved through the use of passive elastic devices.
- The orthosis must be *lightweight*, and especially the addition of distal mass to the limb must be avoided (see subsection 2.3.3).
- The orthosis must be *wearable*, i.e. all components can be attached to the human body without substantially reducing its maneuverability.
- Last but definitely not least, the orthosis must be *ergonomic*. Not only must it be comfortable to wear, but noise, vibrations and heat emission must also be reduced to a minimum.

3.2. Assumptions

As the orthosis fits in a larger design, namely the CYBERLEG ortho-prosthesis, it is important to come to an agreement about the location of the orthosis and the prosthesis. We assumed the orthosis to be located on the left leg while the prosthesis substitutes for the right leg.

Gait data is obtained from [57]. This dataset is valid for normal cadence on a level terrain. It is an average of many test subjects, since there is substantial inter-subject variability. In order to compare test subjects with different weights, the torque data is expressed in Nm/kg. It is thus necessary to define the weight of the test subject for which the ortho-prosthesis is designed. We chose to optimize the design of the orthosis for a 75 kg test subject.

The primary goal of the orthosis is to compensate the additional load on the healthy leg resulting from the use of the prosthesis. Additionally, the human muscles degenerate with age, as explained in subsubsection 2.3.5.2. We found that at the age of 80, a human being can still generate 60-70% of the torque he/she could generate at the age of 30. This decline should be compensated by the orthosis. It is important to take into account that the decline will presumably be even larger in our targetted patients because of the vascular disease. On top of that, the orthosis adds mass to the wearer's leg, increasing the required torques. We will therefore opt to make the orthosis deliver 50% of the required torque. The other half will be generated by the wearer himself.

Finally, we will assume that the orthosis perfectly tracks the biological kinematics. This is only true if the orthosis does not affect the wearer's gait and if the orthosis fits tightly to the leg.

3.3. Joint degrees of freedom

As mentioned in section 3.1 one of the goals of this thesis is to design an orthosis that is comfortable to wear. The restriction of movement of course reduces comfort. Therefore, it seems sensible to incorporate all DOFs of the human lower limbs in the orthosis design. However this greatly increases design complexity and thus most likely also the mass of the exoskeleton, which is preferably avoided (subsection 2.3.3). This is why most exoskeleton designs do not feature the same degrees of freedom as the human lower limbs. An overview and discussion of DOFs of some well-known and well-documented exoskeletons can be found in [13].

In this paragraph, we will discuss the DOFs of human lower limb joints and evaluate the need to incorporate them in our orthosis design.

3.3.1. Hip

The human hip joint has three rotational DOFs and can therefore be considered a ball-and-socket joint [55]. The primary DOF in locomotion is flexion/extension, making it an essential DOF in orthosis design. The other DOFs, abduction/adduction and internal/external rotation, are necessary to allow pelvic motion, which contributes to decreased COM work during gait (subsection 2.2.4). Transverse rotations of the hip joint may also contribute to trailing leg push-off. Frontal plane rotations, on the other hand, make it possible to adjust step width, which is important for control of stability (subsection 2.3.1). Although range of motion during gait is limited for both rotations (about 10°), we feel that these arguments are sufficiently strong to include all these rotations as a DOF in our orthosis design.

3.3.2. Knee

The human knee is a very complex joint, which has one primary DOF (flexion/extension) and two additional DOFs (abduction/adduction and internal/external rotation) with a small arc of motion. Motion in the frontal plane facilitates vertical balance over the limb, particularly during the single support phase of gait, and helps reduce horizontal COM work (subsection 2.2.4). Transverse (internal/external) rotation accommodates the changes in alignment (due to hip transverse rotation) as the body swings from behind to ahead of the supporting limb [41]. As noted in section 2.2, external/internal rotation and abduction/adduction are limited during locomotion. Because frontal plane motion will already be allowed by hip abduction/adduction and foot inversion/eversion and given the small arc of motion, we will not include the abduction/adduction DOF. As mentioned in subsubsection 2.2.6.2 we will constrain this DOF at a fixed adduction angle of 1°. The small quantity of energy absorbed in the internal/external rotation DOF justifies a fixed rotation of 0°.

3.3.3. Ankle

The junction between the foot and the leg, which we call the ankle, is a complex anatomical area [41]. Terminology in the foot is often confusing and lacking in standardization [55]. The primary DOF of the ankle is in the sagittal plane (dorsiflexion/plantarflexion). While 74% of the work done at the hip during a single gait cycle and 85% of the work done at the knee are done in the sagittal plane, no less than 93% of the work done at the ankle is done in the sagittal plane [40]. Inversion/eversion is considered the second DOF, which is used to stabilize the body during gait (subsection 2.3.1). Although the ankle is often modelled as a hinge joint, it would be more correct to describe the ankle by two joints, the *subtalar* and *tibiotalar* joints. Due to the complexity of the ankle-foot complex, eversion/inversion also results in some ankle dorsiflexion/plantarflexion. The combined movement

eversion-dorsiflexion is called *pronation*, the opposite is called *supination*. An extensive discussion of the ankle-foot complex can be found in [37].

Given the important role of the ankle in stability and the coupling of the ankle motions, it seems a sensible choice to allow all motions.

3.3.4. Summary

We suggest a design with a total of seven DOF. This is more than the six DOFs strictly needed to position the foot in any possible way in space, but less than the amount of DOFs of the human leg. Due to practical reasons however, clarified in subsection 5.5.3, we chose not to implement the internal/external rotation joint at the ankle. The designed orthosis is thus left with six DOFs

Joint	**Biological DOFs**	**Orthosis DOFs**
Hip	flexion/extension abduction/adduction internal/external rotation	flexion/extension abduction/adduction internal/external rotation
Knee	flexion/extension abduction/adduction internal/external rotation	flexion/extension
Ankle	plantarflexion/dorsiflexion inversion/eversion internal/external rotation	plantarflexion/dorsiflexion inversion/eversion

Table 3.1.: Comparison of biological and design DOF.

3.4. Joint range of motion

To ensure a safe interaction with the wearer, the ROM of the orthosis must not exceed the biological ROM. Mechanical stops will be designed to keep the orthosis joints from rotating beyond a certain ROM. On the other hand, this ROM must be sufficiently large to allow movement during normal activities, but also to allow the wearer to take corrective measures in case of stumbling. In conclusion, the orthosis' ROM must certainly lie between the maximum biological ROM and the biological ROM during walking. These ROMS are noted down for all orthosis DOFS in Table 3.2, along with the design orthosis ROM. Note that large variablity exists between biological data sets; the biological ROM values should therefore only be used as a guideline. Tests with the actual orthosis will reveal if any adaptations have to be made to the orthosis ROMs.

Joint	DOF	Biol. ROM (max.)[a]	Biol. ROM (walking)[b]	Orthosis ROM
Hip	flexion/extension	+140° to -15°	+22° to -11°	+120° to -15°
	adduction/abduction	+30° to -40°	+6° to -4°	+20° to -30°
	internal/external rotation	+15° to -60°	+5° to -5°	+10° to -50°
Knee	extension/flexion	0° to -140°	-1° to -65°	+0° to -130°
Ankle	dorsiflexion/plantarflexion	+20° to -50°	+10° to -20°	+15° to -40°
	inversion/eversion	+35° to -15°	-7° to -18°	+15° to -15°

[a]Data from [13]
[b]Data from [57] (flexion/extension) and [15] (other DOFs)

Table 3.2.: Joint ranges of motion. The first motion, before the slash (/), is positive.

3.5. Passive or active assistance

To decide whether or not the incorporated DOFs should be actuated it is useful to take a look at the peak power of each DOF. These are listed in Table 3.3.

Joint	DOF	Peak power (W)
Hip	flexion/extension	42
	abduction/adduction	28
	internal/external rotation	6
Knee	flexion/extension	65
Ankle	plantarflexion/dorsiflexion	122
	inversion/eversion	0.5

Table 3.3.: Peak power of the incorporated joints

The peak powers of the sagittal DOFs are noticably larger than the peak powers of the other DOFs. On top of that, they are the most important DOFs in the gait cycle. Therefore they will be actuated in the design.

Hip abduction/adduction exhibits a significant peak power as well. We will thus aim to assist this movement. Nevertheless, the integral of the power during one cycle (which corresponds to the energy expended by this DOF during one cycle) is close to zero, meaning that power is absorbed as much as it is generated. A passive elastic device such as a spring is well-suited for such a task. The assistance will therefore be accomplished passively by means of an abduction/adduction spring (see subsection 5.3.2).

As for the remaining three DOFs, the peak power is negligibly small, respectively 6 and 0.5 Watts. It is safe to assume that the wearer of the orthosis will be able to

generate and absorb the small amounts of energy associated with these DOFs on his own.

3.6. Concept generation

In this section we aim to come up with an actuation system for the sagittal plane DOFs. We will start by presenting a concept that provides a coupling between two joints - the ankle and the knee - to maximize energy transfer: the common spring MACCEPA. After a thorough discussion of this concept, we will figure out a way to achieve energy transfer between all three leg joints and optimize this design. Finally, we will discuss some possible adaptations to the design to accomodate different activities and different gait patterns.

3.6.1. Common spring MACCEPA

3.6.1.1. Basic concept

As mentioned earlier, our goal is to conceive a system that allows energy exchange between the ankle and the knee. A possible way of achieving this is to place one or more biarticular passive elastic elements, i.e. which span the ankle and knee joint. Since ankle and knee are coupled, energy can be transferred from one joint to the other. A drawback of this system is that it delivers a torque which is directly dependent of the joint angles. The residual torques at ankle and knee would still need to be delivered by an active element, e.g. by placing a motor at the ankle and knee joint. Another solution would be to decrease the residual torque by adding parameters to the system. One possibility is to actively adjust lever arm length such that the correct torque is applied. It is on this principle that our concept is based.

The mechanism is based on the MACCEPA actuator [49]. One is placed at the ankle and one at the knee. However one important adaptation has been made: both the ankle and knee MACCEPA lever arms are connected to the same spring. In this way the motor regulating the equilibrium position of the knee MACCEPA will act as the compliance motor of the ankle MACCEPA and vice versa. This mechanism is shown schematicly in Figure 3.1. Note that the motors at knee and ankle are not shown in the sketch.

It is clear that this way energy stored in the spring by the knee can be employed directly by the ankle.

Optimization

To examine whether or not this concept is promising, one has to optimize the design parameters and take a look at the final performance.

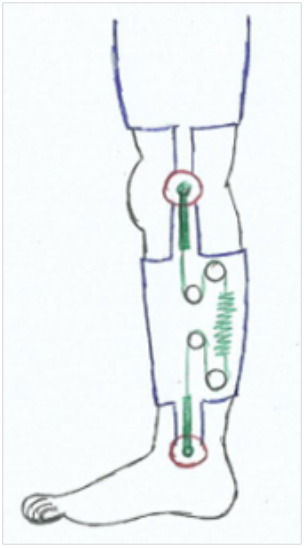

Figure 3.1.: Concept of common spring MACCEPA connecting ankle and knee

There are in total 160 parameters consisting of:

$\alpha_A(i)$	Angle of the lever arm at the ankle (at 50 discrete moments of time i at which the biological angles θ_A are known)
$\alpha_K(i)$	Angle of the lever arm at the knee (at 50 discrete moments of time i at which the biological angles θ_K are known)
k	Constant of the common spring
Δx_0	Initial extension determining pretensioning of the common spring
D_A	Length of the ankle lever arm
D_K	Length of the knee lever arm
L_{0A}	Distance between top of the ankle lever arm and the pulley
L_{0K}	Distance between top of the knee lever arm and the pulley

All parameters are defined in Figure 3.2.

The objective is a function of the parameters and needs to be minimized. It consists of several weighted components:

- ΔT, the difference between the required torque and the actual torque delivered by the orthosis
- P, the power consumption by the motor
- *acc,* the angular acceleration of the lever arm

The first component, ΔT, is the difference between the required torque and the torque generated by the common spring MACCEPA system. Obviously, we want this component to be as small as possible, which would imply that the system is

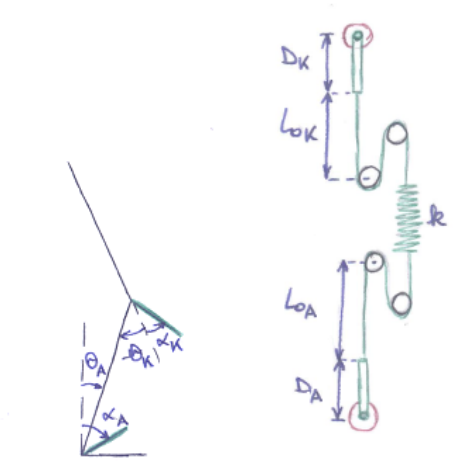

(a) Angle definition **(b)** Definition L_0 and D for both ankle and knee

Figure 3.2.: Parameter definitions for the common spring MACCEPA

capable of generating the correct amount of torque at both ankle and knee. Note that it does not need to be exactly equal to zero because of the nature of the problem. A difference in torque can still be compensated by the wearer. In fact, attempting to exactly reproduce torque data makes little sense, since these data exhibit significant inter-subject variability [57]. The benefit of allowing a small deviation in torque is that this may yield a more energy efficient optimisation result. Torques occuring at high lever arm velocities can be lower, and rapid changes in torque can be slowed down to decrease lever arm velocity. As a result, power will decrease.

The required torque is assumed to be 50% of the biological torque for reasons explained in section 3.2.

The second component, P, is the power necessary to generate the torque. It will thus determine the size of the motor needed to actuate the orthosis. In order to be energy efficient, it is important to keep this term as small as possible.

The third and last component, acc, contains the accelerations of the lever arms. It is included in the objective function in order to obtain a smoother trajectory of the lever arm. This is of course not a primary objective. The acceleration term therefore has a small weighting coefficient, which is of the order of 10^{-3} relative to the other coefficients.

Calculations of the components are clarified in section A.1. The Matlab program defining the objective can be found in section A.2. Note that the objective function is equal to the sum of squares of all three components.

Each parameter is subject to at least one constraint. Most constraints are obvious,

e.g. spring constants or lengths cannot become smaller than zero. An additional constraint on the dimensional parameters is that the system should be compact enough to attach it to the wearer's leg without surpassing the dimensions of the leg too much. Numerical values can be found in section A.2.

Results

The optimized parameter values are summarised in section A.3.

An important observation is that the optimization led to zero pretensioning of the common spring. It is tempting to conclude that pretensioning is thus not necessary. However, when the walking speed changes, torque and power requirements change as well. It is by adapting this parameter that an optimal functioning of the device is ensured at different walking speeds. The actual influence of pretensioning will be verified later on (section 3.7).

One can see in Figure 3.3a that the MACCEPA system generates the required amount of torque both at the ankle and the knee. Even though there are small deviations, this poses no problem for the operation of the orthosis.

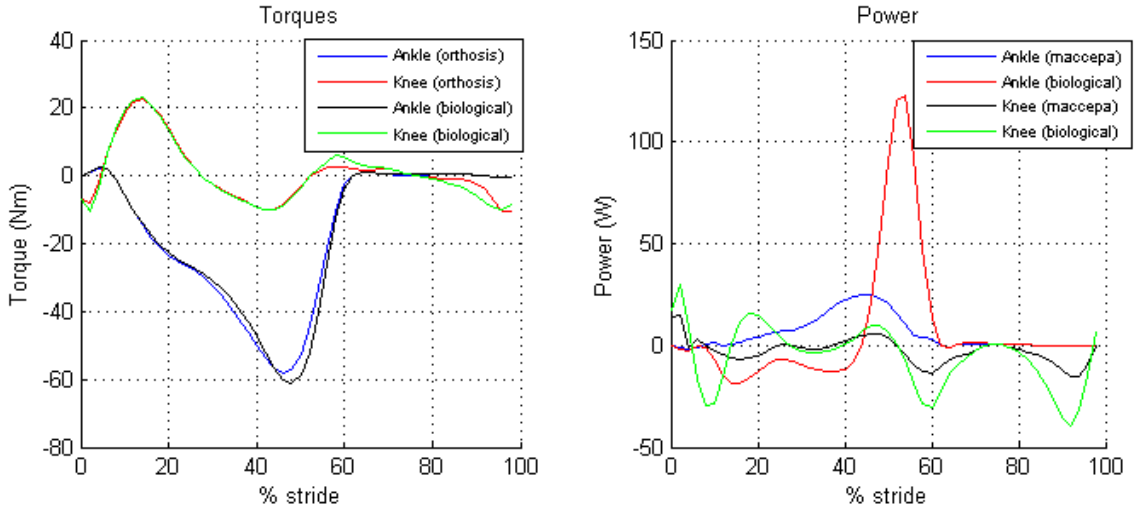

(a) Generated vs. required torques

(b) Biological vs. motor power

Figure 3.3.: Generated torques and required motor power for the ankle-knee common spring MACCEPA

As expected the peak power required to supply half of the biological torque is significantly smaller using the common spring MACCEPA than what it would be with a conventional motor (Figure 3.3b). The peak power is reduced from 120 W to 25 W for the ankle and from 40 W to 15 W for the knee. This is a reduction of respectively 79% and 62% which strengthens our faith in the concept.

It is also useful to take a look at the amount of energy transferred between the ankle and knee joint to ensure proper operation of the system. Table 3.4 gives an

overview of the energy generated/absorbed at each joint. We refer to section E.2 for the formulas. E_m is the MACCEPA motor energy, $E_{orthosis}$ is the energy generated/absorbed by the orthosis, and E_{biol} is the energy which is provided if the torque requirements are exactly met. Note that E_{biol} corresponds to half of the biological energy.

	E_m(J)	$E_{orthosis}$(J)	E_{biol} (J)
ankle	6.48	6.21	8.31
knee	-2.99	-2.68	-6.12

Table 3.4.: Energies from the ankle-knee MACCEPA optimization.

As noted before, the optimization does not impose the torque to be completely supplied by the orthosis, but small deviations from the required torque are allowed. This results in orthosis joint powers which are lower than the biological ones, and as such in lower energies.

From these results, one can conclude that approximately 0.3 J ($E_{orthosis} - E_m$, see section E.2) is transferred from the ankle to the knee. This is rather unexpected since the opposite, energy transfer from the knee to the ankle, is desired. The addition of parallel springs may however greatly influence this result.

3.6.1.2. Addition of parallel springs

In subsubsection 2.2.6.1, we studied the angle-torque characteristic of the knee (Figure 3.4). We noted that, during loading response and mid-stance (2-40% stride), the curve is approximately linear, which indicates spring behaviour. It is possible to dimension a spring (spring 1 in Figure 3.4) to cover this region of the graph. This would improve the energy efficiency of the orthosis, since part of the torque requirements are provided by passive elements instead of the common spring MACCEPA system. Note that during mid and terminal swing, the knee displays a linear torque behavior as well, which is covered by spring 2. The optimization will be expanded with two additional knee springs, of which the approximate position is sketched in Figure 3.4.

Note that spring 1, which was included to meet the torque requirements during loading response and mid-stance, should only be functional in these phases of the gait cycle. This creates the need for a locking mechanism engaging and disengaging the spring, thus complicating the design. To provide some relief, it is favorable to lock and unlock when the spring is at its equilibrium position, i.e. at zero torque.

The addition of spring 2 has another important advantage next to decreasing the energy consumption of the orthosis. It advances the beginning the K3 region of negative power (Figure 2.19). This can be understood as follows. The power P at the knee joint is the sum of the knee MACCEPA power and the power due to knee

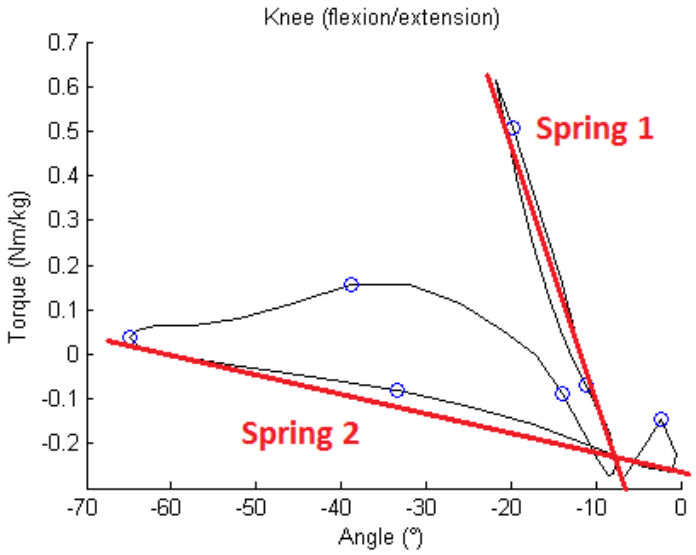

Figure 3.4.: Angle-torque characteristic of the knee

springs 1 and 2. Knee spring 2 delivers a power of $P_2 = T_2 \cdot \omega$, where T_2 is the torque due to spring 2 and ω is the angular acceleration of the joint. By increasing T_2, P_2 increases accordingly. As a result, the residual torque which is to be delivered by the ankle-knee MACCEPA is smaller, and so is its power. In a system without springs, the MACCEPA must deliver a negative torque at the end of terminal stance (between approximately -10 and -17 degrees). However, if spring 2 delivers a sufficiently large negative torque, the MACCEPA will need to deliver a positive torque. In other words, the torque changes sign and so does the power. The knee MACCEPA will absorb power rather than generating it. The result is that the onset of the A2 region of positive power at the ankle now corresponds approximately with the beginning of the extended K3 region. The common MACCEPA can therefore directly transfer the K3 energy generated at the knee to the ankle.

Recall that the ankle angle-torque graph (Figure 2.16) displays a linear part during loading response as well. In order to further improve energy efficiency, an additional spring at the ankle will also be included.

Optimization

The addition of three springs elevates the number of parameters from 106 to 112. The extra parameters are:

k_{A1}	Spring constant of the parallel ankle spring
θ_{0A1}	Neutral position of the ankle spring
k_{K1}	Spring constant of spring 1 at the knee
θ_{0K1}	Neutral position of spring 1 at the knee
k_{K2}	Spring constant of spring 2 at the knee

θ_{0K2} Neutral position of spring 2 at the knee

Spring torque is now proportional to the angle of the joint. The additional springs are therefore torsion springs rather than linear ones. They act in parallel to the MACCEPA, so that their torques add.

The contribution of these springs to the torque delivered by the orthosis should of course be taken into account in the optimization. All mathematical formulas and Matlab programs can be found in Appendix B as well as the numerical values of the constraints.

Results

The optimized parameters are summarised in section B.3.

Note that the spring constant of the ankle spring is set to zero, which indicates that it does not contribute towards minimizing the objective. The design will thus only be expanded with two knee springs. The two springs are indicated in Figure 3.5 by the red and the black curve. Note that spring 1 is shifted upward. The amount of torque to be delivered by spring 1 is elevated because it needs to compensate the negative torque supplied by spring 2 during loading response and mid stance.

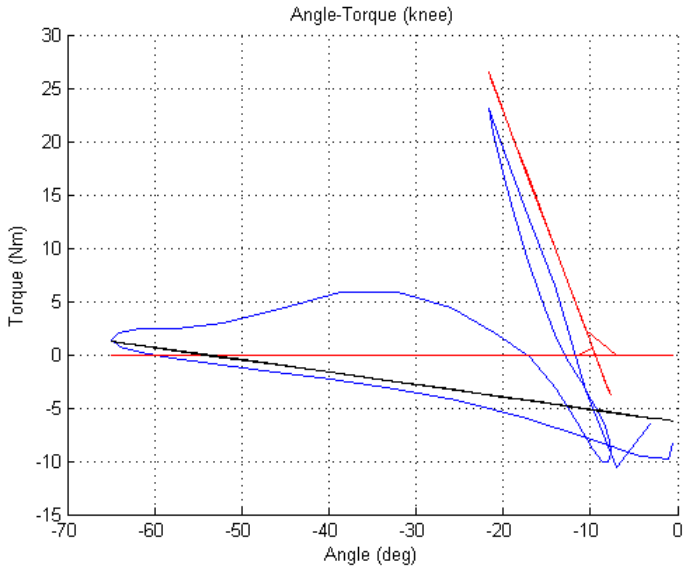

Figure 3.5.: Optimization of the additional knee springs

The torque graphs have not changed substantially (for completeness the graph is added to section B.3). The orthosis is still capable of generating the required amount of torque. The power graphs will be discussed in the next subsection.

Joint energies are shown in Table 3.5. As expected, the energy is now transferred from knee to ankle. The amount of energy transferred is 1.5J, which represents 35% of the energy absorbed by the orthosis knee joint.

	E_m(J)	$E_{orthosis}$(J)	E_{biol} (J)
ankle	5.51	7.06	8.31
knee	-2.80	-4.31	-6.12

Table 3.5.: Energies from the ankle-knee MACCEPA optimization with springs

We can conclude from this discussion that the common spring MACCEPA is a viable solution for the actuation of the knee and ankle joint if we include parallel springs in the design. The next step in the design process is to include the hip and further ameliorate the results.

3.6.1.3. Evaluation of the common MACCEPA concept

The common spring MACCEPA concept was introduced in section 3.6. It was tuned for optimal performance in the orthosis, a performance which was compared to that of a conventional motor. In this subsection, we will further evaluate the common MACCEPA by comparing it to a mechanism with two separate MACCEPAs. Furthermore, we will try to gain a deeper understanding of the system by studying the power flows.

Comparison with two separate MACCEPAs

In subsubsection 3.6.1.2, we optimized the common spring MACCEPA together with some parallel springs and found that 1.5J was transferred from the knee to the ankle. As we explained, the major difference between a common spring MACCEPA and two separate MACCEPAs is the fact that the spring is shared between both joints. Does this slight modification significantly ameliorate system performance? In order to answer this question, we once again ran the optimization described in subsubsection 3.6.1.2, now replacing the common spring MACCEPA with two separate MACCEPAs. No modifications were made in the cost function.

Looking at the optimized spring constants and equilibrium angles (Figure 3.6), we remark that knee spring 1, which was to be engaged during stance, has been eliminated by the optimization. The MACCEPA fully takes over the function of this spring, storing and releasing the energy involved in this phase. This can however also be accomplished with a common spring MACCEPA, as shown in subsection 3.6.1.

The resulting MACCEPA powers are plotted in Figure 3.7b. At first glance, the differences between the common spring MACCEPA (Figure 3.7a) and the separate MACCEPAs in terms of power are rather small. Both mechanisms are compared in Table 3.6 in terms of RMS value of the power and peak powers. From this table, one may conclude that two separate MACCEPAs are slightly better than the common spring MACCEPA. The required energies however give another view. Comparing these energies to Table 3.5 in Table 3.7, we find that the energy that is actually delivered/absorbed by the orthosis, $E_{orthosis}$, is lower for the separate MACCEPA

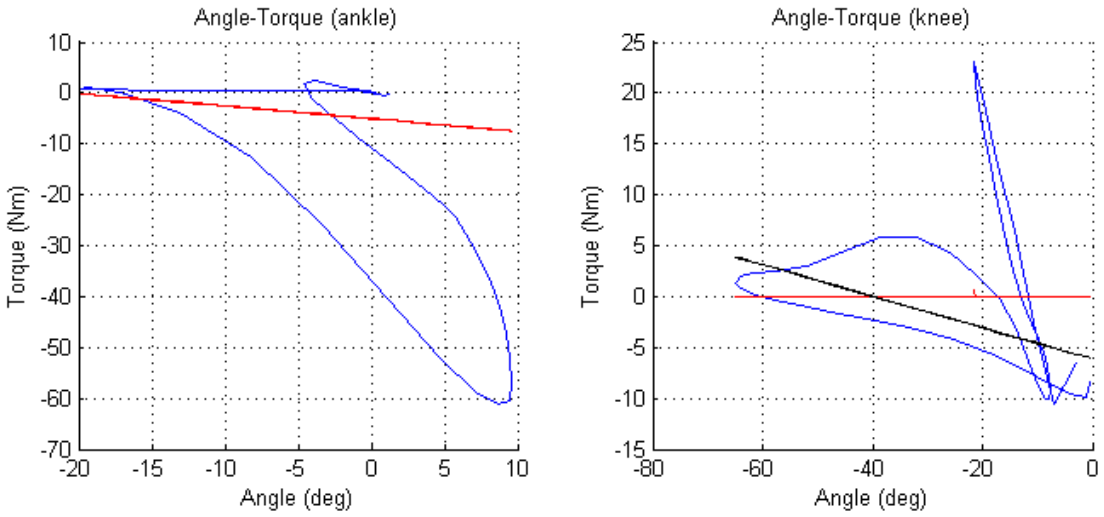

Figure 3.6.: Parallel springs for the separate MACCEPAs

mechanism compared to that of the common spring MACCEPA. This is especially the case at the knee, where 1.27J less is absorbed, which is no less than 21% of E_{biol}. Furthermore, the energy required by the motor, E_m, is far smaller for the common spring MACCEPA thanks to the transfer of energy. This seems contradictory to the similar RMS values of power, although it is not. The RMS value is dominated by the peak powers since it is the square root of a sum of squares, whereas powers are not squared for the calculation of E_m. Peak powers for the common MACCEPA are higher, explaining the elevated RMS value.

	ankle		knee	
	P_{RMS}(W)	P_{peak}(W)	P_{RMS}(W)	P_{peak}(W)
separate MACCEPAs	9.6	23.6	5.4	15.9
common spring MACCEPA	9.7	25.9	5.4	16.8

Table 3.6.: Comparison of separate MACCEPAs and common spring MACCEPA

	E_m(J)	$E_{orthosis}$(J)	E_{biol} (J)
ankle	6.24 (5.51)	6.30 (7.06)	8.31
knee	-3.04 (-2.80)	-3.04 (-4.31)	-6.12

Table 3.7.: Energies from the separate MACCEPAs optimization. Energies of the common spring MACCEPA are noted in brackets.

A closer look at Figure 3.7b immediately reveals the potential for energy exchange. During 10-23, 50-61, 72-86 and 98-4% stride, ankle and knee power have opposite sign, meaning that energy is absorbed at one joint while it is generated at the other. In other words, a potential for energy exchange exists during 44% of the gait cycle. Reviewing Figure 3.7a, we see that the common spring MACCEPA has effectively

exploited this potential. The only significant region of opposite powers that remains lies between 22 and 32% stride. We will further discuss this in the Power flows paragraph.

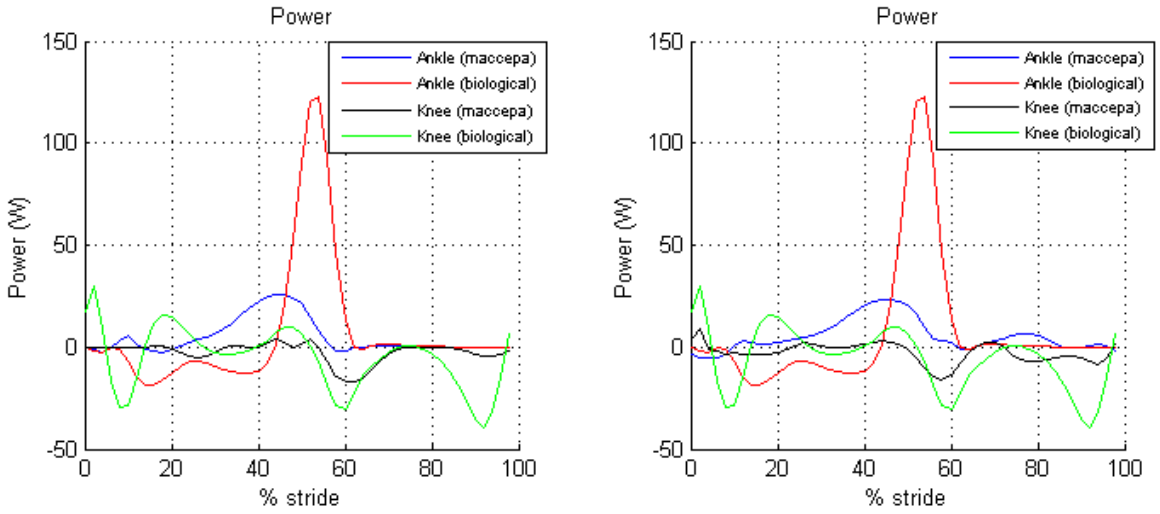

(a) Common spring MACCEPA **(b)** Two separate MACCEPAs

Figure 3.7.: Comparison of motor powers

In conclusion, the common spring MACCEPA with springs matches the energy requirements better and delivers the energy in a more effective way. Peak powers however are higher.

Power flows

The orthosis owes its energy efficiency to the six springs, which allow for energy storage, return and transfer. A study of power flows will help to understand how each spring contributes to the performance of the orthosis. All formulas and definitions can be found in section E.1. In this section, we will once again confine ourselves to the discussion of the common spring MACCEPA with parallel springs.

If the optimization is carried out well, the orthosis power P_{orth} should roughly be equal to the required power P_{biol}. Figure 3.8 shows the power flows for the common spring MACCEPA with parallel springs. The green curve ("parallel springs") is the P_{A1} curve in Figure 3.8a and the sum of P_{K1} and P_{K2} in Figure 3.8b, A1 denoting the parallel ankle spring and K1/K2 denoting parallel knee springs 1 and 2. The cyan curve ("Common spring") is a plot of the common MACCEPA spring power, P_{Sp}.

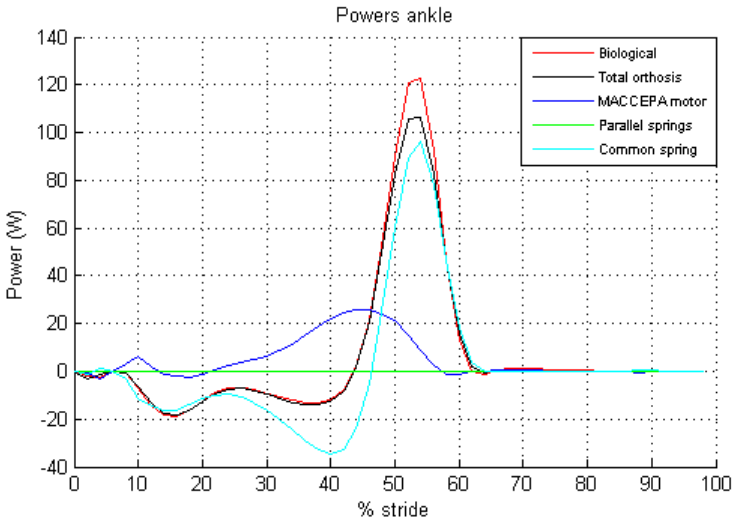

(a) Ankle

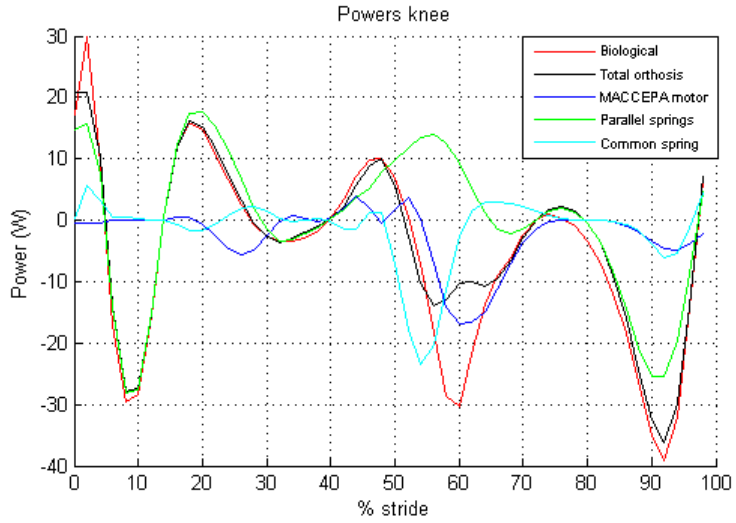

(b) Knee

Figure 3.8.: Power flows for the common spring MACCEPA.

Figure 3.8a clearly highlights the benefit of a MACCEPA system. Most of the power requirements are met by the common MACCEPA spring. It stores energy during stance (8-44% stride) which would normally be dissipated, and releases it during plantarflexion (46-62% stride). The lever arm motor only has to provide a small amount of power, drastically decreasing peak power in comparison to a conventional motor. From this plot we can deduce that during 22-46% stride, the motor is in fact tensioning the spring, storing energy that is released during plantarflexion.

In subsubsection 3.6.1.2, we discussed the importance of parallel springs for power transfer. Figure 3.8b gives a clear explanation. As we noted before, the purpose of knee spring 2 was to influence the beginning of the negative power region K3. It does so by delivering a burst of positive power between 40 and 65% stride, which has to be compensated by negative power from the common spring to obtain a total knee joint power that is more or less equal to the required knee power, in accordance with Equation E.6. Negative spring power means that energy is absorbed by the common spring. This energy is directly employed at the ankle, during the positive burst in common spring power (45-65% stride). The parallel springs also provide most of the power requirements during loading response/mid-stance (2-40% stride) and mid-swing/terminal swing (73-100% stride). The knee motor mainly dissipates the energy that cannot be stored in the spring.

One can clearly see that the integral of the power over one cycle is negative for the knee and positive for the ankle. Both integrals are equal and of opposite sign; they represent the energy transferred between joints.

In subsubsection 3.6.1.3, we already noted that during 22-32% stride ankle and knee motor powers are opposite, and proposed that the potential of energy exchange is not fully exploited in this region. Figure 3.8 shows why. At the ankle, positive motor power is used to extend the spring. At the knee, however, the spring shortens, giving off its energy to the knee motor (negative power). In other words, the ankle motor is putting energy in the system that is dissipated by the knee motor. This is of course undesirable. So why does the simulation not adjust the MACCEPA lever arm angles to eliminate this behaviour? Recall that acceleration was one of the parameters that was minimized (subsection 3.6.1). The optimal set of angles is therefore not necessarily the energetically most favourable, since this would most likely require unfeasibly large accelerations of the lever arm angle.

3.6.1.4. Conclusions

The common MACCEPA proposed in subsection 3.6.1 effectively transfers energy from the knee to the ankle. Well-dimensioned parallel springs influence the power to be delivered by the common MACCEPA system in such a way that a better match between power regions of opposite sign is obtained at the ankle and knee. This was shown to be beneficial to the energy transfer (subsubsection 3.6.1.2). Up to 35% of the absorbed knee energy was transferred to the ankle with this configuration.

The main advantage of the common MACCEPA system is its simplicity. It basically offers the same functionality as a mechanism with separate MACCEPAs at both joints and an additional spring for energy transfer, but it has two springs less. Energy transfer is inherent to the common MACCEPA, so that an additional spring connecting joints is no longer necessary. This makes it a more compact solution. An important disadvantage, however, is that the motor has to deliver torque every instant that the lever arm is not parallel to the leg (provided that the spring is

tensioned). In other words, even during passive motions, when the lever arm is kept at a constant position and the motor does not turn, a current will run through the motor windings to deliver a torque. An option is to use a non-backdrivable gear system, but these are generally less efficient than the backdrivable variants. The most energy-efficient solution would be to eliminate one of the motors. This is what we will look into in the next subsection.

3.6.2. Addition of hip and elimination of the knee motor

The previous concept is now expanded by adding the hip to the optimization. A common spring MACCEPA such as the one used at the ankle and knee is not the best option, since it would require a second motor at the knee. We therefore opt for a biarticular MACCEPA at the hip, with a spring that spans both hip and knee joint. This is in fact the same principle as the common MACCEPA concept illustrated in Figure 3.1, but with a fixed lever arm angle at the knee instead of one operated by a motor. Again, some of the energy absorbed at the knee can be transferred to the hip, as was the case with the common spring MACCEPA.

In this concept, only the ankle and hip motors would deliver a net positive energy to the joint. Since the knee now has two options to transfer its energy to, an attempt will be made to eliminate the knee motor. This will save weight and make the orthosis less bulky. The final concept is sketched in Figure 3.9.

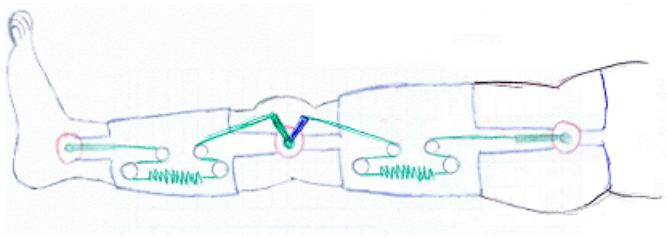

Figure 3.9.: Final orthosis concept

Optimization

In this design phase, the objective function was somewhat modified. Using the previous objective function, high torques may be demanded from the motors, leading to oversizing. This is resolved by adding the sum of the squared motor torques as a new term in the objective function.

Another important modification is the addition of an upper bound on the actual MACCEPA stiffness. Without this limitation, the optimization resulted in a MACCEPA behaviour which was too stiff, especially at the hip. In other words, a small disturbance in the angles α or θ would lead to a large difference in torque, resulting in a spike in power. Details can be found in subsection C.2.3.

The parameters which are to be optimized are listed in subsection C.2.1. As before they consist of lever arm angles, lever arm lengths, pulley distances and spring constants with their neutral positions.

Detailed formulas, a full description of the constraints and the complete Matlab program can be found in Appendix C.

Results

The optimized parameters are again summarised in section C.3.

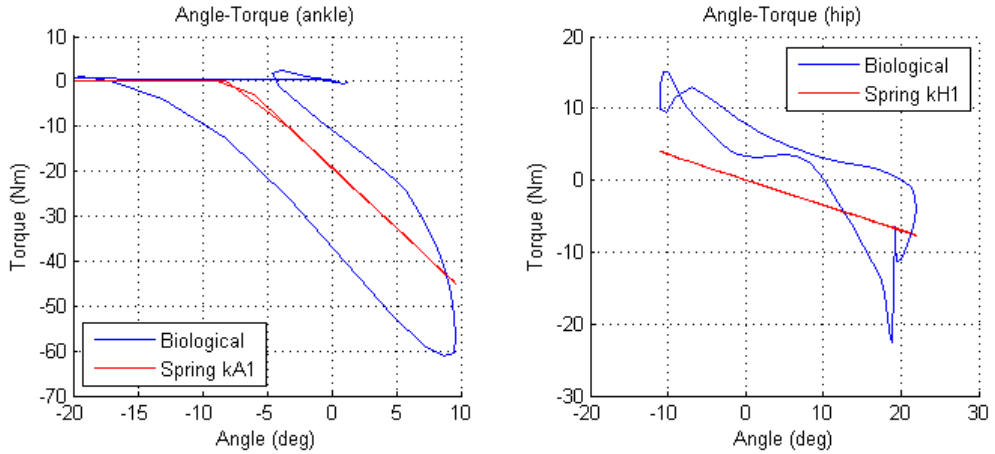

Figure 3.10.: Optimization of the parallel springs at the ankle and the hip.

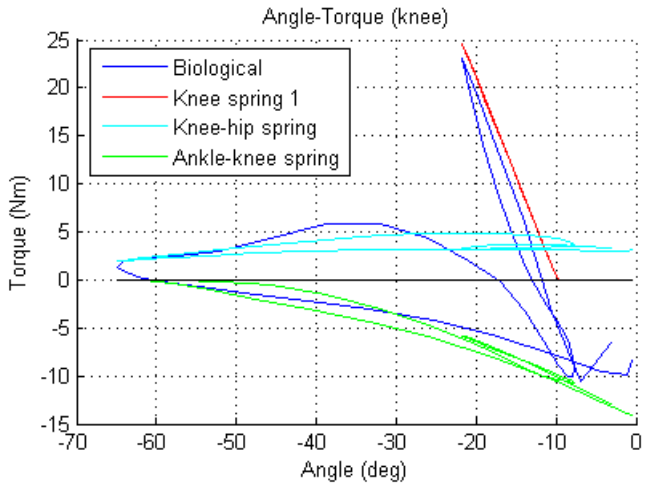

Figure 3.11.: Optimization of the parallel springs at the knee. The torques delivered by the ankle-knee (green) and knee-hip (cyan) spring are plotted as well.

Figure 3.10 and Figure 3.11 give a graphical representation of the optimized parallel springs. In Figure 3.11, the angle-torque characteristic of the knee-hip (cyan) and ankle-knee (green) spring are indicated as well. The area inside these loops represents the energy transferred by this spring from one joint to the other during one

entire cycle. The exact amount will be quantified further on. Figure 3.11 shows that the ankle-knee spring in fact plays the role of knee spring 2 in the previous section, delivering nearly all torque during mid and terminal swing. Knee spring 2 itself is no longer in use, its stiffness is set to zero by the optimization. The parallel ankle spring has a stiffness and equilibrium angle that fully corresponds to the expectations, in a way that it minimizes the torque to be delivered by the ankle MACCEPA motor. The parallel hip spring's equilibrium angle, on the other hand, is 10 to 15 degrees lower than one may expect. Because of this, the hip MACCEPA motor will need to deliver a positive torque throughout most of the gait cycle. Figure 3.11 reveals the benefit of this low equilibrium angle: the hip motor provides a positive torque at the knee, which is necessary to obtain a total torque which is close to the required torque. In an enhanced design, a constant torque spring may be considered to deliver this torque. This would lower the torque requirements of the hip MACCEPA and raise the equilibrium angle of the hip MACCEPA spring to the expected 10-15 degrees.

Orthosis and biological torques are plotted in Figure 3.12. It is clear that the orthosis is reasonably capable of delivering the desired torque.

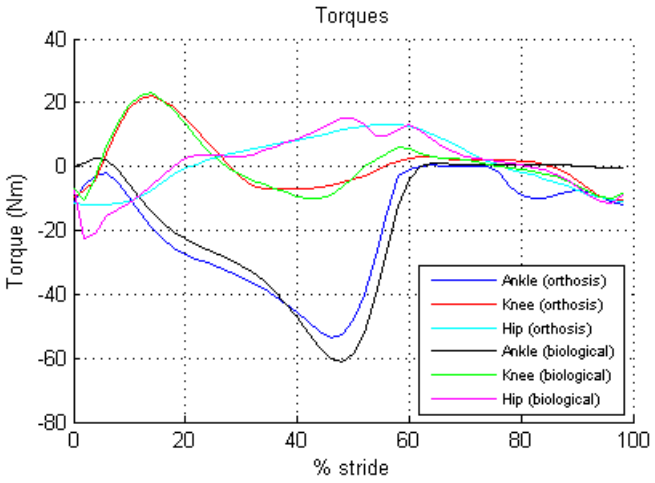

Figure 3.12.: Delivered torques during one gait cycle from the ankle-knee-hip optimization

Figure 3.13 shows the power supplied by the motor during one gait cycle. Peak powers are again lower than the ones that would be obtained with a conventional motor: 32W at the ankle instead of 120W and 13W at the hip instead of 25W. Compared to the common spring MACCEPA with springs, peak ankle power is 6W higher, which can of course be expected due to the elimination of the knee motor. Interesting are the two ankle motor power peaks which occur during swing, and which were not observed in the common spring MACCEPA. The 80% stride peak

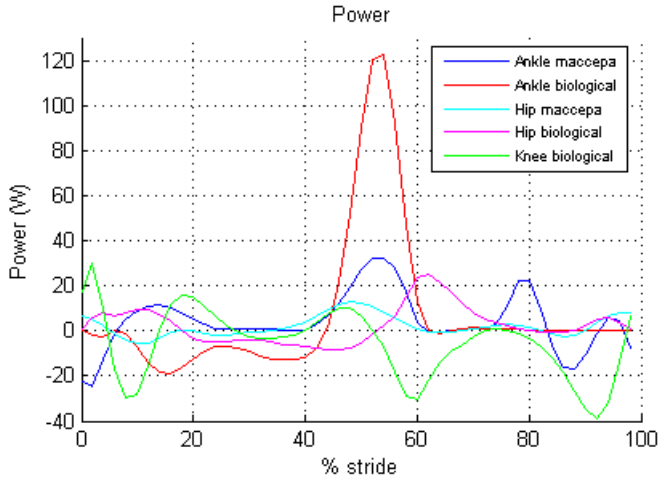

Figure 3.13.: Biological and motor power from the ankle-knee-hip optimization

in ankle motor power is due to the loading of the parallel spring, which starts at 72% stride. This is also the cause for the peak at 2% stride. The common spring MACCEPA did not have this parallel spring, explaining the absence of this bump. The 86% stride peak is due to power absorption at the knee, which has to be taken care of by the MACCEPA motor.

	E_m(J)	$E_{orthosis}$(J)	E_{biol} (J)
ankle	4.79	5.88	8.31
knee	0	-2.28	-6.12
hip	2.38	3.58	2.94

Table 3.8.: Energies from the ankle-knee-hip optimization

Converting these power graphs to energies (Table 3.8) leads to the conclusion that 2.3J is extracted from the knee, of which 1.1J is transferred to the ankle and 1.2J to the hip. Interestingly, the orthosis hip provides 122% of the required hip energy E_{biol}, which corresponds to 61% of the biological hip energy. The orthosis knee, on the other hand, only absorbs 2.28J out of the desired 6.12J. This however is not a big issue, since absorbing energy is metabolically less costly than generating it [17].

3.6.3. Prosthesis side hip

The hip on the prosthesis side is actuated by means of a MACCEPA and a parallel spring.

Optimization

Following parameters are optimized:

$\alpha_{Hp}(i)$	Angle of the lever arm (at 50 discrete moments of time i at which the biological angles θ_H are known)
k_{Hp}	Spring constant of the common spring
Δx_{0Hp}	Initial extension determining pretensioning of the common spring
D_{Hp}	Length of the lever arm
L_{0Hp}	Distance between top of the lever arm and the pulley
k_{H1p}	Spring constant of the parallel spring
θ_{0H1p}	Neutral position of the parallel spring

The results of the optimization can be found in Table D.2.

A graphical representation of the optimized hip spring (red line) is given in Figure 3.14. A torque comparison can be found in Figure 3.15. Except for the peak at 2% stride, the orthosis is reasonably capable of delivering the required torque. Figure 3.16 reveals that peak power is only 10W (compared to 25W for a conventional motor).

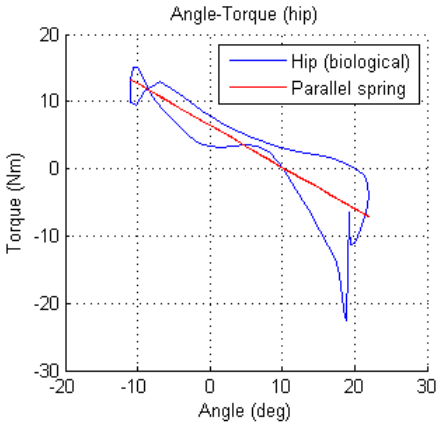

Figure 3.14.: Optimization of the prosthesis side hip parallel spring

The energy supplied by the orthosis at this joint, $E_{orthosis}$, is 2.36J per gait cycle. This is 80% of the required orthosis energy (E_{biol} = 2.94J). Because no energy exchange takes place at this joint, 2.36J is also the amount of energy delivered by the MACCEPA motor (E_m).

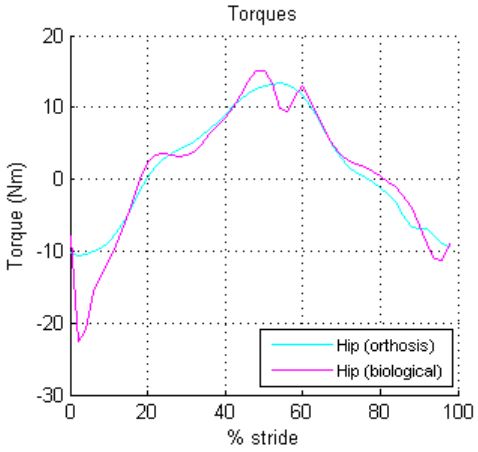

Figure 3.15.: Delivered torques during one gait cycle from the prosthesis side hip optimization

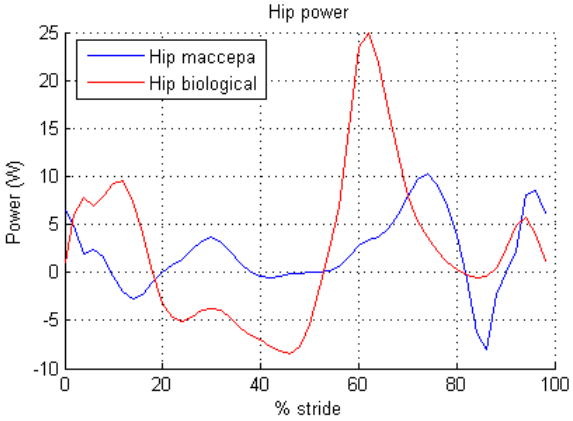

Figure 3.16.: Biological and motor power from the prosthesis side hip optimization

3.7. Possible adaptations to the design

3.7.1. Addition of a knee motor

In the current design, the knee torque depends entirely on the ankle and hip MACCEPA. The position of the lever arms is chosen so that the knee torque delivered by the ankle and hip MACCEPA is optimal for walking. For other activities, however, a knee motor will be needed to deliver the correct amount of torque. It will especially be useful when power generation is demanded from the knee. This is for instance the case during stair climbing, where the knee in fact exhibits the largest burst of generated power [34].

A Matlab optimization was carried out to have an idea of the size of the additional knee motor, if it were used to deliver the residual torque at the knee for level walking. Actuation was performed by a MACCEPA system such as the one at the prosthesis

side hip. The optimization revealed that a 7W motor would already be sufficient[1].

Adding a motor, however, also has the disadvantage of making the orthosis heavier and bulkier. Not only the motor and its transmission and control unit increase the mass, but also secondary effects such as the need for increased battery capacity and strength requirements add weight and volume. As we discussed in subsection 2.3.3, adding mass to the leg increases metabolic energy consumption, whereas humans can absorb energy at relatively low metabolical cost [17]. The extra motor was therefore not deemed worthwile for this orthosis, which is optimized for level walking. When the orthosis is further developed for other activities such as stair climbing, the additional knee motor can be sized based on the requirements for those activities, which are likely to be more demanding.

3.7.2. Stiffening the MACCEPA

Gait patterns differ among different persons. One of the main reasons is a difference in preferred walking speed. Different walking speeds result in different joint kinematics and kinetics. Joint angles do not vary much with walking speed, but joint torques are, in general, clearly higher (Figure 3.17). In other words, joint behaviour is stiffer at higher walking speeds. To adapt the orthosis to different walking speeds, stiffening the MACCEPA is a simple solution that does not require any changes in the control algorithms. It can be done in three ways: by replacing the spring with one that has a higher spring constant, by pretensioning the spring or by changing the lever arm length D. Replacing the spring is a rather impractical solution, we will therefore only look into the other two possibilities.

One can immediately foresee that changing the MACCEPA stiffness alone will not be sufficient. The knee extensor torque at 14% GC is almost completely delivered by stance spring 1. To accomodate the large (about 85%) increase in extensor torque for fast cadence, the only option is to change the spring stiffness of these parallel springs.

[1]For more details on how motors and transmissions are selected, we refer to subsection 5.1.2. We will not describe the complete procedure for selecting this motor, because it is not part of the final design.

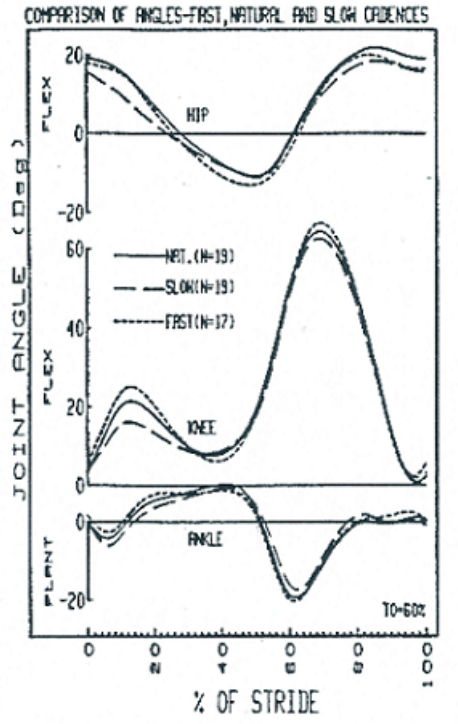

(a) Joint angles

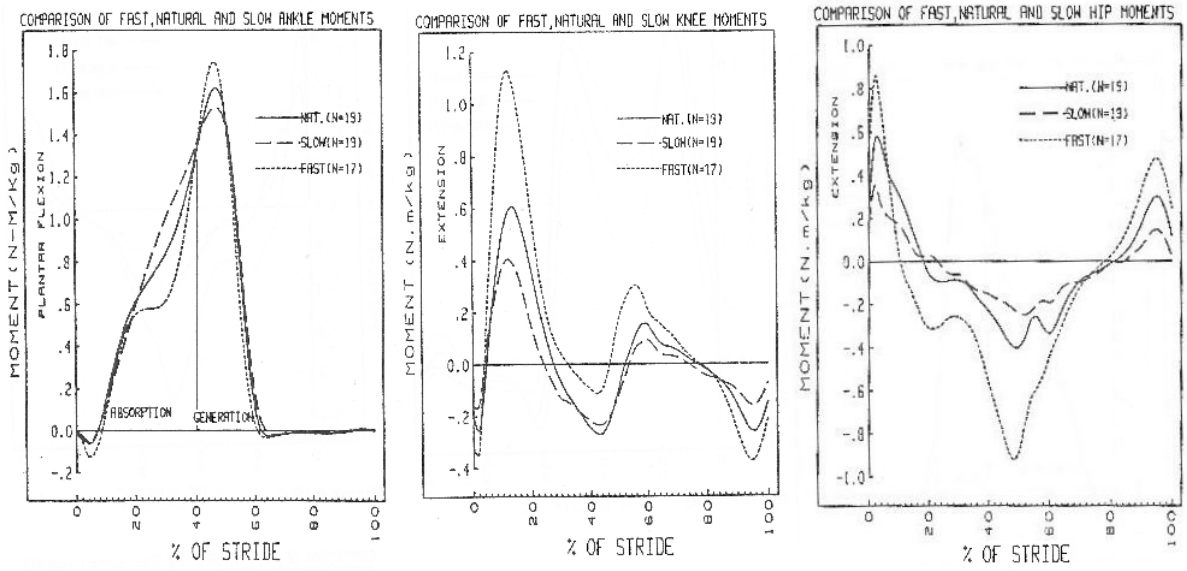

(b) Joint torques

Figure 3.17.: Joint kinematics and kinetics for different cadences [57]

The results in case of increased pretension are shown in Figure 3.18. Pretension

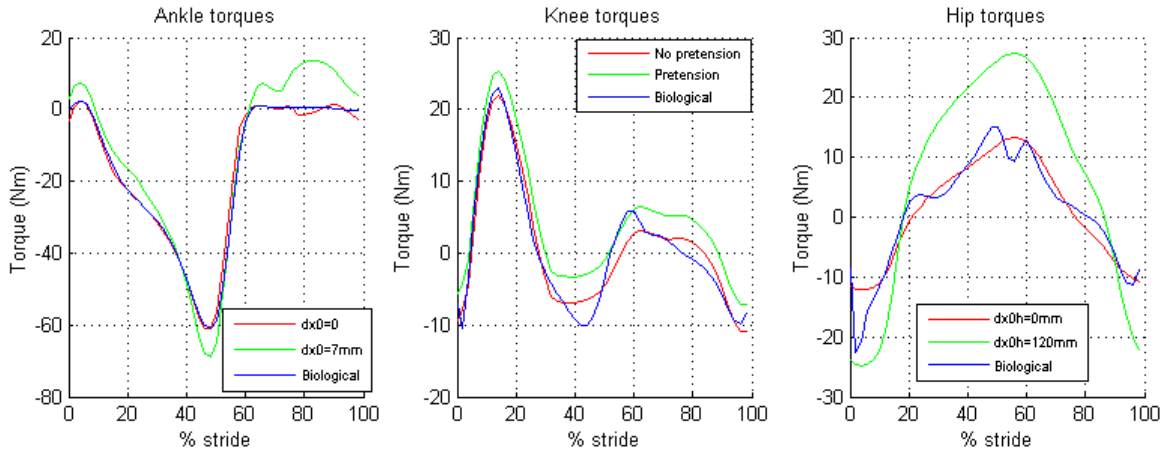

Figure 3.18.: Increased pretension results

was chosen so that the maximum torque more or less meets the fast cadence torque requirements, although kinematics were kept unchanged. Increasing hip pretension clearly works out quite well, with no significant problems. At the ankle, everything goes well during stance, but during swing results are nothing short but dramatic. Due to the presence of the parallel spring, a counteracting torque needs to be generated by the ankle MACCEPA during swing, which is amplified by pretensioning. The resulting torque of maximum 14Nm is unacceptable compared to the low required torque (which is almost zero), especially considering the low moment of inertia of the ankle. Adapting the parallel spring stiffness is an option, although it may be better to not pretension the MACCEPA spring at all because of the small difference in ankle torque for fast cadence compared to normal cadence. Following the latter strategy results in the knee torques shown in Figure 3.19.

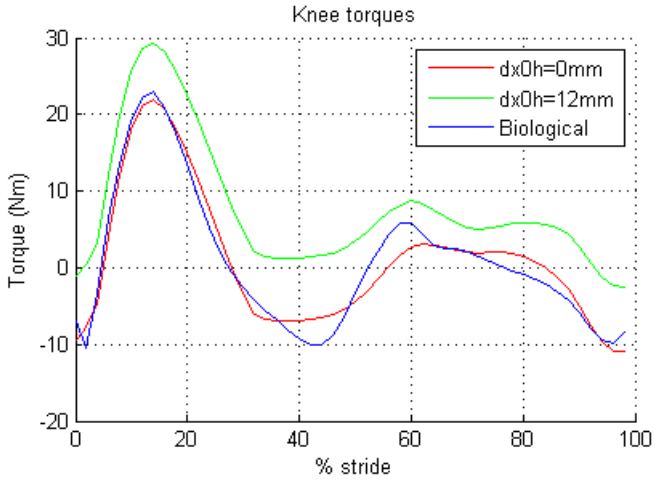

Figure 3.19.: Behavior of the knee in case of pretensioning only the knee-hip MACCEPA spring

We can clearly see that the knee torque is shifted higher by pretensioning the knee-hip MACCEPA spring. This behavior is also seen in Figure 3.17, except during late swing, where the biological torque decreases for fast cadence. Nevertheless, it shows that the biarticular hip MACCEPA actually mimicks the behaviour of the human biarticular muscles quite well. In conclusion, pretensioning only the knee-hip spring is a decent way of coping with faster cadences.

The results obtained by changing the lever arm lengths (D_A=150mm, D_{Kh}=60mm, D_H=95mm) are similar to those presented in Figure 3.18 and will therefore not be repeated. The issues are the same.

3.7.3. Conclusions

The orthosis was optimized for its energy-efficiency during walking at a normal pace, but this comes at the cost of adaptivity. Simple actions such as changing pretension and lever arm length of the MACCEPAs do not suffice for adapting the orthosis to the wearer's walking velocity. Replacing springs and/or adapting the control algorithm may be necessary to achieve the desired performance. Leaving out the knee motor saves weight, making it an excellent option for level walking, but performing other actions without an additional actuator at the knee will be more difficult. It is clear that the use of parallel springs (especially the one at the ankle) and the use of a knee motor will need to be reconsidered when designing a more multi-functional orthosis.

3.8. Final conclusions

An orthosis with six degrees of freedom is proposed for maximum comfort and maneuverability. The three sagittal plane DOFs will be actuated by means of two biarticular MACCEPA systems. This way only two motors are required: one at the ankle and one at the hip. Parallel springs are used at each joint to further enhance energy efficiency by storing and releasing passive elastic energy. The hip abduction/adduction joint will be equipped with a spring to provide the necessary abduction torque. The remaining two DOFs will be left free. The actuated joints will provide almost 50% of the biological torque.

The orthosis is optimized for level walking at a normal speed, based on Winter's data [57]. The motors, transmissions and springs will be chosen based on these optimization results. A design review is advised at different gait speeds or when other daily-life activities are to be performed.

4. Control aspects

4.1. Introduction

The control system must basically do three things:

- It must control the motors so that the lever arms are set in the desired positions
- It must be able to detect the beginning and end of a gait cycle
- It must lift the pawl for the knee locking mechanism at the correct moment

In this chapter, we will discuss possible control strategies for the orthosis.

4.2. Motor control

The purpose of the MACCEPAs is to deliver an assistive torque to the orthosis wearer. The goal is to deliver the correct amount of torque, despite possible deviations in the angular kinematics of the human leg during walking. The most challenging part, however, is to make sure that the orthosis does not force the wearer's legs to move when this is not desired, e.g. when he/she is stumbling or when he/she simply stops walking.

A possibility is to control the torque applied by the motor. This way, the deviations in angular kinematics do not influence the delivered torque, and the torque delivered by the orthosis is predictable and repeatable. Torque control can easily be implemented by controlling the motor current, which is proportional to the motor torque. However, the ratio between motor current and lever arm torque is influenced by the speed- and time-dependent motor efficiency and transmission efficiency. This makes it more difficult to impose the set values that will lead to the exact desired torque.

A simpler approach is to control the position of the lever arm. The torque will now be dependent of the kinematics of the leg. This is not necessarily a disadvantage, because it gives the wearer some room to adapt his gait to get optimal assistance from the orthosis. Since motor torque (and thus current) is a measure of the difference between the lever arm angle and the biological angle, it can be used to track whether or not the wearer has different intentions than walking. If the motor torque surpasses a certain limit, the control unit can decide to stop assistance so that the wearer can move unimpededly. This limit must be sufficiently strict to stop assistance in time,

but it must also be sufficiently permissive to ensure that the orthosis does not suddenly stop its assistance during normal walking. It can be specified in function of % stride to obtain optimal results. Note that this method can be used to detect if the wearer has stopped walking.

4.3. Detection of gait cycle

At some point, a signal is needed to tell the orthosis to start assisting the wearer's walking. This signal can be provided by the user, e.g. by pressing a button, but it would be nice if the orthosis could detect the user's intention to start walking. The priority is to have a detection method that does not switch on the orthosis unexpectedly. Skipping one or two gait cycles is considered less crucial.

Using angular kinematics and/or kinetics is one possibility. However, due to the variability in gait data and the difficulty in distinguishing walking from other leg movements, we feel that this strategy is too unreliable. We suggest a method that requires placing two sensors on the foot: one on the forefoot and one on the heel. The sequence presented in Table 4.1 will detect the intention of the wearer to start walking.

	Heel sensor	Forefoot sensor
Foot is lifted from ground	0	0
Heel contact	1	0
Forefoot contact	X	1
Heel leaves ground	0	1
Forefoot leaves ground (TO)	0	0
Heel contact	1	0

Table 4.1.: Walking onset detection sequence. Sensor output is 1 if the sensor detects contact, X if sensor output does not matter

For this sequence to be completed, it is important that the wearer touches the ground heel-first and that the heel is lifted before the foot leaves the ground. This is necessary to differentiate between simply putting the foot on the ground and starting to walk. The orthosis immediately starts working after the sequence is completed, i.e. at heel contact (0% stride). The wearer will thus need to complete one entire gait cycle without assistance. A time limit of two seconds is set between the first and second heel contact to prevent the system from being activated unwantedly. We feel that this strategy will effectively and robustly detect the user's intention to start walking.

The sensors are checked continuously for this sequence, also during walking. A disturbance in the sequence can be interpreted to signal the wearer's intent to stop walking. The motors will consequently be switched off by the control algorithm.

To detect contact, a hinging plate operating a contact switch can be used. Earlier work has shown that this is a better solution than force sensing resistors, because the latter are sensible to wear and show hysteresis, resulting in unreliable readings [11]. The hinging plate is used for several reasons. If the sensor were placed directly under the the foot, the full body weight would push on it. If a hinging plate is used, the switch can be placed next to the foot instead of under it, with the hinging plate operating the switch. In this case, the sensor must not cope with the body weight, and it must not endure the friction resulting from direct contact with the ground.

4.4. Locking mechanism

In subsection 5.4.1, we already proposed using the hip kinematics to determine the period during which the pawl is lifted. Unless this is realised mechanically, e.g. by means of a wire connecting the hip to the pawl, an angle transducer will be needed to track the hip angle. The control algorithm will power the locking mechanism solenoid, lifting the pawl and thus releasing the ratchet.

An option is to use a commercially available absolute rotary encoder. A digital encoder will produce a unique binary code for each distinct hip angle. This solution actually offers more than we need: we do not need to know the precise angle, we just want to detect whether we are in the range of 5° hip extension or more. A custom-made optical encoder that only has two states - above or below 5° extension - can easily be built: an optical disc with well-defined opaque and transparant areas, with a light source at one side and a photodetector at the other Figure 4.1. This solution is clearly simpler than the absolute encoder. It only has one track and two possible outputs, while an absolute encoder needs 8 tracks to reach a resolution of $\frac{360°}{2^8}$=1.4°, having 2^8 possible outputs. The absolute encoder does have the advantage that the hip angle at which the pawl is released can be altered by simply adjusting the control algorithm. This is certainly a bonus when adaptivity of the concept is considered.

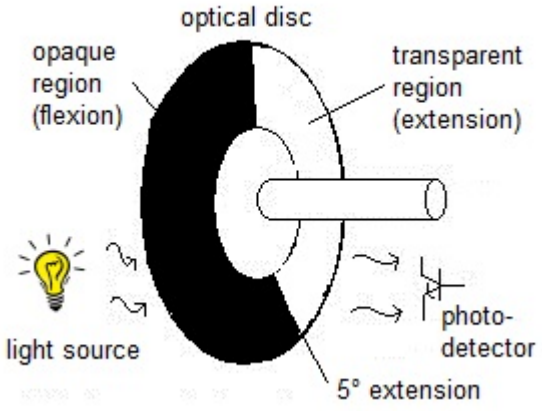

Figure 4.1.: Principle of the custom-made encoder

5. Mechanical implementation

5.1. Component selection

In this section, we will discuss the springs, drive systems and power supply used in the orthosis. We will briefly explore the different options and explain why a particular option was chosen.

5.1.1. Springs

No less than seven springs are used in the orthosis, some of which were modeled as extension springs, others as torsion springs. For the actual design however, a choice can be made between several types of springs. Discussing all of them - if that were possible - would lead us too far, so we will confine ourselves to the spring types that were actually considered.

Compression and extension springs are the most common spring types. The first offer resistance to a compressive force while the latter offer resistance to extension. A variant of the compression spring is the *die spring*, which can have higher spring constants for the same deflection. They are also more suited for dynamic loads than common compression springs. Several other types of springs are designed to resist compression. *Belleville springs* are interesting due to their compactness and their ability to handle large loads over a short range of motion. By stacking them, one can obtain a large variety of spring constants. However, frictional losses occur when stacking Belleville springs in a parallel configuration. Since the orthosis' (MACCEPA) springs undergo quite large deflections, a series configuration with a large number of springs would be necessary, cancelling out their benefit of compactness. *Torsion springs* are another major category. Torsion springs provide a torque when twisted. Helical torsion springs are perhaps the most recognisable type, but other types exist such as the *spiral torsion spring*.

The springs in the orthosis serve two purposes: they work as a parallel spring to provide torque to the joint, or they act as a MACCEPA spring. In this subsection, we will discuss the selected springs and their design.

5.1.1.1. Parallel springs

Torsion springs are chosen as parallel springs. They can easily be placed between two links to provide a torque proportional to the angle in between. Most manufacturers offer custom-made torsion springs, so we will simply calculate the torsion springs ourselves rather than picking them from a catalog.

The goal is to achieve a torsion spring constant k which matches the optimization torsion spring constant k_o. The torsion spring constant k (in Nmm/rad) is calculated as

$$k = \frac{d^4 \cdot E \cdot \pi}{64 \cdot D_m \cdot n_w} \tag{5.1}$$

in which (Figure 5.1):

d	Wire diameter (in mm)
E	Young's modulus of the spring material (in N/mm^2), 190 000 N/mm^2 for stainless steel
D_m	Mean coil diameter (in mm)
n_w	Number of active coils

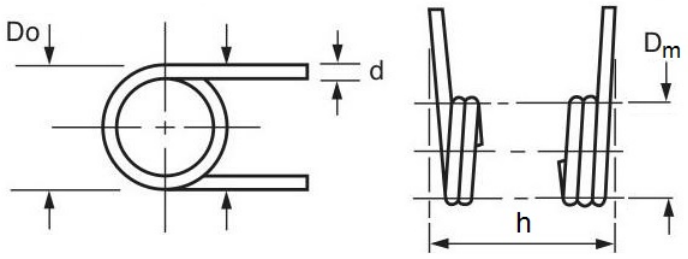

Figure 5.1.: Torsion spring parameter definition (adapted from [2])

A good design is a compact one, i.e. the torsion spring height $h = n_w \cdot d$ and the outer diameter $D_o = D_m + d$ should be small. Furthermore, the spring must be able to withstand the extension it is subjected to. The strength is checked according to EN-10270-1-NS. Following formula is used to determine the permissible bending stress σ_{max} (in N/mm^2):

$$\sigma_{max} = 0.7 \cdot 0.85 \cdot (2220 - 820 \cdot \log d) \tag{5.2}$$

This formula applies to stainless steel torsion springs. The actual bending stress σ_b (in N/mm^2), which must be lower than σ_{max}, is found with

$$\sigma_b = \frac{32 \cdot M}{\pi \cdot d^3} \tag{5.3}$$

where M is the moment acting on the spring (in Nmm).

Four torsion springs are used in the orthosis design: parallel springs k_{A1} at the ankle, k_{H1} at the hip (both prosthesis and orthosis side) and k_{K1} at the knee. Table 5.1 gives an overview of the torsion springs which are used in the orthosis, along with their critical design parameters. All torsion springs are made of stainless steel.

	k_{A1}	k_{K1}	k_{H1O}	k_{H1P}
Wire diameter d (mm)	9.0	7.2	5.0	6.0
Outer diameter D_o(mm)	59.5	34.2	51.0	61.0
Number of active coils n_w	2.5	2.5	2	2
Height of spring h (mm)	22.5	18.0	10.0	12.0
Spring constant k (Nm/rad)	154.3	118.2	20.2	35.5
Optimization spring constant k_o (Nm/rad)	154.4	117.9	20.1	35.6

Table 5.1.: Torsion spring design: overview

5.1.1.2. MACCEPA spring

Three MACCEPAs are used in the orthosis, so three springs need to be selected: k_A between ankle and knee, k_{HO} between knee and hip and k_{HP} at the prosthesis side hip. We opted for extension springs. This is the natural spring choice, since the MACCEPA lever arm pulls the wire which it is connected to. However, compression or die springs may be used if the extension is converted into a compressive force. An example is the common *drawbar spring*. Extension springs have the advantage of being easy to install: their ends can simply be attached to the wire, without the need for a spring container or mandrel. Additionally they do not have the possibility of buckling, which is an issue with compression or die springs.

The selected spring must match the optimization spring constant k_o as closely as possible, while being able to achieve the maximum extension required by the simulation. Many spring manufacturers have suitable springs in their catalog; we therefore chose to select springs from the Associated Spring catalog [2]. Table 5.2 shows the main parameters of the selected springs. The definition of these parameters is clarified in Figure 5.2.

5.1.2. Motor and transmission

5.1.2.1. Motor selection

The energy consumption of the motor is desired to be as low as possible, meaning that its maximum efficiency must be high and that it operates close to its nominal point of operation (i.e. at its maximum effiency). Furthermore, we want the motor to be compact and light-weight. Last but not least, a suitable motor must comply to following requirements:

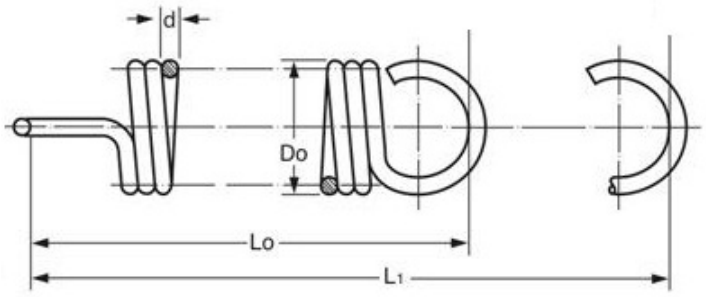

Figure 5.2.: Extension spring parameter definition (adapted from [2])

	k_A	k_{HO}	k_{HP}
Part number	T32920	E10001256500S	E10001256000X
Wire diameter d (mm)	3.60	3.18	2.16
Outer diameter D_o(mm)	18.0	25.4	19.05
Free length L_0 (mm)	111	165.10	88.9
Maximum extension $L_1 - L_0$ (mm)	24.4	113.79	70.36
Optimization maximum extension (mm)	20.8	85.01	30.00
Spring constant k (N/mm)	22.9	2.02	1.47
Optimization spring constant k_o (N/mm)	23.1	2.02	1.47

Table 5.2.: MACCEPA spring selection: overview

- Motor maximum speed must not exceed the maximum permissible speed specified by the constructor
- Motor RMS torque must not exceed the maximum continuous torque specified by the constructor
- Motor peak torque must not exceed the maximum torque for short term operation, as defined by the constructor.

These requirements can be met if the transmission and the motor are well chosen. Both transmission ratio and transmission efficiency affect the torque which is to be delivered by the motor. Motor and transmission selection must therefore be carried out simultaneously.

5.1.2.2. Transmission selection

In order to have an energy comsumption which is as low as possible, an efficient transmission is necessary. Also, the orthosis may not become too bulky and heavy, meaning that transmission size and weight must be as low as possible. Furthermore, a noisy transmission will not be tolerated by the user and therefore has to be avoided.

Several types of gears are available on the market. Gears that transform rotational into linear motion, such as a rack and pinion gear or a ballscrew, are of no use for our

design and are therefore not considered. Based on the arrangement of the input and output shafts, we can distinguish two major types of gears: parallel and nonparallel axes gears. The latter are particularly useful to achieve a compact design.

Parallel axes gears

Spur gears The most commonly used gear. Can only be used in a parallel shaft arrangement. High efficiencies (up to 98%) can be attained at low gear ratios. Does not produce axial thrust forces.

Helical gears Similar to a spur gear, but with helical instead of straight teeth. Run smoother and quieter than spur gears, can withstand higher loads and can achieve higher efficiencies. However, these gears produce an axial thrust force.

Nonparallel axes gears

Bevel gears Used in a perpendicular shaft arrangement. Similarly to spur gears and helical gears, straight and spiral bevel gears exist. Spiral bevel gears have less noise, less vibrations and a higher efficiency than straight bevel gears because they engage more gradually, but produce an axial thrust force.

Hypoid gears Are similar to spiral bevel gears, but the shaft axes do not intersect. Can achieve very high ratios (up to 200) with good efficiency. Have a higher tooth contact area compared to spiral bevel gears, resulting in a higher torque throughput capacity, higher durability and smoother/quieter operation.

Worm gears Large reduction ratios can be obtained, but efficiencies are low. Have self-locking ability at high ratios.

Compact gear systems

Harmonic drive Have no backlash, are compact and light-weight and can achieve high ratios.

Cycloidal drive Compact and capable of high ratios. Not backdrivable. Uses an eccentrically mounted disk, which causes vibrations.

Planetary gears Large reductions possible. Compact.

It is interesting to place the motor parallel to the foot or leg rather than along the joint axis. The motor axis will thus be perpendicular to the joint axis, meaning that a nonparallel axes gear will be needed. We prefer a hypoid gear (if high reductions are necessary) or a spiral bevel gear, because of their good efficiency. The gear is chosen from the KHK catalog [3]. An allowable torque, which is obtained experimentally with the pinion at 600 rpm, is given as a reference. In the final design subsubsection 5.1.2.3, the maximum pinion speed is below this reference speed for

most joints. In this case, we can therefore safely assume that the gear is sufficiently strong if the allowable torque is not exceeded. The only joint that has a higher pinion speed (677 rpm) is the prosthesis side hip. The torque however is about half the allowable torque, so the gear can be expected to withstand this load without any problem. High ratio hypoid gears will not be selected, because the diameter and the weight of the gear wheel is unreasonably high.

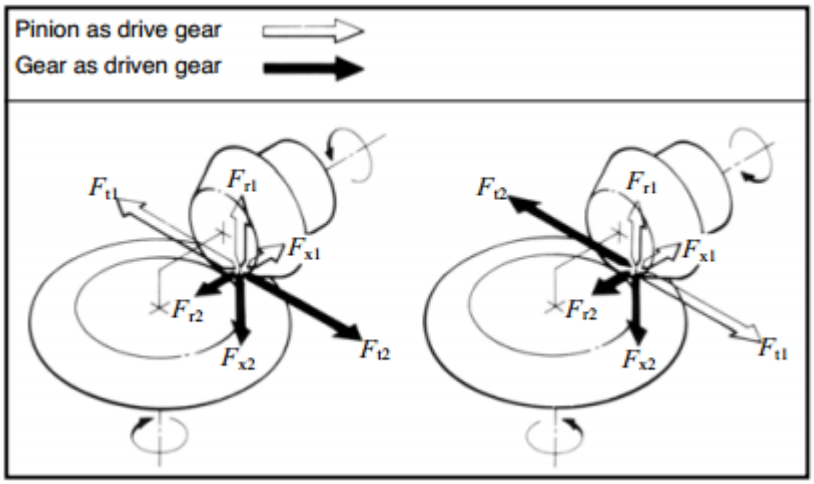

Figure 5.3.: Gear forces. F_{r1}, F_{t1} and F_{x1} are the radial, tangential and thrust forces acting on the pinion, F_{r2}, F_{t2} and F_{x2} are the radial, tangential and thrust forces acting on the wheel.

The load on the gear teeth can be decomposed in a tangential, radial and thrust force (Figure 5.3). These forces are particularly important for the calculation of the motor bearings. For the pinion, the forces can be calculated by

$$F_{radial} = \frac{W_{KP} \cdot T_W}{i} \tag{5.4}$$

$$F_{thrust} = \frac{W_{NP} \cdot T_W}{i} \tag{5.5}$$

$$F_{tangential} = \frac{T_W}{i \cdot r_P} \tag{5.6}$$

where W_{KP} is the radial load coefficient of the pinion, W_{NP} is the thrust load coefficient of the pinion, T_W is torque at the gear wheel, i is the transmission ratio and r_P is pinion wheel radius. Load coefficients are specified by the manufacturer. Note that the direction of the thrust force is dependent of the direction of rotation (Figure 5.4).

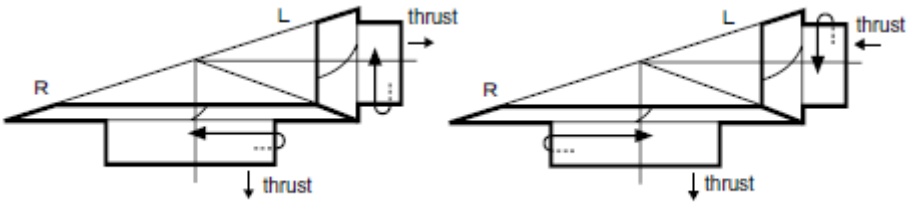

Figure 5.4.: Thrust force and its direction, which is dependent of the direction of rotation

For the gear wheel, the formulas are

$$F_{radial} = W_{KW} \cdot T_W \tag{5.7}$$

$$F_{thrust} = W_{NW} \cdot T_W \tag{5.8}$$

$$F_{tangential} = \frac{T_W}{r_W} \tag{5.9}$$

where W_{KW} is the radial load coefficient of the pinion, W_{NW} is the thrust load coefficient of the pinion and r_P is pinion wheel radius.

The hypoid gears in the KHK catalog have a maximum ratio of 200, which is insufficient. A second gear will therefore be needed in combination with the hypoid gear. Maxon offers modular systems comprising of a motor and a matching planetary gearhead. We will choose an appropriate Maxon gearhead/motor combination for our application. The planetary gearhead must comply to following requirements:

- It must fit the selected motor (appropriate planetary gearheads are mentioned in the motor data sheet)
- The operating torque (RMS torque) must not exceed the gearhead maximum continuous torque specified by the constructor
- The maximum torque must not exceed the intermittently permissible torque specified by the constructor

Maxon states that their gears usually achieve 1000 to 3000 operating hours in continuous operation at the maximum permissible load and recommended input speed. If these limits are not pushed, service life can be extended considerably [6]. Recommended speed may be exceeded, but this will adversely affect the service life. We will therefore try to pick a gearhead with an appropriate recommended speed.

5.1.2.3. Final design

Based on the above criteria, suitable drive systems are selected for the ankle and both hip joints. They can be found in Appendix F. Notice that the planetary gearhead maximum speed exceeds the recommended input speed, reducing the projected lifetime of the transmission. However, the torques are considerably lower than the permissible torques, in turn increasing lifetime.

5.1.3. Power supply

5.1.3.1. Introduction

One of the most important components is the power supply, since the motors will only function correctly if they are supplied with the power that matches their needs. Many things must be taken into consideration when selecting a power supply.

- The power supply must be rechargeable.
- The power supply must have sufficient autonomy, so that the wearer can go a full day without recharging the batteries. This means that the *power capacity*, which is the amount of energy that is stored in the power source (expressed in Wh), must be sufficiently high. For batteries, power capacity is expressed in Ah. This can easily be converted to Wh by multiplying it by the nominal voltage.
- The power supply must be lightweight and compact. The higher the *energy density* (in Wh/kg), the lighter the power source is for a specific power capacity.
- The power supply must not cause any discomfort to the wearer. Noise, vibration, and high temperatures must be avoided.

5.1.3.2. Types of power supplies

A study of possible orthosis power sources can be found in [23]. In terms of energy density and recharge time - the fuel tank only needs to be refilled - *internal combustion engines* are probably the most interesting power source. However, their large power output, the weight of the engine itself and the issues of noise, vibrations and heat make them unsuitable for this application. *Fuel cells* do not have problems with noise and vibrations and work at relatively low temperatures (60-100°C for PEM fuel cells). However, this technology is still in development. Issues such as poor reliability and hydrogen storage still need to be addressed.

Another option is the use of batteries. Although their energy density is lower, they do not have the problems of the technologies listed above. This makes them a suitable power supply for our orthosis. Several types of batteries exist. The highest energy

densities for commercially available, rechargeable batteries are found in lithium-ion and lithium-ion polymer batteries (up to 250 Wh/kg).

An important remark must be made concerning the power capacity of batteries. The power capacity of a battery pack is dependent of the amount of current that is drawn for it. If that current is higher, the batteries will deplete faster. Battery manufacturers therefore often specify a *discharge rate.* This is the amount of current which was drawn to measure the power capacity. It is expressed in C, which is the Ah capacity divided by one hour. A battery of 0.5C and 10Ah, for instance, will have 10Ah power capacity if 5A is drawn. If the RMS value of current goes above the discharge rate, power capacity will be lower than specified and the expected lifetime of the battery will decrease.

5.1.3.3. Battery requirements and selection

We will calculate the minimum battery requirements for the orthosis. First of all, we must determine the time during which the orthosis must be capable of operating autonomously. We will assume that the batteries will be recharged once a day. The number of hours during which the wearer effectively uses the orthosis is highly dependent of his/her lifestyle. An estimate of five hours of walking is made, which is equivalent to approximately 16 000 gait cycles (walking at normal speed).

Second, the electrical energy consumed by the orthosis during this period must be estimated. This can be inferred from the mechanical energy consumption. The energies associated with the movement of the lever arm were calculated in subsection 3.6.2 by integrating the motor power graph in time. However, these values are of no use for the calculation of energy consumption, since the area below the % stride axis is counted negative, meaning that energy is stored by the motor. A correct representation of energy consumption can be obtained by integrating the absolute value of power over one gait cycle:

$$E_{lever} = \int_{GC} |P| dt \tag{5.10}$$

The mechanical energy of the motor shaft is actually higher because of transmission losses, which are taken into account by dividing by $\eta_{transmission}$:

$$E_{motor,m} = E_{lever}/\eta_{transmission} \tag{5.11}$$

Finally, the electrical energy input $E_{motor,el}$ can be calculated by dividing $E_{motor,mech}$ by the motor efficiency η_{motor}:

$$E_{motor,el} = E_{motor,mech}/\eta_{motor} \tag{5.12}$$

These three quantities are calculated for the three orthosis motors (Table 5.3). Mo-

tor and transmission efficiencies can be found in subsubsection 5.1.2.3.

	E_{lever}	$E_{motor,m}$	$E_{motor,el}$
Ankle	10.0 J	19.9 J	22.9 J
Hip (orthosis)	4.0 J	6.2 J	6.8 J
Hip (prosthesis)	3.6 J	5.6 J	6.2 J
Total	17.5 J	31.7 J	35.8 J

Table 5.3.: Energy consumption for one gait cycle

Note that the manufacturer actually specifies the maximum motor efficiency, because motor efficiency varies with speed and torque. The motors of the orthosis do not operate at a constant speed or torque and will therefore certainly not constantly achieve their maximum efficiency Figure 5.5. As a result, motor energy consumption

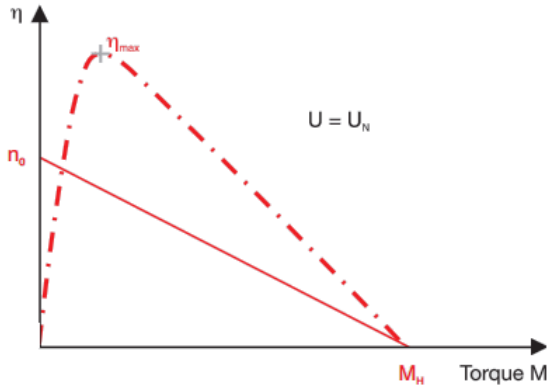

Figure 5.5.: A typical motor efficiency curve at constant speed. As a rule of thumb, maximum efficiency η_{max} occurs at roughly one seventh of the stall torque M_H [5].

will be higher than predicted by $E_{motor,el}$. A second thing to consider when selecting the batteries, is that electronics and solenoids also need to be powered, even though the motors will consume most energy. In conclusion, the batteries must be able to deliver far more than the total electrical motor energy of 35.8 J found in Table 5.3. If we demand 150% of this value, this leads to a required 54J per gait cycle. If we multiply this by the number of steps the wearer is expected to do in one day (16 000), we find the minimum power capacity of the battery pack: 849 kJ or 236 Wh. Note that this only covers the energy expenditure of the orthosis. If the prosthesis is connected to the orthosis, it must carry its own power supply, or higher capacity batteries must be chosen to serve the total energy need.

The number of battery cells required is determined by the voltage of one cell, which is fixed, and the maximum voltage needed by the motor. This voltage U can be calculated as follows:

$$U = k_n \cdot (n + k_{ST} \cdot T) \tag{5.13}$$

where k_n and k_{ST} are the speed constant and the torque gradient of the motor, both specified by the manufacturer, n is the motor speed, and T is the motor torque. The maximum voltages needed for each joint can be found in Table 5.4. A minimum battery voltage of 42V is required. The voltage of one Li-poly battery cell is typically 3.7 V, so a minimum of 12 battery cells are required.

	Max. speed	Speed constant	Max. voltage
Ankle	50 346 rpm	1 470 rpm/V	35.3
Hip orthosis	9 962 rpm	249 rpm/V	41.3
Hip prosthesis	9 482 rpm	249 rpm/V	38.1

Table 5.4.: Maximum motor speed and corresponding voltage

As noted before, total RMS current must be calculated and compared to the discharge rate and the maximum continuous currents specified by the manufacturer. Peak RMS currents must be lower than the maximum peak current. These values can be obtained by multiplying motor torques by the motor torque constant (Table 5.5). Total RMS current is 3.6 A, peak current is 5.0 A.

	RMS torque	Torque constant	RMS current
Ankle	15 mNm	6.49 mNm/A	2.3 A
Hip orthosis	23 mNm	32.3 mNm/A	0.7 A
Hip prosthesis	21 mNm	32.3 mNm/A	0.6 A

Table 5.5.: RMS currents

A battery pack is composed consisting of 13 Kokam SLPB 75106100 lithium-polymer battery cells (Appendix H). The properties of this battery pack are summarized in Table 5.6.

Number of cells	13
Power capacity[a]	333 Wh
Nominal voltage	48,1 V
Weight	2,015 kg
Energy density	179 Wh/kg

[a] At 0.5C=3.75A

Table 5.6.: Battery pack properties

5.2. The orthosis as a whole

Selection of the components is one thing, but the real challenge is to fit them all onto the orthosis in a compact and organized way. In Figure 5.6, the orthosis is

shown. Note that the cuffs at the shank, thigh and hip (displayed in black) as well as the foot sole are inserted only to illustrate the connection between the device and the wearer. In reality, these cuffs will be made based on a mold of the subject's leg. The cuffs at the shank and the hips are half open and are to be closed by means of a Velcro strap. Prudence is called for at the thigh connection. Since the thighs almost touch each other while walking, we opted for a cuff at the outside and the back of the leg in combination with a strap closing the cuff via the inside of the leg. This will take a lot less place than a rigid cuff would.

It is important to mention that the dimensions of the part were based on an Inventor model of the human body (Figure 5.6). This way we can immediately check whether the device hinders a real life person or not, even though this does not guarantee proper functioning of the orthosis. Elaborate testing is certainly neccesary were this device to be used in practice.

We chose to keep the three flexion/extension joints in the same plane, because the kinetic data we used is also calculated in one plane, i.e. the plane of progression [57]. The orthosis' flexion joints are placed beside the leg so that the axes go through the biological joints.

Note that the sole of the orthosis is flexible and follows the shape of the foot from heel-off to toe-off. The sole is strapped firmly to the foot.

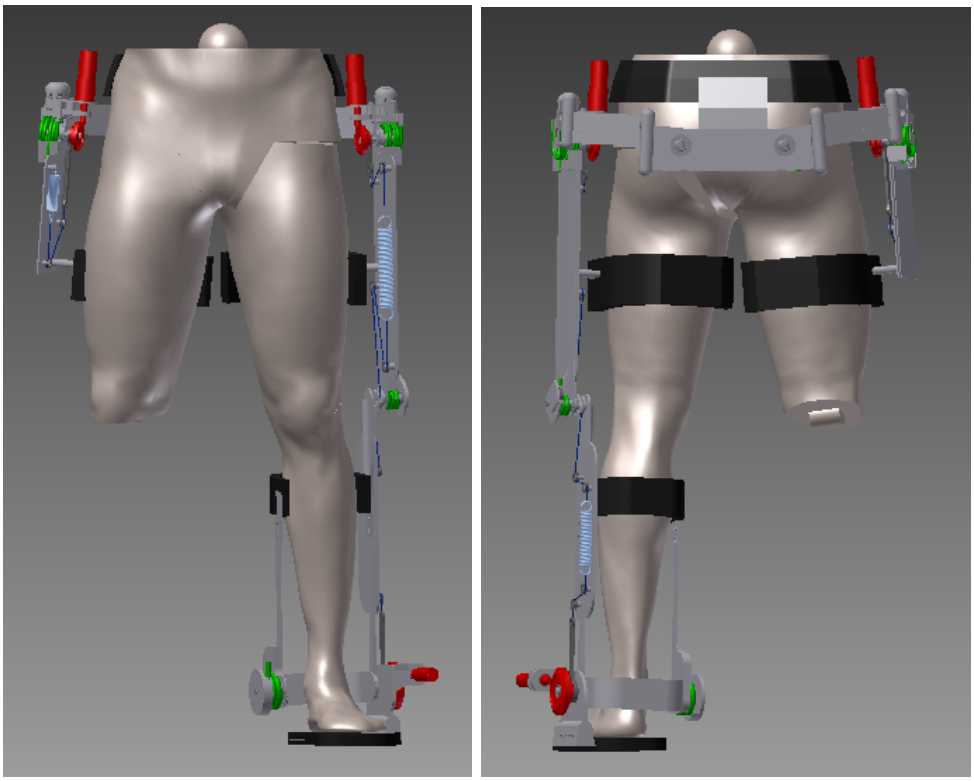

(a) Front view **(b)** Back view

Figure 5.6.: The orthosis

5.3. Hip design

5.3.1. Flexion/extension

As already mentioned, the flexion joint is placed next to the leg so that the biological and orthosis joint axis coincide. The necessary torque is partially delivered by the biarticular MACCEPA and partially by hip spring H1. The knee-hip (KH) spring is mounted between the KH plate and the leg. Note that for safety reasons a cover should be added, separating the spring (and any other moving part) from the wearer's limbs.

The H1 spring is modeled as a torsion spring. As they are to be loaded only in the direction in which the legs of the spring come together, we need to implement two of them. One spring will deliver the extensor torque, the other the flexor torque. In Figure 5.7 one can see that the springs are mounted between the KH plate (in grey) and the rotation joint (in blue). Note that two slots are created in the KH plate to ensure that they are not loaded in the wrong direction.

A bearing for the pinion is placed as close as possible to the hypoid gear wheel, to avoid bending of the shaft. The consequences of a bending shaft are increased wear,

noise and possibly even failure of the shaft due to fatigue.

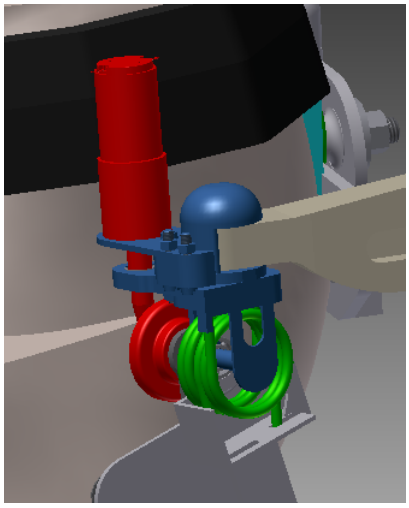

Figure 5.7.: Hip flexion/extension joint

5.3.2. Abduction/adduction

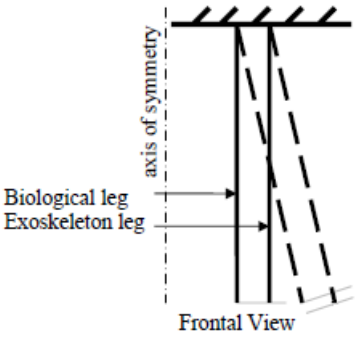

Figure 5.8.: Misalignment due to hip abduction/adduction. In this case, the exoskeleton abduction/adduction joint axis does not run through the biological hip joint. As the leg abducts/adducts (dashed line), the knee joints (grey lines) are no longer aligned.

Special care should be taken when implementing the abduction/adduction DOF. If the orthosis abduction/adduction joint axis does not pass through the human hip joint, a misalignment between the biological and orthosis knee joint will occur as illustrated in Figure 5.8. This can cause discomfort, which is unwanted. Adjusting leg length is one way of dealing with this problem, but it necessitates mechanisms such as the cam mechanism described in [45]. In this design, we prefer to eliminate

the problem by aligning biological and orthosis abduction/adduction joints. This approach was also used by the designers of BLEEX [24].

In subsubsection 2.2.7.2 we already noted the similarity between the hip abductor/adductor torque and angle characteristics during gait. This makes this DOF a prime candidate for the implementation of a spring. The maximum abductor torque of 1.2 Nm/kg is attained at 12% stride, at an angle of 5.5 degrees (Figure 2.26). Since we want to deliver half of the biological torque for a 75kg person, this comes down to a torque of 45 Nm. As equilibrium angle 1° is chosen, so that no torque is delivered during swing. This leads to a desired spring constant of

$$k = \frac{45\,Nm}{4.5\ \text{deg}} = 10\,Nm/deg \tag{5.14}$$

This can be achieved by a simple torsion spring, of which the parameters are listed in Table 5.7.

Wire diameter d	11.7 mm
Outer diameter D_o	39 mm
Number of active coils n_w	2.5
Height of spring h	29.25 mm
Spring constant k	9.96 Nm/deg

Table 5.7.: Abduction torsion spring

The actual placement in the orthosis is shown in Figure 5.9. The torsion springs are colored green.

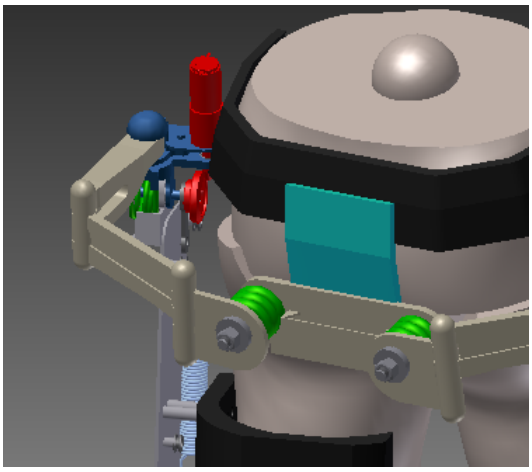

Figure 5.9.: Orthosis hip abduction/adduction joint

5.3.3. Internal/external rotation

It is impossible to design an internal/external rotation joint of which the axis passes through the biological hip joint without obstructing normal movement. The rotation joint was therefore placed next to the leg. This choice necessitates the design of a flexible connection between the rotation joint and the connection to the wearer's backside. The mechanism is explained in section 5.6.

5.4. Knee design

5.4.1. Stance spring locking mechanism

A locking mechanism is required to lock and release stance spring 1 (subsection 3.6.2), so that it only contributes to the knee torque during loading response and mid-stance. More specifically, the spring must be active from to 4% GC to 32% GC.

A pawl-ratchet mechanism is particularly interesting, because it allows motion in one direction while blocking it in the other. This allows to lock and release at a range of angles rather than at one specific angle. A serious design consideration is whether the pawl's resting position is pressed against the ratchet or pulled away from it. In the prior case, the ratchet will be locked if no action is performed by the actuator (or whatever means to remove the pawl from the ratchet). In the latter, the ratchet will be released. If the resting position of the mechanism is locked, the stance spring will be engaged once the knee is extended more than 9.78 degrees when the orthosis is switched off. This may pose some difficulties to the wearer, e.g. when he/she tries to sit down. The wearer will then try to flex his knee, but with the locked mechanism, the stance spring will impose an extension torque. On the other hand, if the resting position of the stance spring is unlocked, the stance spring will not be engaged if something is wrong with the actuator. If this occurs during walking, the wearer of the orthosis, relying on the extra torque supplied by this spring during loading response, may fall due to the unexpected absence of this torque. This is of course completely unacceptable. For now, the locking mechanism will be designed so that the pawl rests in the locked position, which is the safest option. A mechanism may be added that allows the wearer to manually lock the pawl into a position that releases the ratchet, so that e.g. sitting down is no longer a problem. This still does not solve the problem of a missed release of the pawl though, which would result in an extension torque during pre-swing and swing, possibly causing the wearer to trip. We will not further elaborate any measures to cope with these issues, since a detailed design of the locking mechanism is beyond the scope of this thesis, yet we stress that a more carefully designed locking mechanism is essential for a usable and safe orthosis.

Several methods - passive or active - exist to perform this release, some of which are described in [58]. As noted before, we will not design the locking mechanism

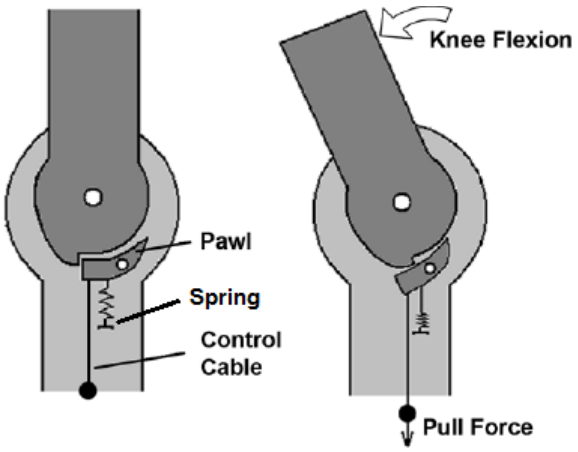

Figure 5.10.: Principle of the ratchet-pawl mechanism (adapted from [58]). A (compression) spring pushes the pawl against the ratchet wheel, so that it locks if the knee is sufficiently extended (left figure). A pull force, which can be exerted by a linear actuator such as a solenoid, pulls the pawl away from the ratchet so that it unlocks and the knee can flex freely (right figure).

into this much detail, but we will simply assume that the release is taken care of by a pull-type solenoid. The solenoid must not be able to provide large forces, since unlocking takes place under zero torque. Only friction needs to be overcome.

The time during which the solenoid is energized must now be determined. With the locked resting position design, release of the pawl must be forced at approximately 46% GC (when the knee reaches the locking angle during the terminal stance phase of gait). The pawl can remain released between 32 and 4% GC (when the stance spring is not active). It is sensible though to define a time range which is sufficiently large for the solenoid to attain its maximum stroke and which allows some safety margin, but which is sufficiently small to not waste power. The hip kinematics provide an interesting trigger for the control unit to start energizing. The hip is extended 5 degrees or more between 38% and 61% GC. If we energize the coil during this period, the solenoid actuator will have sufficient time (8% GC or 91 ms) to attain its maximum stroke at 46% GC. Proper release of the ratchet will also be assured, since the knee is already flexed 42 degrees at 61% GC, so that the pawl pushes against the ratchet in an unlocked position. Note that the pawl may also be pulled back mechanically, e.g. by attaching a cord to the hip that pulls the pawl when it is extended over 5 degrees.

The mechanism that engages and disengages stance spring 1 consists of the ratchet and pawl. The location of the locking mechanism in the orthosis is displayed in Figure 5.11a. The torsion spring is connected to the thigh plate and to the ratchet, both depicted in grey in Figure 5.11b. The pawl (red) is attached to the shank plate (brown), as depicted in Figure 5.11b. When the ratchet is locked, it moves around together with the shank, so that the torsion spring is twisted and a torque

is delivered proportional to the knee angle.

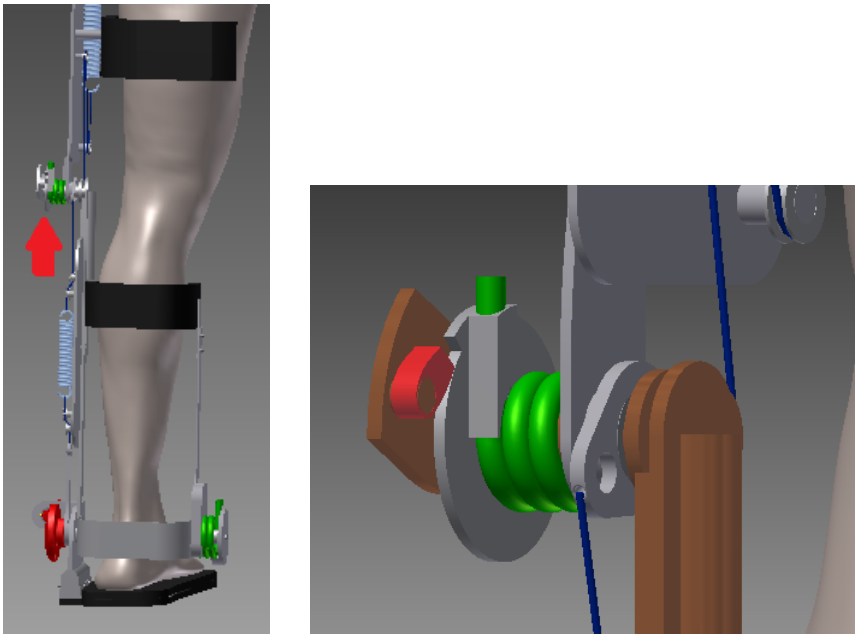

(a) Location in orthosis **(b)** Zoom

Figure 5.11.: Locking mechanism

5.4.2. Flexion/extension

The remainder of the flexion/extension torques are provided by the biarticular MACCEPAs. The biarticular springs span two joints, as the word implies. The ankle-knee (AK) spring is thus attached to a lever arm on the KH plate, while the KH spring is attached to a lever arm on the AK plate (Figure 5.12).

5.4.3. Secondary DOFs

As mentioned in section 3.3, these DOFS are best fixed at 0° (internal/external rotation) and 1° (adduction). We chose to make the ab-/adduction angle 0°. This small deviation is certainly acceptable, and it will make the design a lot easier. It will also eliminate the out-of-plane forces that occur with a 1° adduction angle.

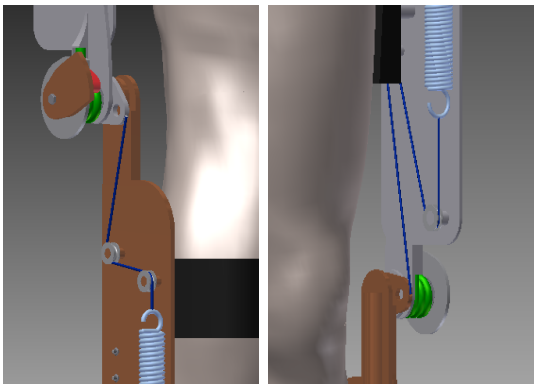

(a) Connection AK spring **(b)** Connection KH spring

Figure 5.12.: Connection of the springs. AK plate is depicted in brown, KH plate in grey

5.5. Ankle design

5.5.1. Flexion/extension

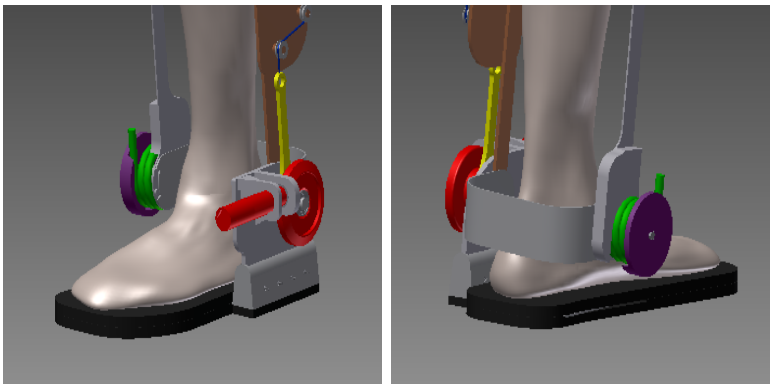

(a) Front view **(b)** Back view

Figure 5.13.: Orthosis ankle

The ankle portion of the orthosis is depicted in Figure 5.13. The motor and gear wheel are displayed in red. The motor is attached to a mounting plate. A bearing is placed as close as possible to the gear wheel to ensure a correct position of the pinion relative to the gear wheel. The lever arm (yellow) is welded onto the gear wheel. The heel buckle, the part that connects the inside and outside of the ankle via the heel, is solidly connected to the motor mounting plate.

The ankle torsion spring (green) is placed on the inside of the ankle in order to keep the orthosis compact. The torsion spring is fixed to a plate on the inside of the leg

(grey), which is attached to the AK plate via the shank cuff. It bumps into a cap (purple) that is screwed into a shaft fixed to the heel buckle. The orientation of this cap with respect to the shaft determines the equilibrium position of the spring. To ensure a correct placement of this cap and to transmit torque, a octagonally shaped axis is used (Figure 5.14).

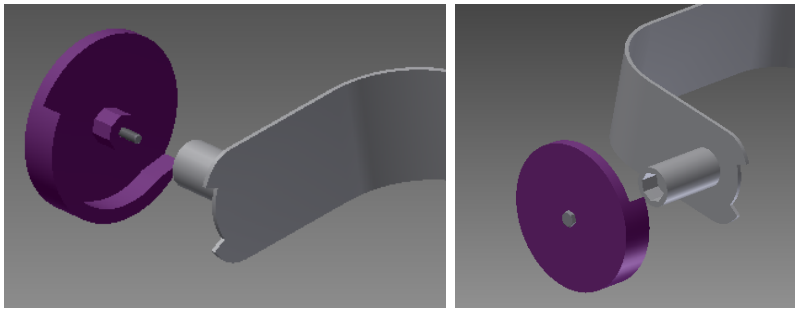

(a) View on cap **(b)** View on heelbuckle

Figure 5.14.: Connection cap - heelbuckle

5.5.2. Inversion/eversion

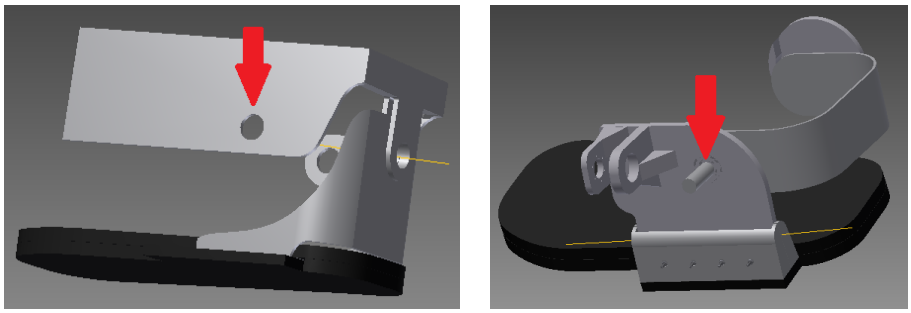

(a) Rejected design **(b)** Final design

Figure 5.15.: Inversion/eversion joint design. The inversion/eversion joint axis is denoted by the yellow line. The red arrow denotes the flexion/extension bearing to which the highest forces are applied.

For ankle inversion/eversion, the same concerns as in subsection 5.3.2 apply. The first design therefore had its abduction/adduction joint axis behind the heel, so that its axis more or less passes through the ankle joint axis (Figure 5.15a). This design was rejected, because the orthosis leg exerts its forces mainly to the left of this joint, causing an unwanted evertor/invertor moment around the joint. This problem can be solved by relocating the joint right beneath the leg structure, so that all forces pass directly through the axis joint (Figure 5.15b). Of course, this solution again

has the problem of non-colocated biological and orthosis joint axes once the ankle inverts/everts. We will assume that the orthosis can move freely parallel to the leg, so that no extra stresses are induced in the material to restrain this movement. This is a reasonable assumption if the orthosis is not too tightly bound to the wearer, or if the interface material is sufficiently compliant. A good attachment to the foot must assure that the joints return to their normal positions once the ankle has stopped inverting/everting.

We stress that this solution is certainly not optimal. Because of the huge importance of foot abduction/adduction for balance (see subsection 2.3.1), we will implement it anyway. The design of a better mechanism is an important area of improvement though.

The abduction/adduction joint is implemented as a hinge joint, restricting radial and axial motion. Rotation is limited mechanically so that the abduction/adduction ROM is as specified in Table 3.2. To make assembly possible, the holding part is divided into two pieces that are connected by means of screws (Figure 5.16).

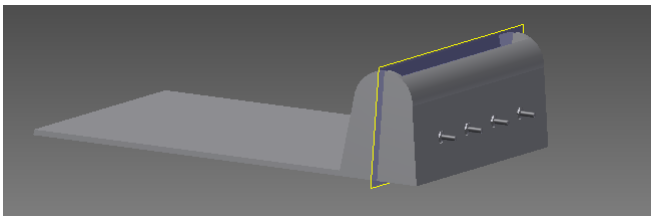

Figure 5.16.: Bearing ankle abduction/adduction joint. The work plane in the picture is positioned at the connection plane of both parts.

5.5.3. Internal/external rotation

It is clear that designing an internal/external rotation joint of which the axis passes through the ankle axis is not an easy task. The only way to achieve this is to place the orthosis joint below the foot. This would require a high heel for the foot plate. Additionally, the material between the orthosis and the wearer's foot will experience friction from the rotating joint, causing it to wear. An alternative that does not suffer from these disadvantages would be to place the joint along the orthosis leg's axis. The range of motion of this DOF is however limited, so we decided to leave this one out for now rather than adopting a suboptimal solution. Turning will be more difficult with the current design, though.

5.6. Hip module design

As the orthosis' rotation joint does not coincide with the biological one, it moves with respect to the subject's back. This is clarified in Figure 5.17. The orthosis is

attached to the wearer's leg, hence as the wearer rotates his leg the device moves along. Both rotate along the biological joint axis, moving the orthosis joint closer to the backplate in case of external rotation (red) of farther from it in case of internal rotation (green). A rigid connection between both is thus not an option. Incorporating two hinges solves the problem, allowing the relative motion between the rotation joint and the backplate. Note that it is important to design the length of the three hinge plates properly so that the orthosis ROM is as specified in Table 3.2.

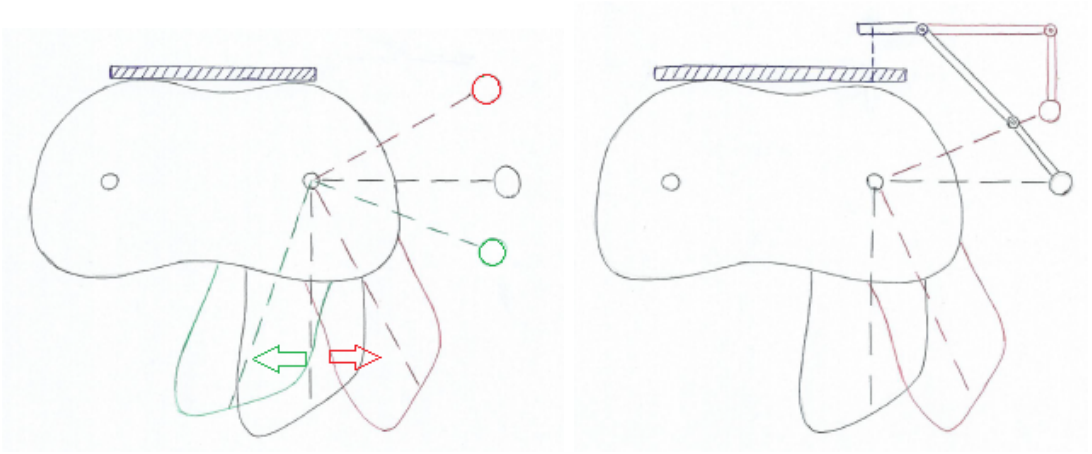

(a) Relative movement between rotation joint and backplate

(b) Relative movement made possible by hinges

Figure 5.17.: Problem caused by and solution for non-collinear rotation axes

5.7. Orthosis operation overview

Using 3D Inventor drawings of the orthosis at some crucial moments during the gait cycle (Figure 5.18), we will give a clear overview of how the orthosis operates. For simplicity this overview is limited to the flexion/extension of the joints. All other DOFs are considered fixed. Notice that the internal/external rotation joint and hip module in the drawings is not the final design, however this does not influence the working principle.

- At initial contact (0% GC), the heel of the orthosis touches the ground (symbolised by the yellow line) and a new gait cycle is detected. At this point, the orthosis hip exerts almost its maximum extensor torque (shown in the inset). About half is supplied by the hip spring, which is close to its maximum twist.
- At 4% GC, the knee is flexed beyond 9.78°. The ratchet is now locked (shown in the inset) and the spring starts twisting. It reaches its maximum extension at 14% GC (maximum extension shown in inset) and is again unloaded at 32% GC. At 14% GC, the hip is also close to its maximum adduction angle and

the twisted abduction spring delivers an abductor torque of 50 Nm. Although it seems that the orthosis foot crosses the line which represents the ground at 14% GC, one must take into account that the sole will deform in reality.

- At 38% GC, the hip is extended 5°, signalling the solenoid to release the pawl of the knee locking mechanism. The knee spring is not loaded at this instant. This is verified in the inset, where the yellow lines represent the edge of the pawl and ratchet. From this figure, it is clear that the pawl and ratchet do not touch, so that the spring can impossibly be loaded.
- At 46% GC, the ankle exerts its maximum torque, of which most is delivered by the ankle spring, which is close to its maximum twist. In the inset the spring deformation is shown.
- At 60% GC, the foot leaves the ground (toe-off). Crossing of the ground line is again the result of disregarding the sole deformation in Inventor. The orthosis hip is now nearly providing its maximum flexor torque. A part is delivered by the hip spring, which is close to its maximum twist (shown in inset).
- At 92% GC, the knee extends beyond 9.78° and the pawl automatically falls down into its locked position. The ratchet can still move though, and the knee spring is not yet twisted.

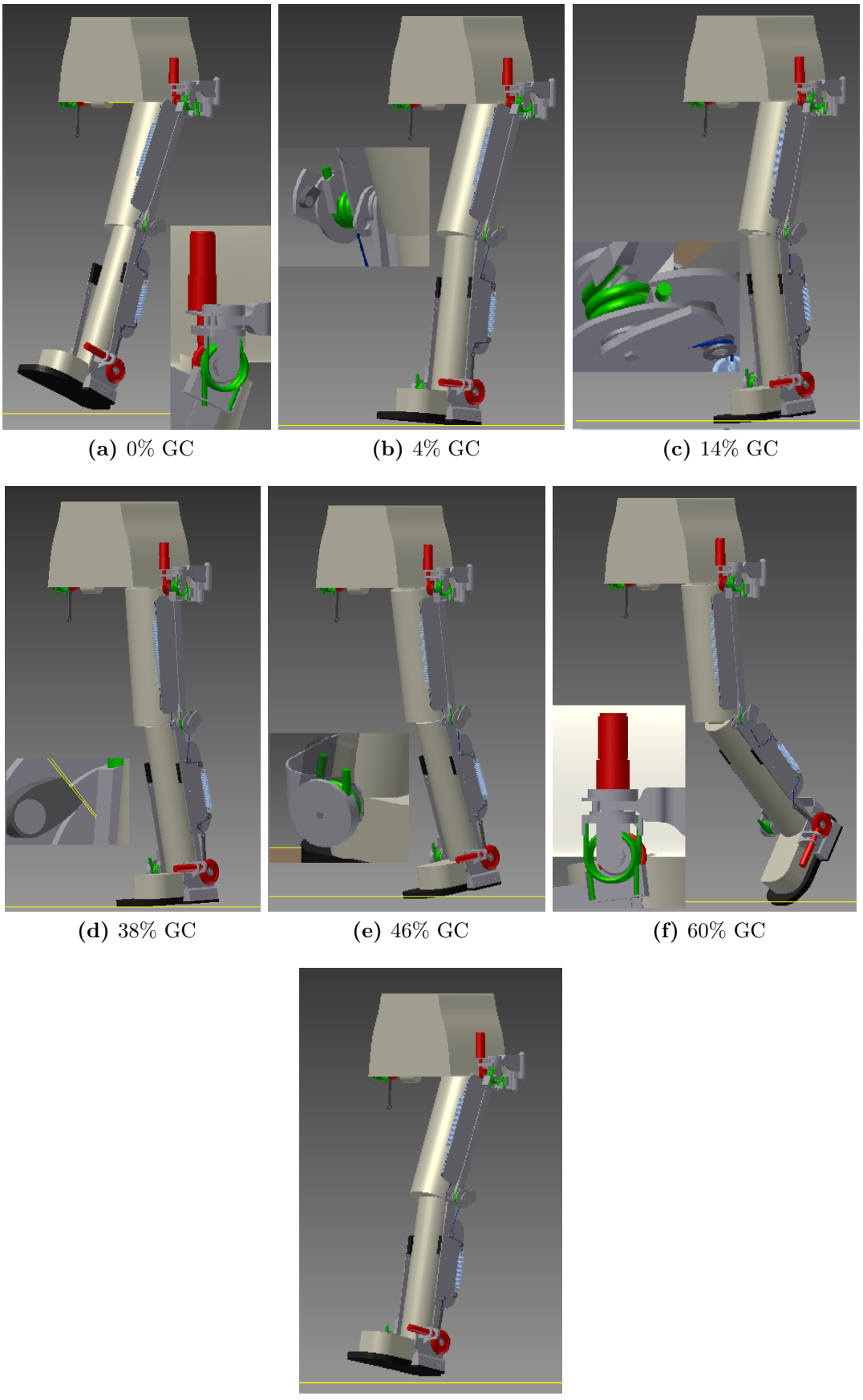

(a) 0% GC **(b)** 4% GC **(c)** 14% GC

(d) 38% GC **(e)** 46% GC **(f)** 60% GC

(g) 92% GC

Figure 5.18.: Orthosis operation on key points in the gait cycle

5.8. Mechanical design and stress analysis

Parts must be created that are as light as possible, but still able to withstand the imposed loads. Performing a stress analysis will allow us to achieve this goal. In this section, we will discuss the mechanical design of a few key parts. We will start with some general considerations, such as material choice and safety factor determination, before moving on to the design of the actual parts. The stress analysis is carried out in *Autodesk Inventor*.

5.8.1. General considerations

5.8.1.1. Material

An aluminium alloy is chosen because of its high strength-to-weight ratio. We will work with AlMgSi1 (also known as Al-6082), which has good machinability, very good weldability and very good corrosion resistance [1]. Material properties are listed in Table 5.8.

(a) AlMgSi1 [36, 1]

Density	2710 kg/m^3
Yield strength	260 N/mm^2
Young's modulus	70 000 N/mm^2
Shear modulus	26 400 N/mm^2
Ultimate tensile strength	310 N/mm^2
Bending fatigue strength	232.5 N/mm^2
Axial fatigue strength	216 N/mm^2
Torsion fatigue strength	154 N/mm^2

(b) Nylon 6-6 (Inventor database and [47])

Density	1130 kg/m^3
Yield strength	82.75 N/mm^2
Young's modulus	2930 N/mm^2
Poisson's ratio	0.35
Ultimate tensile strength	82.68 N/mm^2
Fatigue strength	20 N/mm^2

Table 5.8.: AlMgSi1 and nylon material properties

The cuffs are made out of nylon, which is a common material in orthoses because of its breathability, its low weight and its ability to be thermo-molded to fit the limb.

5.8.1.2. Safety and fatigue correction factors

A static analysis will be performed in Autodesk Inventor, meaning that the stresses in the component will be compared to the yield strength. However, the loads on the orthosis are dynamic rather than static. Fatigue strengths must therefore be used instead of the yield strength. We will therefore introduce correction factors K_f, which are dependent on the type of load (Table 5.9). They are calculated by dividing the yield strength by the fatigue strength for the corresponding load.

	K_f	$K_s \cdot K_f$
axial fatigue	1.20	2.41
bending fatigue	1.12	2.24
torsion fatigue	1.69	3.38

Table 5.9.: Fatigue correction factors for AlMgSi1

A general safety factor $K_s = 2$ is chosen for AlMgSi1.

For nylon, fatigue strength is only specified for axial loads. We will therefore take $K_s = 3$ for nylon, and simply use one fatigue safety factor $K_f = 4.14$. This leads to a total safety factor of $K_s \cdot K_f = 12.41$.

The Autodesk Inventor stress analysis will yield a safety factor S which is defined as

$$S = \frac{yield\,strength}{maximum\,stress} \tag{5.15}$$

The design is accepted if S meets the criterium $S \geq K_s \cdot K_f$.

5.8.1.3. Loads

A part can only be well-designed so far as the loads applied to it are well-defined. For an orthosis, this is certainly not an evident task. The loads imposed by the motors and springs are well-known. They can be directly derived if all system parameters are known. The difficulty however lies in determining the loads applied to the structure by the leg. Unlike a prosthesis, which is placed in series with the leg and supports the entire body weight, the orthosis is a structure parallel to the leg. This allows it to transfer some part of the body weight directly to the ground, lowering the loads on the biological leg. The challenge is now to make a good estimate of the body weight that is carried by the orthosis.

All forces and torques acting upon the natural leg can be assumed proportional to body mass, since they serve to carry the human weight and to overcome the inertia of the body during movement. The orthosis delivers approximately 50% of the biological torque, which we can relate to 50% of the body mass. We will therefore assume that the orthosis carries 50% of the human body weight. This weight is transferred from the leg to the orthosis through the cuffs and the foot plate.

During stance, the foot makes contact with the floor, resulting in a reaction force that carries all of the weight - the so-called ground reaction force which was discussed in subsection 2.2.8. This force must pass through the orthosis, resulting in moments and radial reaction forces in the orthosis joints. The moments are imposed by the actuators of the orthosis and are well-known.

During swing there are no GRF. The joints must react to the weight of the limb segments underneath it and to the inertia of the moving limb. An estimate of the

different limb segments' masses for a 75kg person is shown in Figure 5.19. The total mass of the leg is 12.1 kg or 16% of the total body mass, so we can assume that the highest joint reaction forces will occur during stance. This certainly holds for the joint torques (section 2.2). In other words, we can focus our strength calculations on the stance phase and neglect the loads due to the weight of the limb during stance.

	Mass (kg)
Thigh	7.5
Shank	3.5
Foot	1.1

Figure 5.19.: Mass of the different limb segments [56]

5.8.1.4. Bearings and bolts

Autodesk Inventor offers a tool called *Design Accelerator*, which provides calculators and component generators for bolted connections, pins, shaft, bearings etc. Appropriate components are automatically calculated by Design Accelerator based on specifications (e.g. shaft diameters, loads, safety factors) supplied by the user. We will rely on Design Accelerator for the design of bearings and bolts. These components will therefore not be discussed any further.

5.8.2. Part design

The final design of the orthosis consists of no less than 90 parts. Engineering every single component to an extent that the strength and stiffness requirements are met with the least amount of material is impossible within the limited amount of time available to complete this thesis. Nevertheless, some of the parts are so important that they are worth taking a closer look at. In this subsection, we will discuss the strength analysis of these parts.

5.8.2.1. Ankle motor mounting plate

Large forces are imposed on this plate due to the presence of the gears. Following forces are applied to the plate:

- The expected reaction forces in the hole through which the ankle axis passes. These reaction forces are due to the spring acting on the lever arm and due to the radial and tangential forces on the hypoid gear wheel, but also due to the weight that is transferred to the ground.

- The reaction forces on the bearing and motor mounts. These are due to the thrust, tangential and radial forces on the pinion. To determine the reaction forces, the motor and its shaft are modeled as a beam for the radial and tangential forces (Figure 5.20). F_2 holds the motor in place, while F_1 is the reaction force coming from the bearing that is necessary to reduce the displacement of the pinion. This bearing must support the radial and axial loads that are exerted on the pinion.
- The plate is constrained at the hinge axis (pin constraint + 2 frictionless constraints at the ends).

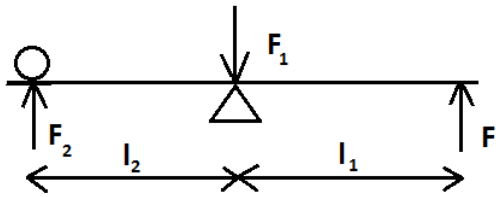

Figure 5.20.: Ankle motor shaft beam model

The loads acting on the hole and pinion during one gait cycle are plotted in Figure 5.21 (transferred weight is not taken into account in this plot). Two loading conditions were considered for strength analysis, at 48% stride and 96% stride. The design is accepted if the safety factor is 2.41 or higher (axial loads).

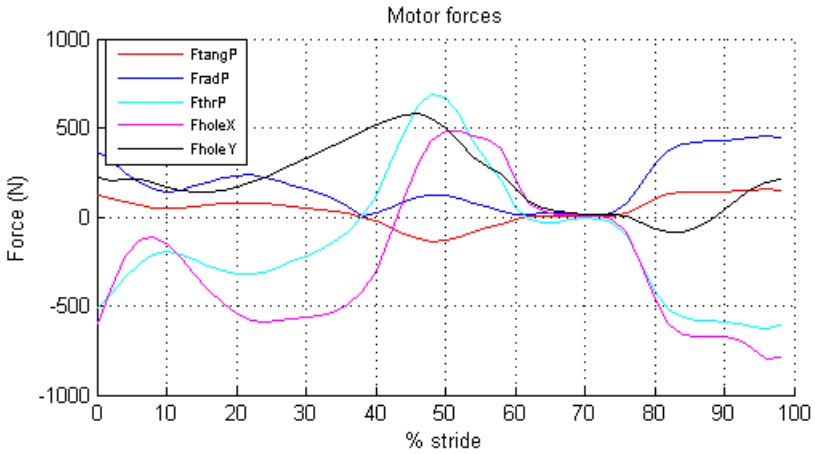

Figure 5.21.: Loads on the ankle motor mounting plate. F_{radP}, F_{tangP} and F_{thrP} are the loads acting on the pinion in the radial, tangential and axial direction. F_{holeX} and F_{holeY} are the forces acting on the ankle axis hole.

The results of the stress analysis are shown in Figure 5.22. The minimum safety factor is higher than the safety factor for axial loading, so the design can be accepted. Support ribs were used to cope with bending forces on the motor mount and bearing.

The deformations of the plate are also important to guarantee the lifetime of the motor and transmission. In this part, deformations up to 0.7mm were recorded by

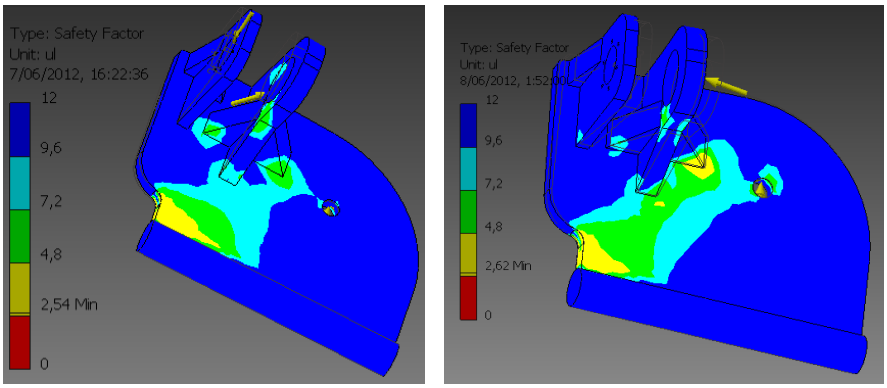

(a) 96% stride **(b)** 48% stride

Figure 5.22.: Safety factors for the ankle mounting plate

the stress analysis. Measures must be taken to ensure that the alignment of the axes is not compromised. Proper bearing selection, the use of special couplings or even making the plate stiffer by adding material or by making the plate out of steel instead of aluminium may help to achieve this goal.

5.8.2.2. Ankle-knee spring plate

The AK spring causes forces which act on the pulleys mounted on the plate. Additionally, the KH spring exerts a force on the plate via the knee lever arm, which is also attached it. Both spring forces are plotted in Figure 5.23. Peak forces occur at 98% GC (AK spring) and 62% GC (KH spring), thus during swing. During stance however, the AK plate transfers some of the weight of the orthosis wearer to the ground. As discussed before, the percentage of weight transferred was estimated to be 50% of the biological weight. The knee torsion spring also exerts a force on the AK plate through the pawl. This maximum torque occurs at 14% GC. It is also the moment at which the second peak in the GRF occurs (subsection 2.2.8). Constraints were placed on the ankle joint hole (pin constraint) and at two sides of the shank cuff (frictionless constraint).

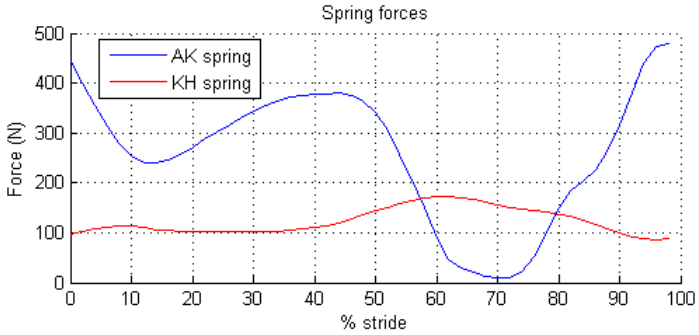

Figure 5.23.: MACCEPA spring forces over one gait cycle

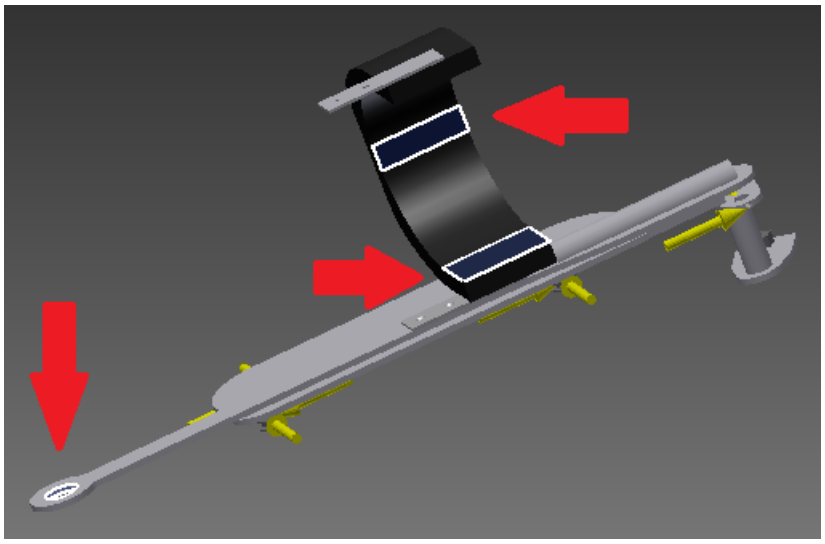

Figure 5.24.: Constraints for the ankle-knee spring plate

For stress analysis, the loading conditions at 14% GC and 98% GC were considered the most important. It was also verified whether the plate could resist the separate peak loads, thus avoiding a compensating influence from the other forces. The design was accepted if the safety factor was 2.41 or higher (axial loads). As we can see in Figure 5.25b, the pulleys and the plate can withstand the highest forces applied to them. The stresses at 14% GC are clearly higher (Figure 5.25a). The minimum safety factor is only 0.25, which is too low, but this stress occurs at the pawl, which was not dimensioned accurately. The stresses in the actual part all lead to safety factors higher than 2.41. A half cilinder, which can be seen in Figure 5.25a, was used as reinforcement to cope with the bending stresses.

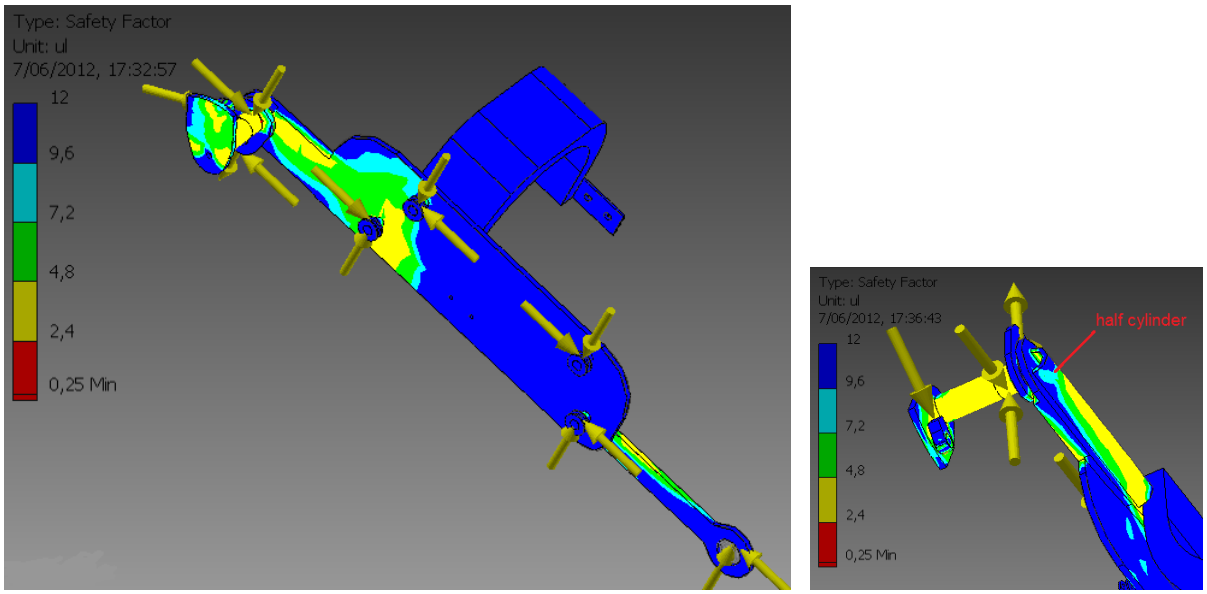

(a) 14% GC

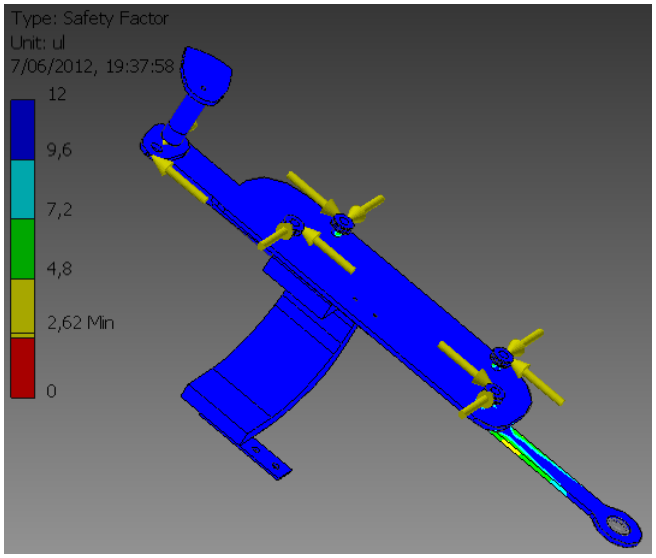

(b) 98% GC

Figure 5.25.: Safety factors for the ankle-knee spring plate

The design of the KH spring plate is similar to the AK spring plate and will therefore not be discussed.

5.8.2.3. Hip motor mounting parts

These parts are designed to hold the motor and serve as the connection between the flexion/extension and the internal/external rotation joint. The forces acting on this

plate are:

- the expected reaction forces on the flexion/extension axis due to the spring acting on the lever arm and due to the radial and tangential forces on the hypoid gear wheel.
- the expected reaction forces due to the weight that is transferred to the ground via the KH plate. These reaction forces are applied to an extrusion specially made for this purpose.
- the force exerted by the torsion springs
- the reaction forces on the motor bearing and mounting holes. These are due to the thrust, tangential and radial forces on the pinion. The motor and its shaft are modeled the same way as in subsubsection 5.8.2.1.
- The plate is constrained at the internal/external rotation joint axis (pin constraint with axial and radial motion constrained) and at the contact area with the KH plate (axial pin constraint)

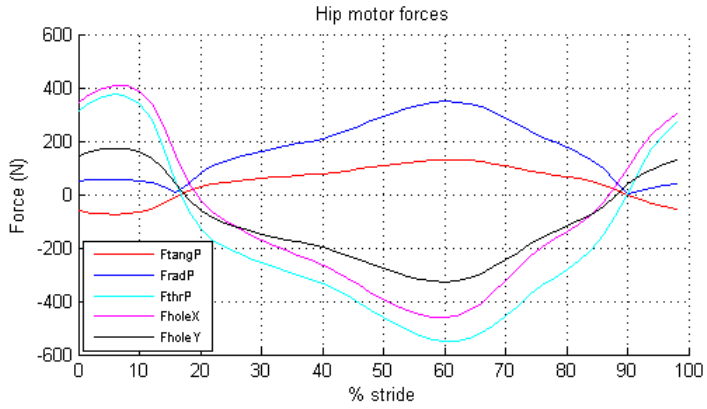

Figure 5.26.: Loads on the hip motor mounting parts. F_{radP}, F_{tangP} and F_{thrP} are the loads acting on the pinion in the radial, tangential and axial direction. F_{holeX} and F_{holeY} are the forces acting on the flexion/extension axle, on the contact surface with the lever arm and gear wheel.

The loads acting on the axis and pinion during one gait cycle are plotted in Figure 5.26 (transferred weight is not taken into account in this plot). Stress analysis was performed for the loading conditions occuring at 6, 48 and 60% GC. The 48% GC loading condition was considered because this is the time at which the second bump in the vertical GRF occurs (subsection 2.2.8). The design is accepted if the safety factor is 2.41 or higher (axial loads).

The results of the stress analysis are shown in Figure 5.27. The minimum safety factor is below 2.4, but the stresses causing it only occur in a small, red-coloured region, which is most pronounced in Figure 5.27a. They are due to the extrusion of the contact surface with the KH plate and should therefore be neglected. Safety

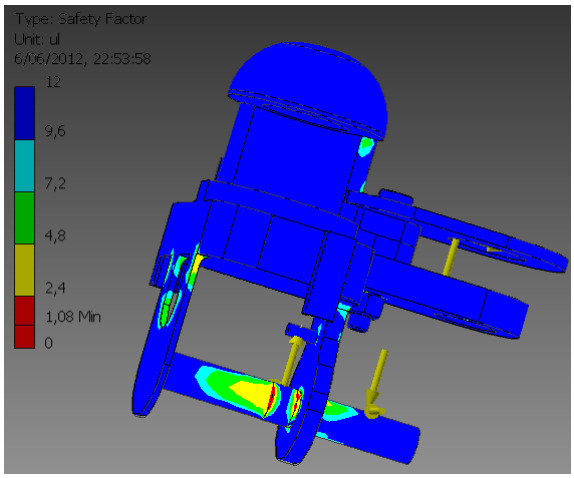

(a) 6% GC

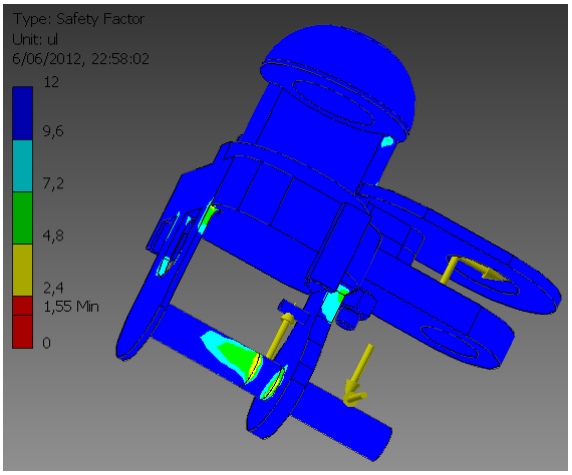

(b) 14% GC

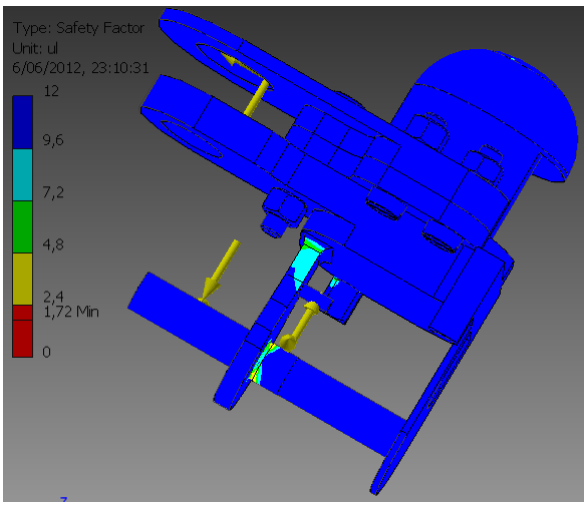

(c) 48% GC

Figure 5.27.: Safety factors for the hip motor mounting parts

factors larger than 10 are seen in the majority of the part, indicating that more material can be removed. However, the stiffness of the part must remain guaranteed not to compromise the alignment of the shafts.

5.8.2.4. Hip module

The hip module was subdued to a stress analysis in its entirety, i.e. as an assembly. The loading conditions at the hip module can be summarized as follows:

- The orthosis is attached to the wearer by means of a belt, the hip cuff, which is attached to a plate (turquoise in Figure 5.9). This plate is connected to the hip module with three bolts at the back. A force of one sixth of the maximum

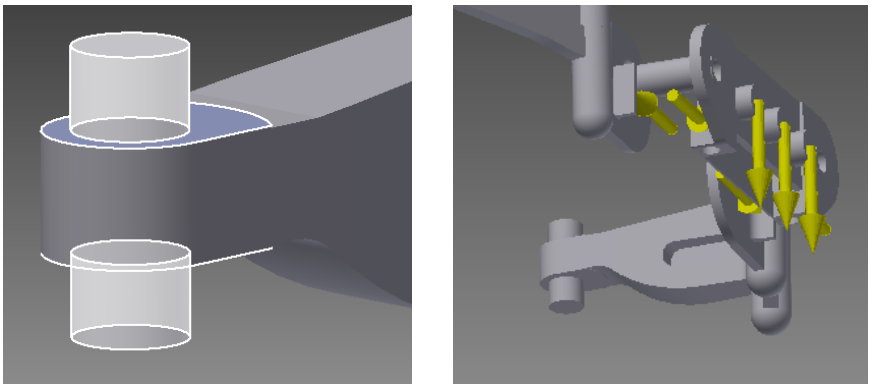

(a) Constraints for the hip module. White: the pin constraint on the axis of rotation, blue: the frictionless constraint on the contact surface.

(b) Loads for the hip module

Figure 5.28.: Contstraints and loads for the hip module

weight (50% of the weight spread over three connections) is applied to the cylindrical pieces that connect the hip module to the plate.

- The hip internal/external rotation axes were constrained as a pin on both sides. A frictionless constraint was used to model the contact with the motor mounting part, restraining axial motion of the joint axis (Figure 5.28a). An extrusion of 0.5mm was used to create the face on which the constraint was applied.
- The maximum forces exerted by the parallel springs are applied to the faces on which they act.

The load on the parts is, in general, a combination of axial, bending and torsion. A minimum safety factor of 2.41 is required (axial loads). Where torsion is significant, we will demand a safety factor of 3.38. The results of the FEA are shown in Figure 5.29. Except for some very small regions, the torsion safety factor is not exceeded. The minimum safety factor of 1.17 was found at the extrusion for the application of the frictionless constraint, and should therefore not be considered.

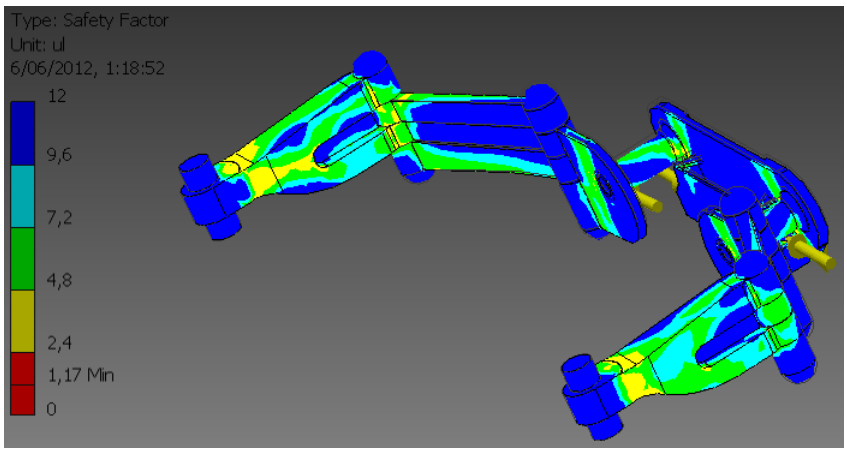

Figure 5.29.: Safety factors for the hip module

5.9. Conclusion

The orthosis was fitted onto a model of a human being in Inventor. A preliminary study has been executed to ensure that the orthosis does not hinder the subject in level walking. An extra safety has been implemented by adding mechanical stops at the actuated joints to prevent injuries in case of orthosis malfunction.

The final design consists of 90 parts, which are all listed with their weight in the bill of materials in Appendix G. The total weight of the orthosis is 10.67 kg. Literature [31, 4] learns us that similar devices such as HAL and ReWalk weigh respectively 15 and 20 kg. The weight of our design is thus more than acceptable.

6. Future work

The design of an actuated orthosis for every-day life is not a one day job. In this thesis, we carefully considered the design requirements before actually designing the orthosis. Despite the authors' effort, the final design still does not meet all of these requirements, so work still remains to be done. The most important and perhaps most challenging issues are listed and discussed below.

6.1. Design of locking mechanism

A possible embodiment for the locking mechanism was presented in subsection 5.4.1, but it was not completely elaborated. As we explained in this subsection, a carefully designed locking mechanism is essential to guarantee the orthosis' safety and wearability. A detailed study of its behaviour during various activities (e.g. sitting, stair descent and ascent) must be conducted to ensure that it does not hamper the wearer, and if it does, measures must be taken to avoid this. The locking must also be secure, so that the wearer can confidently rely on the system to carry his/her weight. A compact, silent, lightweight design that incorporates these features will undoubtedly contribute to the success of an energy-efficient orthosis. Despite years of experience with knee locking mechanisms in stance-control knee-ankle-foot orthoses, the ideal solution is yet to be found, making this an interesting area of research for the coming years [58].

6.2. Design of ankle inversion/eversion joint

Because the ankle inversion/eversion joint is not collinear with the ankle joint, the orthosis will undergo a vertical displacement when the ankle is inverted/everted. This causes the orthosis to slide along the wearer's leg and the orthosis and biological joints to not longer be colocated. In short, the current design could cause some discomfort to the wearer. To the author's knowledge, orthoses with an inversion/eversion joint that succesfully copes with this problem are yet to be reported. The development of such a joint is an important challenge for the future.

6.3. Testing

The design was based on several assumptions (section 3.2). Tests with a prototype can reveal

- whether the allowed ROM of the orthosis is not too strict, nor too permissive
- whether the secondary DOFs are sufficient to allow comfortable motion
- whether the delivered torque (50%) is sufficient
- the exact amount of weight that is transferred to the ground by the orthosis

Test results will be pivotal to gaining a better understanding of assistive exoskeletons and will eventually lead to better a design.

6.4. Ability to perform other activities

The orthosis was optimized for level walking. The final goal of the CYBERLEGs project, however, is to build an orthosis that can be worn the entire day. Thus, it will also be participate in activities such as sitting, stair ascent/descent, walking on a slope,... These activities each have their own kinematics and kinetics, which will have to be studied thoroughly. The performance of the orthosis in these circumstances will need to be evaluated, motor control has to be adapted to perform the correct actions for different activities and strategies have to be developed to recognise these activities. Likely outcomes are that motors will need to be resized or added (in particular a knee motor) and that compliance of the springs will need to be adapted. The parallel springs may even require new locking mechanisms or may be suppressed completely. This is illustrated in the following, simple example.

In a passive activity such as sitting, we would want the exoskeleton to not deliver any torque at any joint. However, when seated, the knee is flexed approximately 90°. The parallel springs at the hips have equilibrium angles of 0° (orthosis side) and 10° (prosthesis side) and are designed for walking, providing the correct amount of torque in a ROM from 11° extension to 22° flexion. 90° of flexion would lead to extension torques of 30 Nm (orthosis side hip) and 50 Nm (prosthesis side hip). These torques not only make sitting uncomfortable, but the springs are in fact not even designed to withstand them. A locking mechanism would thus be required to allow the torsion springs to move freely at some instances.

Of course, locking mechanisms add to the complexity of the design and - together with the parallel springs they engage - to the total mass of the orthosis. When the parallel springs are not active, the entire mechanism is simply carried around as dead weight. The benefit of having them instead of a larger motor must therefore be reassessed when a broader range of activities is considered.

7. General conclusions

The goal of this thesis was to design an actuated, wearable, assistive orthosis for transfemoral amputees. A literature study on exoskeletons revealed the importance of defining the right requirements for the orthosis. A significant portion of the time reserved for this thesis was thus dedicated to specifying and understanding these requirements.

The amount of assistance the orthosis has to provide was estimated based on isokinetic torque data from young and elderly people. This led to the conclusion that the orthosis would need to supply about 50% of the biological torque.

Another important consideration is the amount of degrees of freedom the orthosis should have and which should be actuated. Based on the kinematics and kinetics of walking and considerations such as balance, we suggested an orthosis with six DOFs of which the flexion/extension DOFs - the primary DOFs for walking - are all actuated. Hip abduction/adduction torque was to be delivered by a spring.

Minimizing weight was seen as one of the major design challenges. An important step towards this goal can be taken by maximizing energy-efficiency. For this purpose, we sought to transfer the energy absorbed in the knee to the ankle and hip joints. This search led to the concept of the common spring MACCEPA, which was thoroughly discussed. The common spring MACCEPA was found to effectively transfer energy from one joint to the other. The parallel springs were identified as an important tool for tuning the moment at which the energy is made available for transfer.

Nevertheless, for the actual design, another concept was favored. Two biarticular MACCEPAs were used, connecting the ankle and hip to the knee, with motors only at the ankle and hip joint. Simulations showed that, despite the absence of a knee motor, the torques provided by the orthosis were reasonably close to the biological ones. With this concept, 2.3J is transferred from the knee to the ankle and hip, which represents 19% of the total available biological energy. The total energy consumption of the orthosis - disregarding electronics - is 32J per step, which is consumed by a 40W motor at the ankle and two 15W motors at the hips. A 2,015kg battery pack was considered sufficient to cover the orthosis' energy needs for one entire day.

Incorporating the secondary DOFs was found to be one of the most challenging issues. In a design with many DOFs, it is inevitable to have non-colocated joints. These will cause the orthosis to move relative to the wearer, hampering normal movement and causing discomfort. Tests should reveal how badly this affects walking

comfort and metabolic consumption, and consequently how many effort must be put into designing mechanisms that minimize the effect.

Although the orthosis was designed with the sole goal of assisting walking at a well-defined speed, we always mentioned the importance of adaptivity for a wearable design. The addition of a knee motor is most likely inevitable if activities such as stair climbing and rising from a chair are considered, and the use of parallel springs must be reviewed for every activity other than walking. In short, it is very likely that adaptations will have to be made to the design to make it fully functional for daily life.

In conclusion, we have designed an actuated orthosis that incorporates the principles of energy transfer and energy storage and release through passive elastic elements. Even though there is still a long way to go to reach the ambitious goal of designing an orthosis that provides assistance to the dysvascular transfemoral amputee during all of his every-day activities, with this thesis, we hope to have provided valuable insights that will one day lead to attaining this admirable goal.

Appendix

A. Ankle-knee common spring MACCEPA

A.1. Mathematical expressions

Determination of the amount of spring extension will allow us to calculate the spring force and thus the torque applied to the joint by the MACCEPA system. Note that the spring will be extended by movement of both ankle and knee lever arm. The total change in spring length will thus be the summation of spring extension at the knee and spring extension at the ankle (Equation A.1).

$$\Delta l = \Delta x_A + \Delta x_K \tag{A.1}$$

Let us first look at the ankle. In Figure A.1 one can find the schematics of the design at the ankle without the active component.

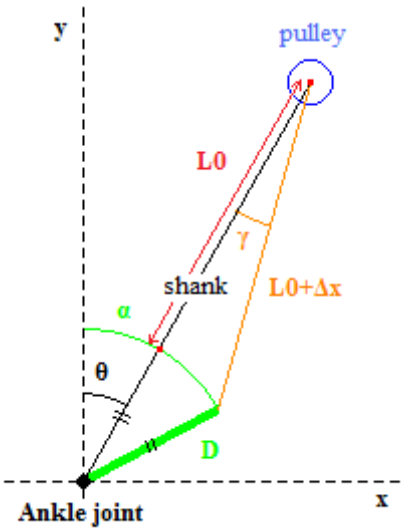

Figure A.1.: Ankle-knee common MACCEPA schematics for the ankle

The parameters in the schematic represent:

y-axis Reference axis

θ	The angle between the shank and the y-axis, positive if the foot is dorsiflexed
α	The angle between the lever arm and the y-axis
D	Length of the lever arm
L_0	Distance between the top of the lever arm (in upright position) and the pulley
Δx_A	Spring extension resulting from ankle motion
γ	Angle between the shank and the cable

Using the law of cosines, one can calculate the varying spring extension.

$$(\Delta x_A + L_0)^2 = (L_0 + D)^2 + D^2 - 2(L_0 + D) \cdot D \cdot cos(\alpha - \theta)$$

$$\Rightarrow \Delta x_A = \sqrt{(L_0 + D)^2 + D^2 - 2 \cdot D \cdot (L_0 + D) \cdot cos(\alpha - \theta)} - L_0 \tag{A.2}$$

As for the knee, the schematics of the design, without the active component, can be found in Figure A.2.

For clarity we used the same symbols although one has to take in mind that the reference is chosen differently:

y-axis	Reference axis
θ	The angle between the shank and the thigh, negative if the knee is flexed
α	The angle between the lever arm and the thigh
D	Length of the lever arm
L_0	Distance between the top of the lever arm (in upright position) and the pulley
Δx_K	Spring extension resulting from knee motion
γ	Angle between the shank and the cable

To keep the calculations simple, we worked with a positive angle θ the same way we did at the ankle. In case of the knee this corresponds to an overstretched leg. Note that this is greatly exaggerated in the schematic for clarity. Application of the law of cosines and the law of sines results in the exact same formula (Equation A.2) for the spring extension caused by knee motion. One has to take into account though that the parameters L_0, α and D have specific values for each joint.

At this point we are able to calculate the total spring extension Δl as a function of the design parameters. The next step is to determine the relation between this extension and the torque exerted at the knee and ankle joint.

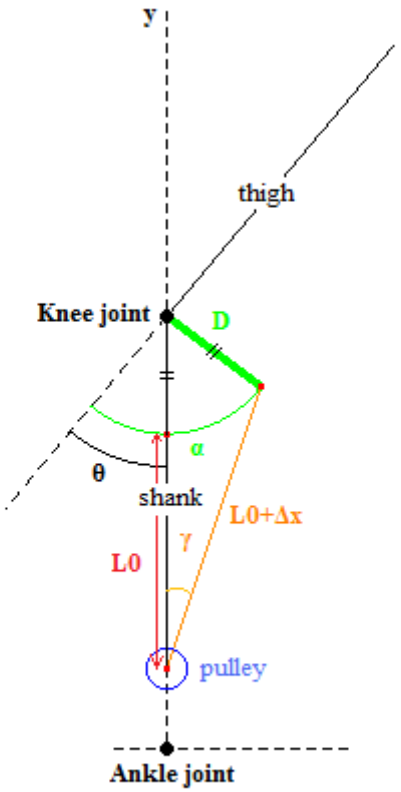

Figure A.2.: Ankle-knee common MACCEPA schematics for the knee

The spring force F_V can be determined if one knows the spring constant k, spring extension Δl and pretensioning Δx_0 of the spring.

$$F_V = k \cdot (\Delta l + \Delta x_0) \tag{A.3}$$

Keep in mind that it is only the projection of the spring force perpendicular to the leg that contributes in the joint torque. Therefore it is necessary to express the angle γ in the chosen parameters. Application of the law of sines allows us to do so.

$$\frac{D}{sin\gamma} = \frac{L_0 + \Delta x}{sin(\alpha - \theta)}$$

$$\Rightarrow sin\gamma = \frac{D \cdot sin(\alpha - \theta)}{L_0 + \Delta x} \tag{A.4}$$

This formula is again valid for both the case of the ankle and the knee. One only has to fill in the appropriate parameter values. Use of Equation A.1, Equation A.2,

Equation A.3 and Equation A.4 allows us to express the torque as follows:

$$\begin{aligned} T &= F_V \cdot sin\gamma \cdot (L_0 + D) \\ &= k \cdot (\Delta l + \Delta x_0) \cdot sin\gamma \cdot (L_0 + D) \\ &= k \cdot (\Delta x_A + \Delta x_K + \Delta x_0) \cdot sin\gamma \cdot (L_0 + D) \end{aligned} \tag{A.5}$$

The required motor power for repositioning the lever arm is calculated by multiplying the exerted torque with the angular velocity $\dot{\alpha}$. For each position of the lever arm, the torque can be calculated using Equation A.5. Since the lever arm angles α are only known at discrete points throughout the gait cycle, we cannot determine the angular velocity continuously. We will calculate $\dot{\alpha}$ by numerical differentiation. We chose to use the central formulation (Equation A.6).

$$\dot{\alpha_i} = \frac{\alpha_{i+1} - \alpha_{i-1}}{2dt} \tag{A.6}$$

The angular acceleration is calculated in the same manner (Equation A.7).

$$\ddot{\alpha_i} = \frac{\alpha_{i+1} - 2\alpha_i + \alpha_{i-1}}{dt^2} \tag{A.7}$$

The same formulas are applied to calculate the angular velocities and accelerations of the biological joints, $\dot{\theta}$ and $\ddot{\theta}$.

A.2. Matlab optimization

The optimization is carried out using Matlab's fmincon solver.

A.2.1. Biological data

Biological data retreived from [57], which is used as a reference for kinematics and kinetics. Torques are scaled by 50% and data is applied to a 75kg subject.

```
% biological data: [ankle knee hip]
% data is for a 75kg person and is scaled: only 50% of the biological
    torque should be delivered by the orthosis

%angle in degrees
BAngle = [
0.30     -3.09    19.15;
-2.06    -7.00    18.92;
-3.88    -10.52   18.45;
-4.60    -14.12   17.94;
-3.98    -17.38   17.30;
-2.40    -19.84   16.40;
```

```
−0.45    −21.27   15.18;
1.45     −21.67   13.67;
3.04     −21.22   11.97;
4.27     −20.20   10.21;
5.13     −18.86   8.48;
5.71     −17.35   6.74;
6.10     −15.73   4.94;
6.43     −14.08   3.13;
6.76     −12.50   1.42;
7.12     −11.09   −0.13;
7.54     −9.91    −1.54;
7.99     −8.97    −2.87;
8.44     −8.28    −4.12;
8.86     −7.86    −5.30;
9.23     −7.72    −6.40;
9.51     −7.94    −7.43;
9.62     −8.60    −8.39;
9.43     −9.76    −9.27;
8.70     −11.50   −10.02;
7.20     −13.86   −10.61;
4.69     −16.97   −10.95;
1.15     −20.96   −10.91;
−3.26    −26.00   −10.31;
−8.17    −32.03   −9.00;
−13.05   −38.74   −6.95;
−17.13   −45.60   −4.25;
−19.52   −52.05   −1.05;
−19.77   −57.54   2.42;
−18.12   −61.66   5.93;
−15.29   −64.12   9.22;
−12.04   −64.86   12.11;
−8.85    −63.95   14.55;
−5.96    −61.59   16.53;
−3.51    −57.97   18.13;
−1.64    −53.27   19.45;
−0.50    −47.58   20.54;
−0.07    −40.94   21.38;
−0.16    −33.46   21.84;
−0.42    −25.38   21.87;
−0.52    −17.27   21.50;
−0.26    −9.94    20.84;
0.36     −4.31    20.09;
1.00     −1.12    19.50;
1.20     −0.54    19.18];

%torque in Nm
BTorque = [
0        −6.5625  −6.375;
1.275    −10.5375         −22.5;
2.4      −3.375   −20.85;
1.9125   6.4875   −15.6;
−1.05    13.575   −13.4625;
```

```
−5.3625  19.05    −11.4375;
−9.75    22.2375  −9.1875;
−13.8    23.0625  −5.9625;
−17.5875          20.85    −3.15;
−20.4375          17.5875  0;
−22.5375          13.575   2.4;
−24.375  9.15     3.45;
−25.95   5.2875   3.675;
−27.6    1.95     3.45;
−29.25   −0.7125  3.1875;
−30.9375          −2.625   3.3;
−33.0375          −4.275   3.75;
−35.6625          −5.5875  4.875;
−38.8875          −6.7875  6.3;
−42.9    −8.1375  7.4625;
−47.25   −9.2625  8.6625;
−52.05   −10.0875          10.0875;
−56.7375          −10.125  11.7;
−60.3    −8.8875  13.65;
−61.05   −6.4125  15.0375;
−58.6875          −3.2625  15.15;
−52.05   −0.15    13.35;
−40.2375          2.025    9.825;
−25.875  4.35     9.4125;
−12.5625          5.8875   11.625;
−3.825   5.85     12.9;
0.0375   4.275    11.0625;
1.05     3        8.55;
0.8625   2.475    6.3375;
0.7125   2.4      4.725;
0.5625   1.9875   3.3375;
0.45     1.3875   2.5875;
0.375    0.75     2.1375;
0.375    0.15     1.65;
0.375    −0.3375  0.975;
0.4125   −0.8625  0.3375;
0.45     −1.5     −0.3;
0.4875   −2.2125  −1.0875;
0.4875   −3.075   −2.25;
0.4125   −4.275   −3.975;
0.225    −5.925   −6.375;
−0.0375  −7.9125  −9.075;
−0.2625  −9.4875  −11.1;
−0.4125  −9.8625  −11.2875;
−0.375   −8.4     −8.8875];

%power in W
BPower = [
0.00     16.23    0.63;
−2.04    29.97    6.03;
−2.33    9.20     7.82;
−0.07    −17.03   6.87;
```

```
−0.88    −29.72   7.94;
−7.25    −28.36   9.28;
−14.37   −15.58   9.60;
−18.43   0.44     7.33;
−18.98   11.73    4.17;
−16.35   15.89    0.00;
−12.42   14.81    −3.19;
−9.05    10.96    −4.67;
−7.15    6.62     −5.08;
−6.97    2.41     −4.65;
−7.72    −0.82    −3.98;
−9.24    −2.60    −3.74;
−11.00   −3.47    −3.93;
−12.28   −3.49    −4.81;
−12.95   −2.88    −5.86;
−12.97   −1.74    −6.51;
−11.76   0.28     −7.06;
−7.77    3.40     −7.68;
1.74     7.05     −8.24;
21.23    9.86     −8.52;
52.11    10.06    −7.71;
90.07    6.83     −5.39;
120.53   0.41     −1.53;
122.44   −7.00    2.41;
92.30    −18.43   6.88;
47.07    −28.71   14.95;
13.12    −30.38   23.45;
−0.09    −21.78   24.98;
−1.06    −13.71   21.83;
0.46     −9.10    16.93;
1.22     −6.04    12.30;
1.31     −2.43    7.89;
1.11     0.09     5.28;
0.87     0.94     3.62;
0.77     0.34     2.26;
0.62     −1.07    1.09;
0.48     −3.43    0.31;
0.27     −7.08    −0.22;
0.06     −11.96   −0.54;
−0.07    −18.31   −0.42;
−0.06    −26.49   0.52;
0.01     −35.01   2.51;
−0.01    −39.25   4.90;
−0.13    −32.03   5.69;
−0.13    −14.23   3.93;
0.10     6.33     1.19];

%data generation
thetaA = BAngle(:,1)/180*pi; %angle in radians
thetaK = BAngle(:,2)/180*pi; %angle in radians
thetaH = BAngle(:,3)/180*pi; %angle in radians
BTorqueA = BTorque(:,1);
```

```
BTorqueK = BTorque(:,2);
BTorqueH = BTorque(:,3);
BPowerA = BPower(:,1);
BPowerK = BPower(:,2);
BPowerH = BPower(:,3);
thetaAP = BAngle2(:,1)/180*pi; %angle in radians
thetaKP = BAngle2(:,2)/180*pi; %angle in radians
thetaHP = BAngle2(:,3)/180*pi; %angle in radians
BTorqueAP = BTorque2(:,1);
BTorqueKP = BTorque2(:,2);
BTorqueHP = BTorque2(:,3);
BPowerAP = BPower2(:,1);
BPowerKP = BPower2(:,2);
BPowerHP = BPower2(:,3);

%evaluation times in % gait cycle
time = transpose([0:2:98]);

% stride time and delta t
ST = 1.14; %sec
dt = ST/50;

%antropometric data
Lthigh=0.41;
Lshank=0.38;

%angular velocities
omegaA(1)=(thetaA(2)-thetaA(50))/2/dt;
omegaK(1)=(thetaK(2)-thetaK(50))/2/dt;
omegaH(1)=(thetaH(2)-thetaH(50))/2/dt;
for i=2:49
    omegaA(i)=(thetaA(i+1)-thetaA(i-1))/2/dt;
    omegaK(i)=(thetaK(i+1)-thetaK(i-1))/2/dt;
    omegaH(i)=(thetaH(i+1)-thetaH(i-1))/2/dt;
end
omegaA(50)=(thetaA(1)-thetaA(49))/2/dt;
omegaK(50)=(thetaK(1)-thetaK(49))/2/dt;
omegaH(50)=(thetaH(1)-thetaH(49))/2/dt;
omegaAP = [omegaA(26:50) omegaA(1:25)];
omegaKP = [omegaK(26:50) omegaK(1:25)];
omegaHP = [omegaH(26:50) omegaH(1:25)];
```

A.2.2. Objective

```
function f = myobj0(x)
% Optimisation cost function for ankle+knee maccepa without ankle and
    knee springs. First run ConstraintsBounds0 to create constraint,
    bound and initial value matrices. Use nonlconstr0 as non-linear
    constraints in optimtool solver. Bounds LB and UB, Linear
    inequalities A and b.
```

```
BiologicalData; % Insert biological data
% x(1-50) = alfaA    in radians
% x(51-100) = alfaK    in radians
% x(101) = k   in N/m
% x(102) = dx0    in m
% x(103) = DA    in m
% x(104) = DK    in m
% x(105) = L0A    in m
% x(106) = L0K   in m

% calculation of the powers: velocity and torques
for i= 1:50
dlA(i)=sqrt((x(105)+x(103))^2+x(103)^2-2*x(103)*(x(105)+x(103))*cos(
    thetaA(i)-x(i)))-x(105);
dlK(i)=sqrt((x(106)+x(104))^2+x(104)^2-2*x(104)*(x(106)+x(104))*cos(
    thetaK(i)-x(i+50)))-x(106);
TA(i)=x(101)*(x(102)+dlA(i)+dlK(i))*x(103)*sin(x(i)-thetaA(i))/(dlA(i)+
    x(105))*(x(105)+x(103));
TK(i)=x(101)*(x(102)+dlA(i)+dlK(i))*x(104)*sin(x(i+50)-thetaK(i))/(dlK(
    i)+x(106))*(x(106)+x(104));
end

for i= 2:49
velA(i) = (x(i+1)-x(i-1))/2/dt;
velK(i) = (x(i+1+50)-x(i-1+50))/2/dt;
end
velA(1) = (x(2)-x(50))/2/dt;
velK(1) = (x(2+50)-x(50+50))/2/dt;
velA(50) = (x(1)-x(49))/2/dt;
velK(50) = (x(1+50)-x(49+50))/2/dt;

O(1)=0;
for i= 1:50
O(1) = O(1)+ (velA(i)*TA(i))^2 + (velK(i)*TK(i))^2;
end

% calculate acceleration
O(2)=(x(50)-2*x(1)+x(2))^2/dt^4; %sum((accA)^2)
for i=2:49
O(2) = O(2)+(x(i-1)-2*x(i)+x(i+1))^2/dt^4;
end
O(2) = O(2)+(x(49)-2*x(50)+x(1))^2/dt^4;
O(3)=(x(50+50)-2*x(50+1)+x(52))^2/dt^4; %sum((accA)^2)
for i=2:49
O(3) = O(3)+(x(i-1+50)-2*x(i+50)+x(i+51))^2/dt^4;
end
O(3) = O(3)+(x(49+50)-2*x(50+50)+x(1+50))^2/dt^4;

% calculate torque difference
O(4)=0; %sum(dTA^2)
O(5)=0; %sum(dTK^2)
for i= 1:50
```

```
O(4)=O(4)+(BTorqueA(i)-TA(i))^2;
O(5)=O(5)+(BTorqueK(i)-TK(i))^2;
end

f = O(1) + 0.0002*(O(2) + O(3)) + 10*(O(4) + 2*O(5));function f =
    myobj0(x)
% Optimisation cost function for ankle+knee maccepa without ankle and
    knee
% springs.
% First run ConstraintsBounds0 to create constraint, bound and initial
    value matrices.
% Use nonlconstr0 as non-linear constraints in optimtool solver. Bounds
     LB and UB, Linear inequalities A and b.

BiologicalData;
%x(1-50) = alfaA  in radians
%x(51-100) = alfaK  in radians
%x(101) = k  in N/m
%x(102) = dx0  in m
%x(103) = DA  in m
%x(104) = DK  in m
%x(105) = L0A  in m
%x(106) = L0K  in m

% calculation of the powers: velocity and torques
for i= 1:50
    dlA(i)=sqrt((x(105)+x(103))^2+x(103)^2-2*x(103)*(x(105)+x(103))*cos
        (thetaA(i)-x(i)))-x(105);
    dlK(i)=sqrt((x(106)+x(104))^2+x(104)^2-2*x(104)*(x(106)+x(104))*cos
        (thetaK(i)-x(i+50)))-x(106);
    TA(i)=x(101)*(x(102)+dlA(i)+dlK(i))*x(103)*sin(x(i)-thetaA(i))/(dlA
        (i)+x(105))*(x(105)+x(103));
    TK(i)=x(101)*(x(102)+dlA(i)+dlK(i))*x(104)*sin(x(i+50)-thetaK(i))/(
        dlK(i)+x(106))*(x(106)+x(104));
end

for i= 2:49
    velA(i) = (x(i+1)-x(i-1))/2/dt;
    velK(i) = (x(i+1+50)-x(i-1+50))/2/dt;
end
velA(1) = (x(2)-x(50))/2/dt;
velK(1) = (x(2+50)-x(50+50))/2/dt;
velA(50) = (x(1)-x(49))/2/dt;
velK(50) = (x(1+50)-x(49+50))/2/dt;

O(1)=0;
for i= 1:50
    O(1) = O(1)+ (velA(i)*TA(i))^2 + (velK(i)*TK(i))^2;
end

% calculate acceleration
O(2)=(x(50)-2*x(1)+x(2))^2/dt^4; %sum((accA)^2)
```

```
for i=2:49
    O(2) = O(2)+(x(i-1)-2*x(i)+x(i+1))^2/dt^4;
end
O(2) = O(2)+(x(49)-2*x(50)+x(1))^2/dt^4;

O(3)=(x(50+50)-2*x(50+1)+x(52))^2/dt^4; %sum((accA)^2)
for i=2:49
    O(3) = O(3)+(x(i-1+50)-2*x(i+50)+x(i+51))^2/dt^4;
end
O(3) = O(3)+(x(49+50)-2*x(50+50)+x(1+50))^2/dt^4;


% calculate torque difference
O(4)=0; %sum(dTA^2)
O(5)=0; %sum(dTK^2)
for i= 1:50
    O(4)=O(4)+(BTorqueA(i)-TA(i))^2;
    O(5)=O(5)+(BTorqueK(i)-TK(i))^2;
end

f = O(1) + 0.0002*(O(2) + O(3)) + 10*(O(4) + 2*O(5));
```

A.2.3. Constraints

All constraints applicable to the parameters can be found in Table A.1. Note that the constraints on α, L_0 and D are valid for both knee and ankle.

Constraint	Units	Explanation
$-\frac{\pi}{2} \leqslant \alpha \leqslant \frac{\pi}{2}$	rad	These values of α allow us to reach the entire torque range
$-\pi \leqslant \alpha - \theta \leqslant \pi$	rad	These values of α allow us to reach the entire torque range
$0 \leqslant \Delta x_0 \leqslant 0.10$	m	Initial spring extension is limited so that the spring fits in between the pulleys
$0.01 \leqslant L_0 \leqslant 0.20$	m	L_0 should be at least 10 mm te ensure clearance between pulley and lever arm
$0.03 \leqslant D \leqslant 0.12$	m	Range of realistical values for D
$2000 \leqslant k \leqslant 200000$	N/m	Range of realistical values for k
$L_{0A} + L_{0K} + D_A + D_K \leqslant 0.25$	m	Make sure the entire construction fits on the shank
$0 \leqslant \Delta l_A + \Delta l_K \leqslant 0.20$	m	Extended spring should fit in between the pulleys

Table A.1.: Constraints for the ankle-knee MACCEPA optimization

Constraints should be transformed into one of the permitted formulations.

All red constraints are *bounds*: one parameter limited by two numerical values. They

can be inserted in the optimization by means of a matrix equation: $LB \leqslant x \leqslant UB$, with x the vector of all parameters, LB the lower bounds and UB the upper bounds.

The blue constraints are *linear inequalities*: a linear function of the parameters limited by certain numerical values. Linear inequalities should be united in one matrix equation $A \cdot x \leqslant b$. A is a matrix of dimensions $NumberOfLinearConstraints \times NumberOfParameters$, while b is a vector with *NumberOfLinearConstraints* elements.

The green one is a *non-linear constraint* since the extension of the spring, dl, is a non-linear function of the parameters. The non-linear constraints are defined in a separate Matlab file and should be written in the form $f(x) \leqslant 0$.

A.2.3.1. Bounds, linear contraints and initial values

```
% Function that defines matrices containing the lower and upper bounds
    and
% matrices of the linear constraints. Goes with myobj0
% Bounds: Lower bound <= x <= Upper bound
% Units defined in myobj0

% Lower bound
LB = zeros(106,1);
for i = 1:100
    LB(i,1)=-pi/2;
end
LB(101,1) = 2000;
LB(102,1) = 0;
LB(103,1) = 0.03;
LB(104,1) = 0.03;
LB(105,1) = 0.01;
LB(106,1) = 0.01;

%Upper bound
UB = zeros(106,1);
for i = 1:100
    UB(i,1)=pi/2;
end
UB(101,1) = 100000;
UB(102,1) = 0.1;
UB(103,1) = 0.12;
UB(104,1) = 0.12;
UB(105,1) = 0.2;
UB(106,1) = 0.2;

%Linear constraints: Ax <= b
BiologicalData;
A=[eye(50) zeros(50) zeros(50,6);
    -eye(50) zeros(50) zeros(50,6);
    zeros(50) eye(50) zeros(50,6);
    zeros(50) -eye(50) zeros(50,6);
```

```
    zeros(1,50) zeros(1,50) [0 0 1 0 1 0];
    zeros(1,50) zeros(1,50) [0 0 0 1 0 1];
    zeros(1,50) zeros(1,50) [0 0 1 1 1 1]];
b=[pi+thetaA;
    pi-thetaA;
    pi+thetaK;
    pi-thetaK;
    0.25;
    0.25;
    0.25];

% initial values result from Excel-optimization
Init=[
0.008271154;
-0.021179953;
-0.050083445;
-0.067102591;
-0.075396484;
-0.073874055;
-0.065476392;
-0.057424251;
-0.054800108;
-0.055453624;
-0.057830662;
-0.060929999;
-0.063423503;
-0.065955346;
-0.069103873;
-0.073238783;
-0.078774409;
-0.085969333;
-0.094699539;
-0.105011951;
-0.11606867;
-0.127845035;
-0.139681173;
-0.151300016;
-0.162062977;
-0.172483799;
-0.18342071;
-0.19448721;
-0.207623559;
-0.229295894;
-0.263566253;
-0.298974901;
-0.34068827;
-0.345051593;
-0.31625366;
-0.266860843;
-0.210137642;
-0.154461639;
-0.104021623;
```

−0.061261057;
−0.0286234;
−0.008726646;
−0.00122173;
−0.002792527;
−0.007330383;
−0.009075712;
−0.004537856;
0.006283185;
0.017453293;
0.020943951;
−0.120633548;
−0.189106682;
−0.206886399;
−0.194102528;
−0.188454506;
−0.189480451;
−0.191378132;
−0.193533572;
−0.200471496;
−0.20887843;
−0.218701919;
−0.228284861;
−0.232682572;
−0.231130154;
−0.224546967;
−0.215133431;
−0.206546171;
−0.199496464;
−0.195263797;
−0.195002201;
−0.197463725;
−0.202815596;
−0.210367555;
−0.219660742;
−0.232752238;
−0.253559369;
−0.288724884;
−0.344601656;
−0.420010195;
−0.519763872;
−0.642164473;
−0.772333275;
−0.890245786;
−0.986975842;
−1.057484294;
−1.101735664;
−1.119181091;
−1.109405706;
−1.073590999;
−1.01432833;
−0.935338887;

```
-0.838794474;
-0.725530251;
-0.597901499;
-0.4619754;
-0.330520603;
-0.221524318;
-0.148011734;
-0.10796041;
-0.094227795;
55631.25954;
0.016854685;
0.085844102;
0.054595408;
0.113967554;
0.045592936];
```

The initial values allow us to attain a better solution starting from the first run. These values result from an Excel optimization (using the Solver add-in and some manual fine-tuning) which was performed prior to programming in Matlab.

A.2.3.2. Non-linear constraints

```
function [c,ceq] = nonlconstr0(x)
% Non-linear constraints to go with myobj0

BiologicalData; % Insert biological data

g = zeros(50,1);
for i = 1:50
g(i)=-sqrt((x(103)+x(105))^2+x(103)^2-2*x(103)*(x(103)+x(105))*cos(x(i)
    -thetaA(i)))+x(105)-sqrt((x(104)+x(106))^2+x(104)^2-2*x(104)*(x
    (104)+x(106))*cos(x(i+50)-thetaK(i)))+x(106);
end

% non-linear inequalities ( rewrite as: ... <= 0)
c = [g;
        -g - 0.2];

% non-linear equalities
ceq = [];
```

A.3. Results

The parameter values resulting from the optimization can be found in Table A.2.

The lever arm angles are plotted together with the biological joint angles. During swing both become nearly equal, i.e. the lever arm moves together with the leg. This results in a low torque applied by the MACCEPA, in agreement with the low torque which is imposed.

Parameter	Optimized value	Parameter	Optimized value
$\alpha_A(i)$	Figure A.3	D_A	128 mm
$\alpha_K(i)$	Figure A.3	D_K	28.1 mm
k	18.5 N/mm	L_{0A}	83.9 mm
Δx_0	0 mm	L_{0K}	10.0 mm

Table A.2.: Results of the ankle-knee MACCEPA optimization

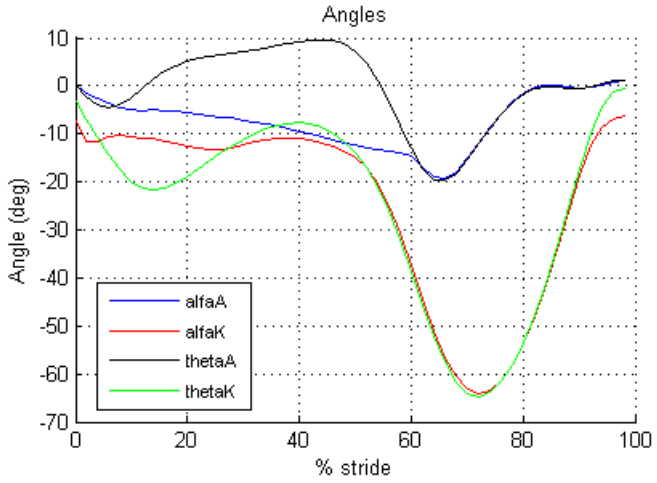

Figure A.3.: Lever arm angles for the ankle-knee common MACCEPA

B. Addition of springs

B.1. Mathematical expressions

When calculating the torque at one joint, the use of Equation A.5 no longer suffices. One needs to take into account the contributions of the added springs.

The torque provided by the ankle spring:

$$T_{A1} = min\,(0, -k_{A1} \cdot (\theta_A - \theta_{0A1})) \tag{B.1}$$

With this formulation, the spring is engaged only when $\theta_A > \theta_{0A}$, i.e. when the ankle is sufficiently dorsiflexed.

The torque provided by spring 1 at the knee:

$$T_{K1} = max\,(0, -k_{K1} \cdot (\theta_K - \theta_{0K1})) \tag{B.2}$$

With this formulation, the spring is engaged only when $\theta_K < \theta_{0K1}$, i.e. when the knee is sufficiently flexed.

For spring 2:

$$T_{K2} = -k_{K2} \cdot (\theta_K - \theta_{0K2}) \tag{B.3}$$

The total amount of torque at the ankle is then calculated by adding Equation A.5 and Equation B.1. Analogously, torque at the knee is calculated by adding Equation A.5 with Equation B.2 and Equation B.3.

B.2. Matlab optimization

B.2.1. Objective

```
function f = myobj1(x)
% Optimisation cost function for ankle+knee maccepa with ankle and knee
% springs.
% First run ConstraintsBounds1 to create constraint, bound and initial
    value matrices.
% Use nonlconstr1 as non-linear constraints in optimtool solver. Bounds
     LB and UB, Linear inequalities A and b.
```

```
BiologicalData;
%x(1-50) = alfaA   in radians
%x(51-100) = alfaK   in radians
%x(101) = k   in N/m
%x(102) = dx0   in m
%x(103) = DA   in m
%x(104) = DK   in m
%x(105) = L0A   in m
%x(106) = L0K   in m
%x(107) = kA1   in Nm/rad
%x(108) = theta0A1   in radians
%x(109) = kK1   in Nm/rad
%x(110) = theta0K1   in radians
%x(111) = kK2   in Nm/rad
%x(112) = theta0K2   in radians

% Calculation torque
% T from spring 1
TK1(1:50)=zeros(1,50);
for i=2:24
    TK1(i)= max(0,-x(109)*(thetaK(i)-x(110)));
end

% T from ankle spring
TA1(1:50)=zeros(1,50);
for i=1:50
    TA1(i)= min(0, -x(107)*(thetaA(i)-x(108)));
end

% T calculation common spring and spring 2
for i= 1:50
    dlA(i)=sqrt((x(105)+x(103))^2+x(103)^2-2*x(103)*(x(105)+x(103))*cos
        (thetaA(i)-x(i)))-x(105);
    dlK(i)=sqrt((x(106)+x(104))^2+x(104)^2-2*x(104)*(x(106)+x(104))*cos
        (thetaK(i)-x(i+50)))-x(106);
    %T common spring at the ankle
    TA(i)=x(101)*(x(102)+dlA(i)+dlK(i))*x(103)*sin(x(i)-thetaA(i))/(dlA
        (i)+x(105))*(x(105)+x(103));
    %T common spring at the knee
    TK(i)=x(101)*(x(102)+dlA(i)+dlK(i))*x(104)*sin(x(i+50)-thetaK(i))/(
        dlK(i)+x(106))*(x(106)+x(104));
    %T spring 2
    TK2(i)= -x(111)*(thetaK(i)-x(112));
    %Total torque = sum of all torque contributions
    Ta(i)=TA(i)+TA1(i);
    Tk(i)=TK(i)+TK1(i)+TK2(i);
end

% Calculate velocities
for i= 2:49
    velA(i) = (x(i+1)-x(i-1))/2/dt;
```

```
    velK(i) = (x(i+1+50)-x(i-1+50))/2/dt;
end
velA(1) = (x(2)-x(50))/2/dt;
velK(1) = (x(2+50)-x(50+50))/2/dt;
velA(50) = (x(1)-x(49))/2/dt;
velK(50) = (x(1+50)-x(49+50))/2/dt;

% Calculate maccepa power
O(1)=0;
for i= 1:50
    O(1) = O(1)+ (velA(i)*TA(i))^2 + (velK(i)*TK(i))^2;
end

% Calculate acceleration
O(2)=(x(50)-2*x(1)+x(2))^2/dt^4; %sum((accA)^2)
for i=2:49
    O(2) = O(2)+(x(i-1)-2*x(i)+x(i+1))^2/dt^4;
end
O(2) = O(2)+(x(49)-2*x(50)+x(1))^2/dt^4;

O(3)=(x(50+50)-2*x(50+1)+x(52))^2/dt^4; %sum((accK)^2)
for i=2:49
    O(3) = O(3)+(x(i-1+50)-2*x(i+50)+x(i+51))^2/dt^4;
end
O(3) = O(3)+(x(49+50)-2*x(50+50)+x(1+50))^2/dt^4;


% calculate torque difference
O(4)=0; %sum(dTA^2)
O(5)=0; %sum(dTK^2)
for i= 1:50
    O(4)=O(4)+(BTorqueA(i)-Ta(i))^2;
    O(5)=O(5)+(BTorqueK(i)-Tk(i))^2;
end

f = O(1) + 0.0005*(O(2) + O(3)) + 13*(O(4) + 2*O(5));
```

B.2.2. Constraints

On the spring constants k and neutral position θ_0 of the added torsion springs, certain limitations are imposed as well. They can be found in Table B.1. Note that all additional limitations are bounds.

Constraints	Units	Explanation
$0 \leqslant k_{A1} \leqslant 500$	Nm/rad	Range of realistical values for k_{A1}
$-\frac{\pi}{9} \leqslant \theta_{0A1} \leqslant \frac{\pi}{18}$	rad	Neutral position falls within the range of motion
$0 \leqslant k_{K1} \leqslant 500$	Nm/rad	Range of realistical values for k_{K1}
$-\frac{7\pi}{18} \leqslant \theta_{0K1} \leqslant -0.1361$	rad	Explained below
$0 \leqslant k_{K2} \leqslant 500$	Nm/rad	Range of realistical values for k_{K2}
$-\frac{7\pi}{18} \leqslant \theta_{0K2} \leqslant \frac{\pi}{18}$	rad	Neutral position falls within the range of motion

Table B.1.: Additional constraints for the torsion springs

The lower bound of θ_{0K1} matches the range of motion of the knee, the upper bound does not. This value can be explained taking a look at Figure B.1. We want the locking mechanism to disengage the spring under zero tension in order to ensure an acceptable lifetime of the locking mechanism. This means that the spring is to be disengaged close to its equilibrium position. During unloading of spring 1 however, the knee never reaches an angle larger than -7.86° or -0.1361 radians (Figure B.1). The spring equilibrium position should therefore not exceed this angle. If it would, the spring would always disengage under tension.

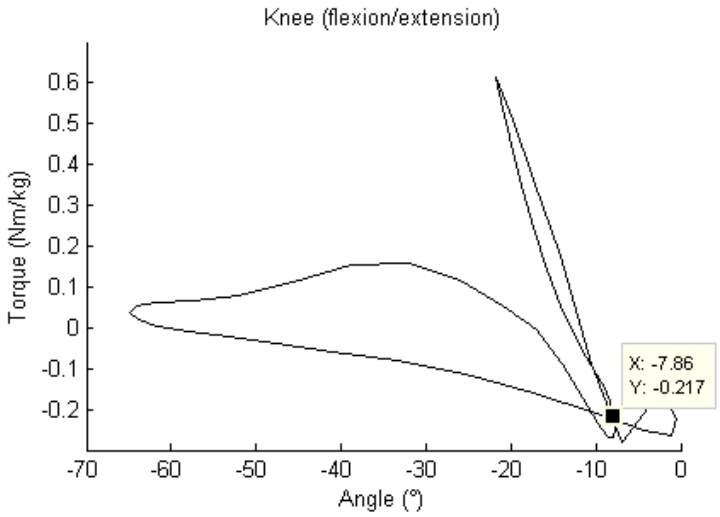

Figure B.1.: Determination of neutral position knee spring 1

B.2.2.1. Bounds, linear constraints and initial values

```
% Function that defines matrices containing the lower and upper bounds and
% matrices of the linear constraints. Goes with myobj1
% Bounds: Lower bound <= x <= Upper bound
% Units defined in myobj1

% Lower bound
```

```
LB = zeros(106,1);
for i = 1:100
    LB(i,1)=-pi/2;
end
LB(101,1) = 2000;
LB(102,1) = 0;
LB(103,1) = 0.03;
LB(104,1) = 0.03;
LB(105,1) = 0.01;
LB(106,1) = 0.01;
LB(107,1) = 0;
LB(108,1) = -20/180*pi;
LB(109,1) = 0;
LB(110,1) = -70*pi/180;
LB(111,1) = 0;
LB(112,1) = -70*pi/180;

%Upper bound
UB = zeros(106,1);
for i = 1:100
    UB(i,1)=pi/2;
end
UB(101,1) = 100000;
UB(102,1) = 0.1;
UB(103,1) = 0.12;
UB(104,1) = 0.12;
UB(105,1) = 0.2;
UB(106,1) = 0.2;
UB(107,1) = 500;
UB(108,1) = 10/180*pi;
UB(109,1) = 500;
UB(110,1) = -0.1361;
UB(111,1) = 500;
UB(112,1) = 10*pi/180;

%Linear constraints: Ax <= b
BiologicalData;
A=[eye(50) zeros(50) zeros(50,12);
    -eye(50) zeros(50) zeros(50,12);
    zeros(50) eye(50) zeros(50,12);
    zeros(50) -eye(50) zeros(50,12);
    zeros(1,50) zeros(1,50) [0 0 1 0 1 0 0 0 0 0 0 0];
    zeros(1,50) zeros(1,50) [0 0 0 1 0 1 0 0 0 0 0 0];
    zeros(1,50) zeros(1,50) [0 0 1 1 1 1 0 0 0 0 0 0]];
b=[pi+thetaA;
    pi-thetaA;
    pi+thetaK;
    pi-thetaK;
    0.25;
    0.25;
    0.25];
```

```
% Initial values
Init=[
0.005236;
-0.035954;
-0.067719;
-0.080285;
-0.080285;
-0.080285;
-0.080285;
-0.080285;
-0.080285;
-0.080285;
-0.080285;
-0.080285;
-0.080285;
-0.080285;
-0.080285;
-0.080285;
-0.080285;
-0.080285;
-0.080285;
-0.096619;
-0.102279;
-0.114593;
-0.122173;
-0.132285;
-0.140130;
-0.149614;
-0.158138;
-0.167415;
-0.179651;
-0.191048;
-0.234767;
-0.298975;
-0.340688;
-0.345052;
-0.316254;
-0.266861;
-0.210138;
-0.154462;
-0.104022;
-0.061261;
-0.028623;
-0.008727;
-0.001222;
-0.002793;
-0.007330;
-0.009076;
-0.004538;
0.006283;
0.017453;
0.020944;
```

```
−0.064170;
−0.102224;
−0.155800;
−0.213526;
−0.271798;
−0.326432;
−0.371232;
−0.378213;
−0.370359;
−0.352557;
−0.329169;
−0.302815;
−0.274540;
−0.245742;
−0.218166;
−0.193557;
−0.172962;
−0.156556;
−0.144513;
−0.110690;
−0.126886;
−0.159777;
−0.198962;
−0.244892;
−0.216449;
−0.188736;
−0.157294;
−0.149778;
−0.148878;
−0.199086;
−0.338977;
−0.505746;
−0.679924;
−0.865668;
−1.096016;
−1.281167;
−1.364103;
−1.371474;
−1.333401;
−1.259400;
−1.159756;
−1.038610;
−0.896946;
−0.742091;
−0.593780;
−0.477634;
−0.402234;
−0.344203;
−0.288619;
−0.194899;
51001.5364;
0.000543884;
```

```
0.072992901;
0.047290909;
0.010000503;
0.169715687;
150;
-4.2*pi/180;
118.9562202;
-0.164119654;
9.289587607;
-0.773534323];
```

B.2.2.2. Non-linear constraints

```
function [c,ceq] = nonlconstr1(x)
%Non-linear constraints to go with myobj1

BiologicalData;
g = zeros(50,1);

for i = 1:50
g(i)=-sqrt((x(103)+x(105))^2+x(103)^2-2*x(103)*(x(103)+x(105))*cos(x(i)
    -thetaA(i)))+x(105)-sqrt((x(104)+x(106))^2+x(104)^2-2*x(104)*(x
    (104)+x(106))*cos(x(i+50)-thetaK(i)))+x(106);
end

c = [g;
        -g - 0.2];
ceq = [];
```

B.3. Results

The values of the optimized parameters are summarised in Table B.2. A comparison of the generated torques and the required ones is depicted in Figure B.2b.

Parameter	Optimized value	Parameter	Optimized value
$\alpha_A(i)$	Figure B.2a	L_{0A}	63.3 mm
$\alpha_K(i)$	Figure B.2a	L_{0K}	11.2 mm
k	19.426 N/mm	k_{A1}	0 Nm/rad
Δx_0	0 mm	θ_{0A1}	irrelevant
D_A	120 mm	k_{K1}	124.4 Nm/rad
D_K	30 mm	θ_{0K1}	-0.1653 rad
L_{0A}	63.3 mm	k_{K2}	6.6 Nm/rad
L_{0K}	11.2 mm	θ_{0K2}	-0.9494 rad

Table B.2.: Results of the optimization with additional springs

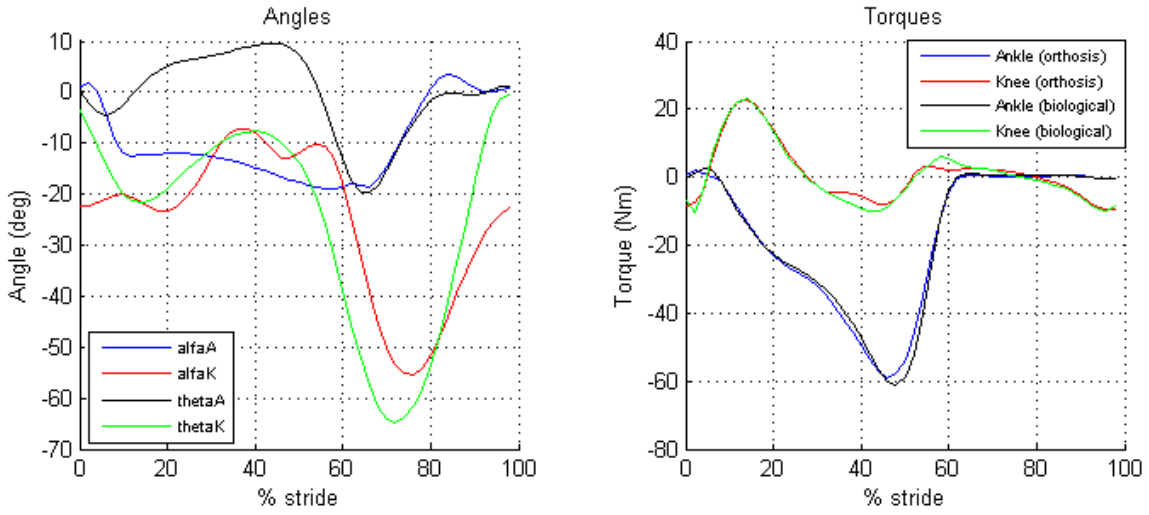

(a) Lever arm angles

(b) Generated vs. required torques

Figure B.2.: Lever arm angles and generated torques for the optimization with additional springs

C. Ankle-knee-hip without knee motor

C.1. Mathematical expressions

For the MACCEPA between the ankle and the knee, the expressions are the same as those found in section A.1. The only exception is that the lever arm angle α is fixed at the knee, i.e. only one value is used instead of 50. The same springs as in Appendix B are used, so that the formulas of this appendix are applicable as well.

The formulas for the MACCEPA between the knee and the hip are very similar to those between the ankle and the knee. The derivation of the formulas is exactly the same as in section A.1, although the final results differ due to a different parameter definition. The parameters are defined in Figure C.1 and are clarified below.

y-axis	Reference axis
θ_K	The angle between the shank and the thigh, negative if the knee is flexed
α_{Kh}	The angle between the knee lever arm and the shank
D	Length of the lever arm
L_0	Distance between the top of the lever arm (in upright position) and the pulley
Δx_{Kh}	Spring extension resulting from knee motion
γ	Angle between the thigh and the cable
θ_H	The angle between the thigh and the trunk (y-axis), positive if the hip is flexed
α_H	The angle between the hip lever arm and the y-axis
Δx_H	Spring extension resulting from hip motion

Unless specified otherwise, we will use the index Kh for the knee and the index H for the hip.

The knee-hip spring extension, Δl_h, has two contributions: Δx_{Kh} and Δx_H.

$$\Delta x_{Kh} = \sqrt{(L_{0Kh} + D_{Kh})^2 + D_{Kh}^2 - 2 \cdot D_{Kh} \cdot (L_{0Kh} + D_{Kh}) \cdot cos(\alpha_{Kh} + \theta_K)} - L_{0Kh}$$

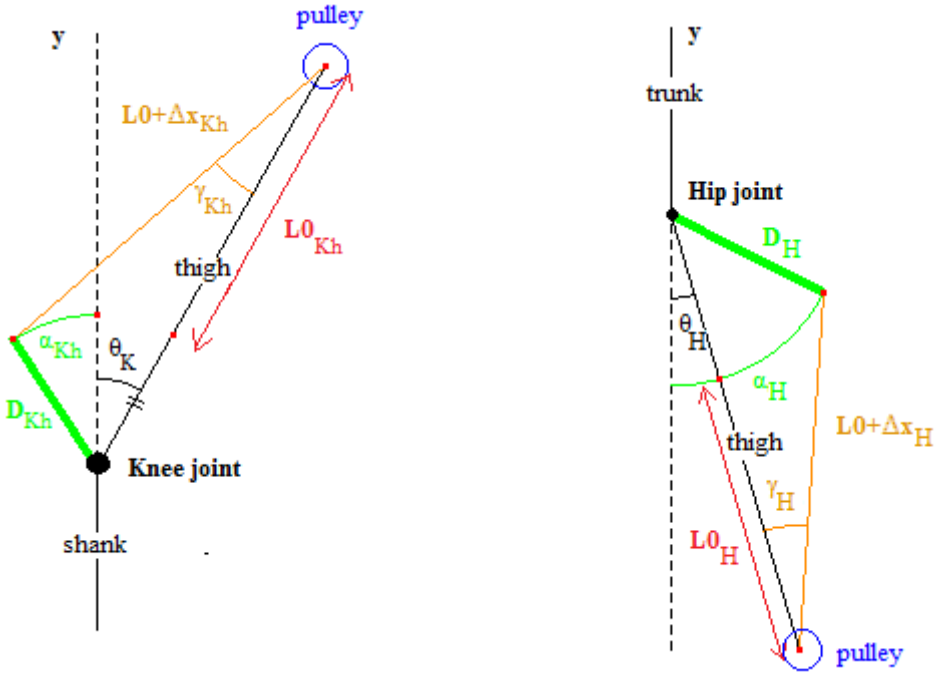

(a) Schematics knee **(b)** Schematics hip

Figure C.1.: Parameter definition for the knee-hip common MACCEPA

(C.1)

$$\Delta x_H = \sqrt{(L_{0H} + D_H)^2 + D_H^2 - 2 \cdot D_H \cdot (L_{0H} + D_H) \cdot cos(\alpha_H - \theta_H)} - L_{0H} \quad \text{(C.2)}$$

$$\Delta l_h = \Delta x_{Kh} + \Delta x_H \quad \text{(C.3)}$$

The spring force can be determined if one knows the spring constant k_h, spring extension Δl and pretensioning Δx_{0h} of the spring.

$$F_V = k_h \cdot (\Delta l_h + \Delta x_{0h}) \quad \text{(C.4)}$$

$$sin\gamma_{Kh} = \frac{D_{Kh} \cdot sin(\alpha_{Kh} + \theta_K)}{L_{0Kh} + \Delta x_{Kh}} \quad \text{(C.5)}$$

$$sin\gamma_H = \frac{D \cdot sin(\alpha_H - \theta_H)}{L_{0H} + \Delta x_H} \tag{C.6}$$

The torque is expressed as follows:

$$T_{Kh} = k_{Kh} \cdot (\Delta l_h + \Delta x_{0h}) \cdot sin\gamma_{Kh} \cdot (L_{0Kh} + D_{Kh}) \tag{C.7}$$

$$T_H = k_H \cdot (\Delta l_h + \Delta x_{0H}) \cdot sin\gamma_H \cdot (L_{0H} + D_H) \tag{C.8}$$

The required motor power for repositioning the lever arm is calculated by multiplying the exerted torque with the angular velocity $\dot{\alpha}$.

The parallel spring is described by:

$$T_{H1} = -k_{H1} \cdot (\theta_H - \theta_{0H1}) \tag{C.9}$$

The total torque at the knee can be found by adding T_{Kh} to the knee torques found in section A.1 and section B.1. The total torque at the hip is the sum of T_H and T_{H1}.

C.2. Matlab optimization

C.2.1. Parameters

The optimization parameters are:

$\alpha_A(i)$	Angle of the lever arm at the ankle (at 50 discrete moments of time i at which the biological angles θ_A are known)
α_K	Angle of the fixed lever arm at the knee (ankle-knee spring)
k_{AK}	Spring constant of the common ankle-knee spring
Δx_{0AK}	Initial extension determining pretensioning of the common ankle-knee spring
D_A	Length of the ankle lever arm
D_K	Length of the knee lever arm of the ankle-knee spring
L_{0A}	Distance between top of the ankle lever arm and the pulley
L_{0K}	Distance between top of the knee lever arm and the pulley (ankle-knee spring)
k_{A1}	Spring constant of the parallel ankle spring

θ_{0A1}	Neutral position of the ankle spring
k_{K1}	Spring constant of spring 1 at the knee
θ_{0K1}	Neutral position of spring 1 at the knee
k_{K2}	Spring constant of spring 2 at the knee
θ_{0K2}	Neutral position of spring 2 at the knee
k_{H1}	Spring constant of the parallel hip spring
θ_{0H1}	Neutral position of the hip spring
$\alpha_H(i)$	Angle of the lever arm at the hip (at 50 discrete moments of time i at which the biological angles θ_H are known)
α_{Kh}	Angle of the fixed lever arm at the knee (knee-hip spring)
k_h	Spring constant of the common knee-hip spring
Δx_{0h}	Initial extension determining pretensioning of the common knee-hip spring
D_H	Length of the hip lever arm
D_{Kh}	Length of the knee lever arm of the knee-hip spring
L_{0H}	Distance between top of the hip lever arm and the pulley
L_{0Kh}	Distance between top of the knee lever arm and the pulley (knee-hip spring)

C.2.2. Objective

```
function f = myobj4quat(x)
% Optimisation cost function for biarticular maccepa between
    ankle-knee and
% knee-hip, together with parallel springs at the ankle,
   knee and hip joints.
% First run ConstraintsBounds4quat to create constraint,
   bound and initial value matrices.
% Use nonlconstr4quat as non-linear constraints in optimtool
    solver. Bounds LB and UB, Linear inequalities A and b.

BiologicalData;

alfaA = x(1:50);
alfaK = x(51);
k = x(52);
dx0 = x(53);
DA = x(54);
```

```
DK = x(55);
L0A = x(56);
L0K = x(57);
kA1 = x(58);
theta0A1 = x(59);
kK1 = x(60);
theta0K1 = x(61);
kK2 = x(62);
theta0K2 = x(63);
kH1 = x(64);
theta0H1 = x(65);
alfaH = x(66:115);
alfaKh = x(116);
kh = x(117);
dx0h = x(118);
DH = x(119);
DKh = x(120);
L0H = x(121);
L0Kh = x(122);

% Calculate torque TK1 due to parallel knee spring kK1
TK1(1:50)=zeros(1,50);
for i=2:24
    TK1(i)= max(0,-kK1*(thetaK(i)-theta0K1));
end

% Calculate torque TA1 due to parallel ankle spring kA1
TA1(1:50)=zeros(1,50);
for i=1:50
    TA1(i)= min(0, -kA1*(thetaA(i)-theta0A1));
end

for i= 1:50
    % Maccepa spring extensions
    dlA(i)=sqrt((L0A+DA)^2+DA^2-2*DA*(L0A+DA)*cos(thetaA(i)-
        alfaA(i)))-L0A;
    dlK(i)=sqrt((L0K+DK)^2+DK^2-2*DK*(L0K+DK)*cos(thetaK(i)-
        alfaK))-L0K;
    dlKh(i)=sqrt((L0Kh+DKh)^2+DKh^2-2*DKh*(L0Kh+DKh)*cos(
        thetaK(i)+alfaKh))-L0Kh;
    dlH(i)=sqrt((L0H+DH)^2+DH^2-2*DH*(L0H+DH)*cos(thetaH(i)-
        alfaH(i)))-L0H;
    % Torques due to maccepa
```

```
    TA(i)=k*(dx0+dlA(i)+dlK(i))*DA*sin(alfaA(i)-thetaA(i))/(
        dlA(i)+L0A)*(L0A+DA);
    TK(i)=k*(dx0+dlA(i)+dlK(i))*DK*sin(alfaK-thetaK(i))/(dlK
        (i)+L0K)*(L0K+DK);
    TKh(i)=-kh*(dx0h+dlH(i)+dlKh(i))*DKh*sin(alfaKh+thetaK(i
        ))/(dlKh(i)+L0Kh)*(L0Kh+DKh);
    TH(i)=kh*(dx0h+dlH(i)+dlKh(i))*DH*sin(alfaH(i)-thetaH(i)
        )/(dlH(i)+L0H)*(L0H+DH);
    % Torque TK2 due to parallel knee spring kK2
    TK2(i)= -kK2*(thetaK(i)-theta0K2);
    % Torque TH1 due to parallel hip spring kH1
    TH1(i)= -kH1*(thetaH(i)-theta0H1);
    % Total torques
    Ta(i)=TA(i)+TA1(i);
    Tk(i)=TK(i)+TK1(i)+TK2(i)+TKh(i);
    Th(i)=TH(i)+TH1(i);
end

for i= 2:49
    velA(i) = (alfaA(i+1)-alfaA(i-1))/2/dt;
    velK(i) = 0;
    velH(i) = (alfaH(i+1)-alfaH(i-1))/2/dt;
end
velA(1) = (alfaA(2)-alfaA(50))/2/dt;
velK(1) = 0;
velA(50) = (alfaA(1)-alfaA(49))/2/dt;
velK(50) = 0;
velH(1) = (alfaH(2)-alfaH(50))/2/dt;
velH(50) = (alfaH(1)-alfaH(49))/2/dt;

% Calculate maccepa power
O(1)=0;
for i= 1:50
    O(1) = O(1)+ (velA(i)*TA(i))^2 + (velK(i)*TK(i))^2 + (
        velH(i)*TH(i))^2;
end

% Calculate acceleration
O(2)=(alfaA(50)-2*alfaA(1)+alfaA(2))^2/dt^4; %sum((accA)^2)
for i=2:49
    O(2) = O(2)+(alfaA(i-1)-2*alfaA(i)+alfaA(i+1))^2/dt^4;
end
O(2) = O(2)+(alfaA(49)-2*alfaA(50)+alfaA(1))^2/dt^4;
```

```
O(3) = 0;

O(6)=(alfaH(50)-2*alfaH(1)+alfaH(2))^2/dt^4; %sum((accH)^2)
for i=2:49
    O(6) = O(6)+(alfaH(i-1)-2*alfaH(i)+alfaH(i+1))^2/dt^4;
end
O(6) = O(6)+(alfaH(49)-2*alfaH(50)+alfaH(1))^2/dt^4;

% calculate torque difference
O(4)=0; %sum(dTA^2)
O(5)=0; %sum(dTK^2)
O(7)=0; %sum(dTH^2)
for i= 1:50
    O(4)=O(4)+(BTorqueA(i)-Ta(i))^2;
    O(5)=O(5)+(BTorqueK(i)-Tk(i))^2;
    O(7)=O(7)+(BTorqueH(i)-Th(i))^2;
end

O(8)=max(abs(TA))+max(abs(TH));

f = 1.5*O(1) + 0.08*(O(2) + O(3) + O(6)) + 22*(1.4*O(4) +
   6.9*O(5) + 0.8*O(7))+17.5*O(8);
```

C.2.3. Constraints

The constraints for the ankle-knee MACCEPA and the parallel springs at the ankle and knee are the same as in subsection A.2.3 and subsection B.2.2 and will therefore not be repeated. All additional constraints for the knee-hip MACCEPA with parallel hip spring are listed in Table C.1. These constraints are similar to those explained in subsection A.2.3 and subsection B.2.2. Note that the constraints on D and L_0 are applied to both hip (index H) and knee (index Kh).

Constraints	Units	Explanation
$0 \leqslant k_{H1} \leqslant 50$	Nm/rad	Range of realistical values for k_{H1}
$-\pi \leqslant \theta_{0H1} \leqslant \pi$	rad	Neutral position is uniquely defined
$-\frac{\pi}{2} \leqslant \alpha_H(i) \leqslant \frac{\pi}{2}$	rad	These values of α_H allow us to reach the entire torque range
$-\frac{\pi}{2} \leqslant \alpha_{Kh} \leqslant \frac{\pi}{2}$	rad	These values of α_{Kh} allow us to reach the entire torque range
$-\pi \leqslant \alpha_H(i) - \theta_H(i) \leqslant \pi$	rad	These values of α_H allow us to reach the entire torque range
$0 \leqslant \Delta x_{0h} \leqslant 0.10$	m	Initial spring extension is limited so that the spring fits in between the pulleys
$0.01 \leqslant L_0 \leqslant 0.20$	m	L_0 should be at least 10 mm te ensure clearance between pulley and lever arm
$0.03 \leqslant D \leqslant 0.12$	m	Range of realistical values for D
$2\,000 \leqslant k_h \leqslant 100\,000$	N/m	Range of realistical values for k_h
$L_{0Kh} + L_{0H} + D_{Kh} + D_H \leqslant 0.25$	m	Make sure the entire construction fits on the thigh
$0 \leqslant \Delta l_h \leqslant 0.20$	m	Extended spring should fit in between the pulleys

Table C.1.: Additional constraints for the knee-hip MACCEPA and parallel hip spring

Red constraints are bounds, blue constraints are linear inequalities and the green constraint is a non-linear inequality.

The first optimizations were executed with these constraints. This resulted in a MACCEPA behaviour which was too stiff. In other words, a small disturbance in the angles α or θ would lead to a large difference in torque, resulting in a spike in power. Since stiffness is not only dependent on spring stiffness k_H but also on pretension Δx_{OH}, simply lowering the upper bound on k_H is too simplistic. The equivalent hip MACCEPA stiffness is therefore calculated as

$$k_{eq} = \frac{\partial T}{\partial(\alpha - \theta)} \tag{C.10}$$

This is in fact the sensitivity of the torque to changes in $\alpha - \theta$, which is exactly what we want to limit. Substituting Equation C.8 or Equation A.5 into the above

expression leads to

$$k_{eq} = kD(L_0+D)cos(\alpha-\theta)\left(1+\frac{\Delta x_0+\Delta x_K-L_0}{\sqrt{(L_0+D)^2+D^2-2D(L_0+D)cos(\alpha-\theta)}}\right) - \frac{kD^2(L_0+D)^2sin^2(\alpha-\theta)(\Delta x_0+\Delta x_K-L_0)}{((L_0+D)^2+D^2-2D(L_0+D)cos(\alpha-\theta))^{3/2}} \quad \text{(C.11)}$$

In Equation C.11, D, L_0, α, and θ must be evaluated at the joint for which the equivalent MACCEPA stiffness is calculated, i.e. the ankle (index A) or the hip (index H). k and Δx_0 are equivalent to k_{AK} and Δx_{0AK} for the ankle-knee MACCEPA and k_h and Δx_{0h} for the knee-hip MACCEPA. Putting a upper bound of 230 Nm/rad on k_{eq} for the hip and 400Nm/rad for the ankle results in a decent sensitivity to changes in $\alpha-\theta$. This results in the additional nonlinear constraints

$$k_{eqH} < 230 \quad \text{(C.12)}$$
$$k_{eqA} < 400 \quad \text{(C.13)}$$

C.2.3.1. Bounds, linear constraints and initial values

```
% Function that defines matrices containing the lower and
   upper bounds and
% matrices of the linear constraints. Goes with myobj4quat.
% Bounds: Lower bound <= x <= Upper bound
% Units defined in myobj4quat

% Lower bound
LB = zeros(122,1);
for i = 1:51
    LB(i,1)=-pi/2;
end
LB(52,1) = 2000;
LB(53,1) = 0;
LB(54,1) = 0.03;
LB(55,1) = 0.03;
LB(56,1) = 0.01;
LB(57,1) = 0.01;
LB(58,1) = 130;
LB(59,1) = -20/180*pi;
LB(60,1) = 100;
LB(61,1) = -70*pi/180;
LB(62,1) = 0;
LB(63,1) = -70*pi/180;
```

```
LB(64,1) = 0;
LB(65,1) = -pi;
for i = 65:116
    LB(i,1)=-pi/2;
end
LB(117,1) = 2000;
LB(118,1) = 0;
LB(119,1) = 0.03;
LB(120,1) = 0.03;
LB(121,1) = 0.01;
LB(122,1) = 0.01;


%Upper bound
UB = zeros(122,1);
for i = 1:51
    UB(i,1)=pi/2;
end
UB(52,1) = 100000;
UB(53,1) = 0.1;
UB(54,1) = 0.12;
UB(55,1) = 0.12;
UB(56,1) = 0.2;
UB(57,1) = 0.2;
UB(58,1) = 170;
UB(59,1) = 10/180*pi;
UB(60,1) = 140;
UB(61,1) = -0.1361;
UB(62,1) = 20;
UB(63,1) = 10*pi/180;
UB(64,1) = 50;
UB(65,1) = pi;
for i = 66:116
    UB(i,1)=pi/2;
end
UB(117,1) = 100000;
UB(118,1) = 0.1;
UB(119,1) = 0.12;
UB(120,1) = 0.12;
UB(121,1) = 0.2;
UB(122,1) = 0.2;

mat=-eye(50,50)+[zeros(48,2) eye(48,48); eye(2,2) zeros
   (2,48)];
```

```
%Linear constraints: Ax <= b
BiologicalData;
A=[eye(50) zeros(50,1) zeros(50,14) zeros(50) zeros(50,7);
    -eye(50) zeros(50,1) zeros(50,14) zeros(50) zeros(50,7);
    zeros(1,50) zeros(1,1) [0 0 1 0 1 0] zeros(1,8) zeros
       (1,50) zeros(1,7);
    zeros(1,50) zeros(1,1) [0 0 0 1 0 1] zeros(1,8) zeros
       (1,50) zeros(1,7);
    zeros(1,50) zeros(1,1) [0 0 1 1 1 1] zeros(1,8) zeros
       (1,50) zeros(1,7);
    zeros(50) zeros(50,1) zeros(50,14) eye(50) zeros(50,7);
    zeros(50) zeros(50,1) zeros(50,14) -eye(50) zeros(50,7);
    zeros(1,50) zeros(1,1) zeros(1,14) zeros(1,50) [0 0 0 1
       1 1 1]];
b=[pi+thetaA;
   pi-thetaA;
   0.25;
   0.25;
   0.25;
   pi+thetaH;
   pi-thetaH;
   0.25];

% Initial values
Init=[
0.005236;
-0.035954;
-0.067719;
-0.080285;
-0.080285;
-0.080285;
-0.080285;
-0.080285;
-0.080285;
-0.080285;
-0.080285;
-0.080285;
-0.080285;
-0.080285;
-0.080285;
-0.080285;
-0.080285;
-0.080285;
-0.080285;
```

```
−0.080285;
−0.096619;
−0.102279;
−0.114593;
−0.122173;
−0.132285;
−0.140130;
−0.149614;
−0.158138;
−0.167415;
−0.179651;
−0.191048;
−0.234767;
−0.298975;
−0.340688;
−0.345052;
−0.316254;
−0.266861;
−0.210138;
−0.154462;
−0.104022;
−0.061261;
−0.028623;
−0.008727;
−0.001222;
−0.002793;
−0.007330;
−0.009076;
−0.004538;
0.006283;
0.017453;
0.020944;
−0.064170;
51001.5364;
0.000543884;
0.072992901;
0.047290909;
0.010000503;
0.169715687;
150;
−4.2∗pi/180;
118.9562202;
−0.164119654;
9.289587607;
```

```
−0.773534323;
28.64788976;
0.20943951;
0.078084221;
−0.023561813;
−0.030107925;
−0.009912038;
−0.006587356;
−0.007926797;
−0.011556581;
−0.011027641;
−0.010288248;
−0.001712417;
0.00741851;
0.011070559;
0.012488064;
0.01485176;
0.018949272;
0.024200575;
0.031055281;
0.041316723;
0.053712158;
0.062594547;
0.067419647;
0.070744043;
0.073703939;
0.07685317;
0.075088314;
0.065330464;
0.047771194;
0.030005218;
0.040493126;
0.073262961;
0.100310611;
0.107633371;
0.110985148;
0.111166459;
0.112341952;
0.113124826;
0.114664882;
0.118835103;
0.129337778;
0.144839209;
0.161249202;
```

```
0.173150191;
0.176933216;
0.169976861;
0.151100872;
0.121614443;
0.087623557;
0.059429564;
0.047960275;
0.056901186;
10/180*pi;
17151.11437;
0.000581485;
0.133208809;
0.133208809;
0.116791191;
0.116791191];
```

C.2.3.2. Non-linear constraints

```
function [c,ceq] = nonlconstr4quat(x)
%Non-linear constraints to go with myobj4

alfaA = x(1:50);
alfaK = x(51);
k = x(52);
dx0 = x(53);
DA = x(54);
DK = x(55);
L0A = x(56);
L0K = x(57);
alfaH = x(66:115);
alfaKh = x(116);
kh = x(117);
dx0h = x(118);
DH = x(119);
DKh = x(120);
L0H = x(121);
L0Kh = x(122);

BiologicalData;
g = zeros(50,1);
h = zeros(50,1);
```

```
for i = 1:50
g(i) = -sqrt((DA+L0A)^2+DA^2-2*DA*(DA+L0A)*cos(alfaA(i)-
    thetaA(i)))+L0A -sqrt((DK+L0K)^2+DK^2-2*DK*(DK+L0K)*cos(
    alfaK-thetaK(i)))+L0K;
h(i) = -sqrt((DH+L0H)^2+DH^2-2*DH*(DH+L0H)*cos(alfaH(i)-
    thetaH(i)))+L0H -sqrt((DKh+L0Kh)^2+DKh^2-2*DKh*(DKh+L0Kh)
    *cos(alfaKh+thetaK(i)))+L0Kh;
end
amt=alfaH(1:50)'-thetaH;
wortel=sqrt((L0H+DH).^2+DH.^2-2.*DH.*(L0H+DH).*cos(amt));
keqH(:,1)=kh.*DH.*cos(amt).*(L0H+DH).*(1+(dx0h+dlKh(:,1)-L0H
    )./wortel)-kh.*DH.^2.*(L0H+DH).^2.*sin(amt).^2.*(dx0h+
    dlKh(:,1)-L0H)./wortel.^3;
keqH=max(abs(keqH));
amtA=x(1:50)'-thetaA;
wortelA=sqrt((L0A+DA).^2+DA.^2-2.*DA.*(L0A+DA).*cos(amtA));
keqA=max(abs(k.*DA.*cos(amtA).*(DA+L0A).*(1+(dx0+dlK'-L0A)./
    wortelA)-k.*DA.^2.*(DA+L0A).^2.*sin(amtA).^2.*(dx0+dlK'-
    L0A)./wortelA.^3));

c = [g;
     -g - 0.2;
     h;
     -h - 0.2;
     keqH-230;
     keqA-400];

ceq = [];
```

C.3. Results

The parameter values are:

Parameter	Optimized value	Parameter	Optimized value
$\alpha_A(i)$	Figure Figure C.2	k_{K2}	0 Nm/rad
α_K	-1.114 rad	θ_{0K2}	irrelevant
k_{AK}	23.072 N/mm	k_{H1}	20.1 Nm/rad
Δx_{0AK}	0 mm	θ_{0H1}	0.0030 rad
D_A	120 mm	$\alpha_H(i)$	Figure Figure C.2
D_K	30 mm	α_{Kh}	-1.571 rad
L_{0A}	14 mm	k_h	2.020 N/mm
L_{0K}	86 mm	Δx_{0h}	0 mm
k_{A1}	154.5 Nm/rad	D_H	58 mm
θ_{0A1}	-0.1237 rad	D_{Kh}	36 mm
k_{K1}	117.9 Nm/rad	L_{0H}	10 mm
θ_{0K1}	-0.1703 rad	L_{0Kh}	146 mm

Table C.2.: Results of the ankle-knee-hip optimization with passive knee

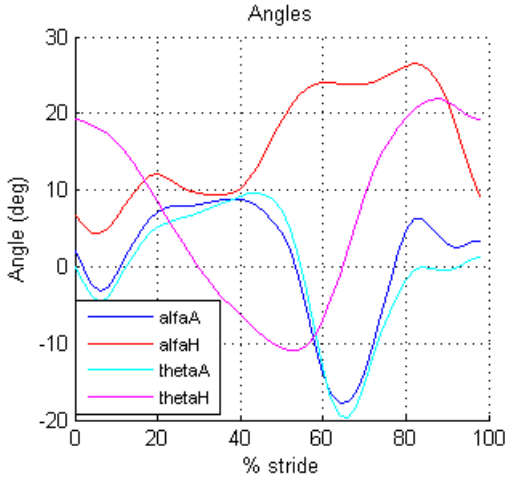

Figure C.2.: Lever arm angles for the the ankle-knee-hip optimization

D. Prosthesis side hip MACCEPA

D.1. Mathematical expressions

The hip on the prosthesis side is a simple MACCEPA system, which can be described with the formulas found in section A.1. Spring extension Δl_{Hp} of course now only has one contribution, which is due to the position of the hip lever arm and the hip motion. The final formula for the hip torque is (index Hp is left out for simplicity):

$$\begin{aligned} T &= \frac{kDsin(\alpha-\theta)(L_0+D)\left(\sqrt{(L_0+D)^2+D^2-2D(L_0+D)cos(\alpha-\theta)}-L_0+\Delta x_0\right)}{\sqrt{(L_0+D)^2+D^2-2D(L_0+D)cos(\alpha-\theta)}} \\ &= kDsin(\alpha-\theta)(L_0+D)\left(1+\frac{\Delta x_0-L_0}{\sqrt{(L_0+D)^2+D^2-2D(L_0+D)\cdot cos(\alpha-\theta)}}\right) \end{aligned} \quad \text{(D.1)}$$

The equivalent MACCEPA stiffness is found by substituting Equation D.1 into Equation C.10:

$$\begin{aligned} k_{eq} &= kD(L_0+D)cos(\alpha-\theta)\left(1+\frac{\Delta x_0-L_0}{\sqrt{(L_0+D)^2+D^2-2D(L_0+D)cos(\alpha-\theta)}}\right) \\ &\quad -\frac{kD^2(L_0+D)^2sin^2(\alpha-\theta)(\Delta x_0-L_0)}{((L_0+D)^2+D^2-2D(L_0+D)cos(\alpha-\theta))^{3/2}} \end{aligned} \quad \text{(D.2)}$$

The parallel spring is described by:

$$T_{H1p} = -k_{H1p}\cdot(\theta_H-\theta_{0H1p}) \quad \text{(D.3)}$$

D.2. Matlab optimization

D.2.1. Objective

```
function f = myobjHip(x)
% Optimisation cost function for hip maccepa with parallel
    spring.
```

```
% First run ConstraintsBoundsHip to create constraint, bound
    and initial value matrices.
% Use nonlconstrHip as non-linear constraints in optimtool
   solver. Bounds LB and UB, Linear inequalities A and b.

BiologicalData;

%x(1-50) = alfaH in radians
%x(51) = kH in N/m
%x(52) = dx0H in m
%x(53) = DH in m
%x(54) = L0H in m
%x(55) = kH1 in Nm/rad
%x(56) = theta0H1 in radians

for i= 1:50
    % Maccepa spring extension
    dlH(i)=sqrt((x(54)+x(53))^2+x(53)^2-2*x(53)*(x(54)+x(53)
       )*cos(thetaH(i)-x(i)))-x(54);
    % Torque due to maccepa
    TH(i)=x(51)*(x(52)+dlH(i))*x(53)*sin(x(i)-thetaH(i))/(
       dlH(i)+x(54))*(x(54)+x(53));
    % Torque TH1 due to parallel hip spring kH1
    TH1(i)= -x(55)*(thetaH(i)-x(56));
    % Total torque
    Th(i)=TH(i)+TH1(i);
end

for i= 2:49
    velH(i) = (x(i+1)-x(i-1))/2/dt;
end
velH(1) = (x(2)-x(50))/2/dt;
velH(50) = (x(1)-x(49))/2/dt;

% Calculate maccepa power
O(1)=0;
for i= 1:50
    O(1) = O(1)+ (velH(i)*TH(i))^2;
end

% Calculate acceleration

O(2)=(x(50)-2*x(1)+x(2))^2/dt^4; %sum((accH)^2)
for i=2:49
```

```
    O(2) = O(2)+(x(i-1)-2*x(i)+x(i+1))^2/dt^4;
end
O(2) = O(2)+(x(49)-2*x(50)+x(1))^2/dt^4;

% calculate torque difference
O(3)=0; %sum(dTH^2)
for i= 1:30
    O(3)=O(3)+(BTorqueH(i)-Th(i))^2;
end
for i= 31:50
    O(3)=O(3)+3*(BTorqueH(i)-Th(i))^2;
end

O(8)=max(TH.^2)+0.4*max(velH.^2);

f = 1.2*O(1) + 0.008*(O(2)) + 10*(O(3))+90*O(8);
```

D.2.2. Constraints and bounds

All constraints applicable to the parameters can be found in Table D.1.

Constraint	Units	Explanation
$-\frac{\pi}{2} \leqslant \alpha_{Hp} \leqslant \frac{\pi}{2}$	rad	These values of α_{Hp} allow us to reach the entire torque range
$-\pi \leqslant \alpha_{Hp} - \theta_H \leqslant \pi$	rad	Constraint to avoid instantaneous changes of α_{Hp} of more than 2π
$0 \leqslant \Delta x_{0Hp} \leqslant 0.10$	m	Initial spring extension is limited so that the spring fits in between the pulleys
$0.01 \leqslant L_{0Hp} \leqslant 0.20$	m	L_{0Hp} should be at least 10 mm te ensure clearance between pulley and lever arm
$0.03 \leqslant D_{Hp} \leqslant 0.12$	m	Range of realistical values for D_{Hp}
$2\,000 \leqslant k_{Hp} \leqslant 20\,000$	N/m	Range of realistical values for k_{Hp}
$L_{0Hp} + D_{Hp} \leqslant 0.25$	m	Make sure the entire construction fits on the thigh
$0 \leqslant \Delta l_{Hp} \leqslant 0.20$	m	Extended spring should fit in between the pulleys
$0 \leqslant k_{H1p} \leqslant 500$	Nm/rad	Range of realistical values for k_{H1}
$-\frac{\pi}{2} \leqslant \theta_{0H1p} \leqslant \frac{\pi}{2}$	rad	Neutral position falls within the range of motion
$k_{eqHp} \leqslant 50$	Nm/rad	Equivalent MACCEPA stiffness is limited to avoid spikes in power

Table D.1.: Constraints for the prosthesis side hip

D.2.2.1. Bounds, linear constraints and initial values

```
% Function that defines matrices containing the lower and
   upper bounds and
% matrices of the linear constraints. Goes with myobjHip.
% Bounds: Lower bound <= x <= Upper bound
% Units defined in myobjHip

% Lower bound
LB = zeros(56,1);
for i = 1:50
    LB(i,1)=-pi/2;
end
LB(51,1) = 200;
LB(52,1) = 0;
LB(53,1) = 0.05;
LB(54,1) = 0.02;
LB(55,1) = 0;
LB(56,1) = -pi/2;

%Upper bound
UB = zeros(56,1);
for i = 1:50
    UB(i,1)=pi/2;
end
UB(51,1) = 10000;
UB(52,1) = 0.05;
UB(53,1) = 0.12;
UB(54,1) = 0.20;
UB(55,1) = 500;
UB(56,1) = pi/2;

%Linear constraints: Ax <= b
BiologicalData;
A=[eye(50) zeros(50,6);
    -eye(50) zeros(50,6);
    zeros(1,50) [0 0 1 1 0 0]];
b=[pi+thetaH;
    pi-thetaH;
    0.25];

% Initial values
Init=[
0.078084221;
```

```
−0.023561813;
−0.030107925;
−0.009912038;
−0.006587356;
−0.007926797;
−0.011556581;
−0.011027641;
−0.010288248;
−0.001712417;
0.00741851;
0.011070559;
0.012488064;
0.01485176;
0.018949272;
0.024200575;
0.031055281;
0.041316723;
0.053712158;
0.062594547;
0.067419647;
0.070744043;
0.073703939;
0.07685317;
0.075088314;
0.065330464;
0.047771194;
0.030005218;
0.040493126;
0.073262961;
0.100310611;
0.107633371;
0.110985148;
0.111166459;
0.112341952;
0.113124826;
0.114664882;
0.118835103;
0.129337778;
0.144839209;
0.161249202;
0.173150191;
0.176933216;
0.169976861;
0.151100872;
```

```
0.121614443;
0.087623557;
0.059429564;
0.047960275;
0.056901186;
17151.11437;
0;
0.133208809;
0.116791191;
28.64788976;
0.20943951];
```

D.2.2.2. Non-linear constraints

```
function [c,ceq] = nonlconstrHip(x)
%Non-linear constraints to go with myobjHip

BiologicalData;
h = zeros(50,1);

for i = 1:50
 h(i) = -sqrt((x(53)+x(54))^2+x(53)^2-2*x(53)*(x(53)+x(54))*
     cos(x(i)-thetaH(i)))+x(54);
end
amt=x(1:50)'-thetaH;
wortel=sqrt((x(54)+x(53))^2+x(53)^2-2*x(53)*(x(54)+x(53)).*
    cos(amt));
keq=x(51).*x(53).*cos(amt).*(x(54)+x(53)).*(1+(x(52)-x(54))
    ./wortel)-x(51).*x(53)^2.*(x(54)+x(53))^2.*sin(amt).^2.*(
    x(52)-x(54))./wortel.^3;
keq_max=max(abs(keq));

c = [-h - 0.2;
     keq_max - 40];
ceq = [];
```

D.3. Results

The results of the optimization are listed in: Table D.2.

Parameter	Optimized value	Parameter	Optimized value
$\alpha_H(i)$	FigureFigure D.1	L_{0Hp}	44 mm
k_{Hp}	2.242 N/mm	k_{H1p}	35.77 Nm/rad
Δx_{0Hp}	42 mm	θ_{0H1p}	0.1816 rad
D_{Hp}	116 mm		

Table D.2.: Prosthesis side hip optimization results

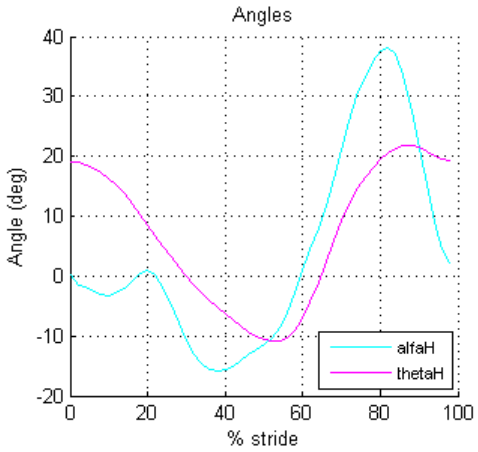

Figure D.1.: Lever arm angles for the prosthesis side hip optimization

E. Powers and energies for the ankle-knee common spring MACCEPA with parallel springs

E.1. Powers

Following notations will be used:

P_{biol}	Required power (half of biological joint power)
P_{orth}	Total power delivered by the orthosis
P_m	MACCEPA motor power
P_{A1}, P_{K1}, P_{K2}	Power of the parallel springs A1, K1 and K2
P_{Sp}	Power of the common MACCEPA spring

An additional index A is used to denote the ankle, K is used for the knee.

The total common MACCEPA spring power, P_{Sp}, has two contributions: one by the ankle (P_{SpA}) and one by the knee (P_{SpK}). The spring has two purposes: it can store and release elastic energy coming from both ankle and knee and it can transfer energy between both joints. P_{Sp}, P_{SpA} and P_{SpK} can be calculated as

$$\begin{aligned} P_{Sp} &= F \cdot \frac{d(\Delta x)}{dt} = -k\Delta x \cdot \frac{d(\Delta x)}{dt} \\ &= -k\Delta x \cdot \frac{d(\Delta x_A)}{dt} - k\Delta x \cdot \frac{d(\Delta x_K)}{dt} \\ &= P_{SpA} + P_{SpK} \end{aligned} \tag{E.1}$$

The parallel spring powers, P_{A1}, P_{K1} and P_{K2}, can be found by multiplying the spring torques with the joint angular acceleration:

$$\begin{aligned} P_{A1} &= T_{A1} \cdot \omega_A \\ P_{K1} &= T_{K1} \cdot \omega_K \\ P_{K2} &= T_{K2} \cdot \omega_K \end{aligned} \tag{E.2}$$

where T_i is the torque exerted by the spring corresponding to the index i and ω_A/ω_K is the angular velocity of the ankle/knee joint.

Orthosis joint powers are calculated as follows:

$$P_{orthosis} = T_{tot} \cdot \omega \tag{E.3}$$

where T_{tot} is the total orthosis joint torque and ω is the angular velocity of the joint.

Finally, one can calculate the MACCEPA joint powers and energies:

$$P_m = T_m \cdot \dot{\alpha} \tag{E.4}$$

where T_m is the torque applied by the MACCEPA and $\dot{\alpha}$ is the angular velocity of the MACCEPA lever arm.

The orthosis power at a specific joint is also the sum of all powers working on that joint:

$$P_{orthA} = P_{mA} + P_{A1} + P_{SpA} \tag{E.5}$$
$$P_{orthK} = P_{mK} + P_{K1} + P_{K2} + P_{SpK} \tag{E.6}$$

E.2. Energies

One can easily calculate the energies E dissipated and generated in the joints by integrating the joint power P over one cycle:

$$E = \int P dt \tag{E.7}$$

Applying this to biological gait data, we find following joint energies:

ankle	knee	hip
16.6	-12.2	5.9

Table E.1.: Biological joint energies in J

Since the orthosis will apply only half of the biological torque to the joints, energies which are to be provided by the orthosis are half of those found in Table E.1. We will name those energies E_{biol}.

Applying Equation E.7 to P_{orth} and P_m, we find $E_{orthosis}$ and E_m. $E_{orthosis}$ is the energy that is generated/absorbed by the orthosis, E_m is the energy that is generated/absorbed by the MACCEPA motor.

Springs do not add energy to a joint over one cycle. The difference in energy $E_{orthosis} - E_m$ is therefore zero, unless energy exchange is made possible by an element coupling two joints. In this case, the difference in energy is the energy transferred from one joint to the other. The transferred energy can also be calculated by integrating the spring power at a specific joint over one gait cycle:

$$E_{transf} = \int P_{SpA} dt = -\int P_{SpK} dt \tag{E.8}$$

F. Motors and transmissions

The selected motors and transmissions are shown in Table F.1, Table F.2 and Table F.3.

Lever[a]	Design
RMS torque (Nm)	11.6
Max. torque (Nm)	20.3
RMS speed (rpm)	14
Max. speed (rpm)	32

Hypoid gear	Design	Permissible
Catalog number[b]	MHP1.5-0453R	
Transmission ratio	15	
Efficiency	0.85	
Max. speed (rpm)	484	
Max. torque (Nm)	20.3	41.2

Planetary gearbox	Design	Permissible
Catalog number[c]	370783	
Transmission ratio	104	
Efficiency	0.59	
RMS Torque (Nm)	0.9	3.0
Max. torque (Nm)	1.4	3.5
Max. speed (rpm)	50 346	17 000

Transmission-total	Design
Transmission ratio	1 560
Efficiency	0.50

Motor	Design	Permissible
Catalog number[d]	386658	
Nominal power (W)	40	
RMS torque (mNm)	14.8	19.7
Max. torque (mNm)	26	30
RMS speed (rpm)	22 260	
Max. speed (rpm)	50 346	60 000
Max. efficiency	0,87	

Total efficiency	0,44

[a]Simulation results
[b]See KHK catalog [3]
[c]See Maxon Planetary Gearhead GP 22 HP data sheet (Appendix H)
[d]See Maxon EC22 data sheet (Appendix H)

Table F.1.: Ankle drive system

Lever[a]	Design
RMS torque (Nm)	6.1
Max. torque (Nm)	10.0
RMS speed (rpm)	10
Max. speed (rpm)	24

Hypoid gear	Design	Permissible
Catalog number[b]	MHP1-0453R	
Transmission ratio	15	
Efficiency	0.85	
Max. speed (rpm)	356	
Max. torque (Nm)	10.0	10.3

Planetary gearbox	Design	Permissible
Catalog number[c]	166937	
Transmission ratio	28	
Efficiency	0.75	
RMS Torque (Nm)	0.48	3.0
Max. torque (Nm)	0.65	3.75
Max. speed (rpm)	9962	8000

Transmission-total	Design
Transmission ratio	420
Efficiency	0.64

Motor	Design	Permissible
Catalog number[d]	226754	
Nominal power (W)	15	
RMS torque (mNm)	22.8	26.1
Max. torque (mNm)	37.2	40
RMS speed (rpm)	4108	
Max. speed (rpm)	9962	11000
Max. efficiency	0.91	

Total efficiency	0.58

[a]Simulation results
[b]See KHK catalog [3]
[c]See Maxon Planetary Gearhead GP 32 C data sheet (Appendix H)
[d]See Maxon RE-max 29 data sheet (Appendix H)

Table F.2.: Orthosis side hip drive system

Lever[a]	Design
RMS torque (Nm)	2.8
Max. torque (Nm)	5.3
RMS speed (rpm)	21
Max. speed (rpm)	45

Hypoid gear	Design	Permissible
Catalog number[b]	MHP1-0453R	
Transmission ratio	15	
Efficiency	0.85	
Max. speed (rpm)	677	
Max. torque (Nm)	5.3	10.3

Planetary gearbox	Design	Permissible
Catalog number[c]	166935	
Transmission ratio	21	
Efficiency	0.75	
RMS Torque (Nm)	0.22	3.0
Max. torque (Nm)	0.36	3.75
Max. speed (rpm)	9482	8000

Transmission-total	Design
Transmission ratio	210
Efficiency	0.64

Motor	Design	Permissible
Catalog number[d]	226754	
Nominal power (W)	15	
RMS torque (mNm)	20.9	26.1
Max. torque (mNm)	39.9	40
RMS speed (rpm)	4424	
Max. speed (rpm)	9482	11000
Max. efficiency	0.91	

Total efficiency	0.58

[a]Simulation results
[b]See KHK catalog [3]
[c]See Maxon Planetary Gearhead GP 32 C data sheet (Appendix H)
[d]See Maxon RE-max 29 data sheet (Appendix H)

Table F.3.: Prosthesis side hip drive system

G. Bill of materials

Part name	Quantity	Weight per part (g)
Inversion bearing	1	327
Motor mounting plate	1	303
Ankle lever arm	1	33
Ankle motor + gear	1	664
Heelbuckle	1	128
Torsion bar	1	144
Ankle torsion spring	1	248
Torsion cap	1	91
Bolted connection inversion bearing	4	1
Bolted connection torsion cap	1	3
Bearing gear + ankle lever arm	1	26
Bearing pinion	1	7
Bearing torsion bar	1	45
AK plate	1	498
Pawl mounting plate	1	26
AK pulley	4	1
AK spring	1	7
Bolted connection mounting plate pawl	1	3
Bearing AK plate	1	6
Connection plate shank brace	2	9
Bolted connection shank brace	4	1
KH plate	1	407
Knee torsion spring	1	93
Ratchet	1	22
KH spring	1	170
KH spring pulley	2	2
KH lever arm pulley	2	1
Bolted connection thigh brace	2	1
Bearing KH plate	1	16

Table G.1.: Bill of material

Part name	Quantity	Weight per part (g)
Bearing ratchet	1	8
Orthosis side (OS) rotation joint	1	168
Prosthesis side (PS) rotation joint	1	181
OS hip motor + gear	1	476
PS hip motor + gear	1	476
OS hip lever arm	1	11
PS hip lever arm	1	16
OS hip torsion spring	2	57
PS hip torsion spring	2	92
Bolted connection rotation joint	6	6
Bearing OS gear + lever arm	1	6
Bearing PS gear + lever arm	1	6
Bearing OS rotation joint	1	8
Bearing PS rotation joint	1	8
Belt rotation axis	2	346
Belt interlink	2	203
Belt link to adduction joint	2	127
Adduction axis	2	35
Axis fixation cap	4	46
Belt fixation part	1	217
Hip adduction spring	2	326
Bolted connection adduction axis	4	113
PS hip plate	1	275
PS pulley	2	1
PS MACCEPA spring	1	44
Bolted connection PS thigh brace	2	1
Battery mounting plate	1	402
Battery	1	2 015
Total	*90*	*10 670*

Table G.2.: Bill of material (continued)

H. Data sheets

This appendix contains the data sheets of all components used in the orthosis design.

Contents

- Motor data sheets
  - RE-max 29 (15W)
  - EC 22 (40W)
- Planetary gears
  - Maxon planetary gearhead GP 22 HP
  - Maxon planetary Gearhead GP 32 C
- Batteries
  - Kokam SLPB 75106100

RE-max 29 ∅29 mm, Precious Metal Brushes CLL, 15 Watt

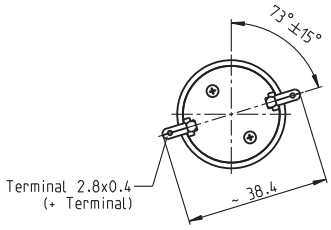

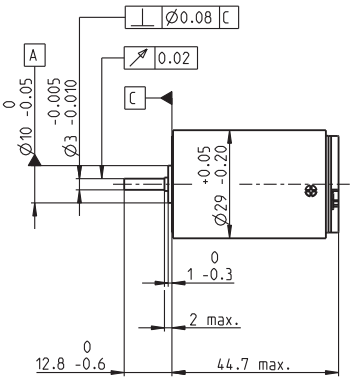

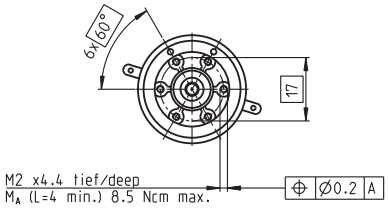

M 1:2

Stock program
Standard program
Special program (on request)

Order Number

			226748	226749	226751	226752	226753	226754	226755	226756	226757	226759	226760	226761	226762	226763	226764
Motor Data																	
	Values at nominal voltage																
1	Nominal voltage	V	7.2	9.0	12.0	18.0	18.0	24.0	30.0	36.0	42.0	48.0	48.0	48.0	48.0	48.0	48.0
2	No load speed	rpm	6480	7190	6160	6820	5630	5960	6170	6640	6710	6280	5400	5000	4160	3350	2790
3	No load current	mA	45.1	43.6	24.7	19.8	14.0	11.6	9.90	9.43	8.25	6.39	4.87	4.26	3.08	2.13	1.57
4	Nominal speed	rpm	6200	6850	5550	6160	4810	5110	5320	5790	5820	5410	4520	4130	3260	2440	1870
5	Nominal torque (max. continuous torque)	mNm	8.44	9.51	15.1	20.7	25.2	26.1	25.8	25.7	24.3	25.2	25.4	25.5	25.2	25.2	24.9
6	Nominal current (max. continuous current)	A	0.840	0.840	0.840	0.840	0.840	0.691	0.566	0.506	0.416	0.352	0.304	0.283	0.232	0.186	0.153
7	Stall torque	mNm	195	200	152	214	173	185	188	201	183	182	157	146	117	93.3	75.6
8	Starting current	A	18.4	16.8	8.22	8.49	5.68	4.81	4.05	3.90	3.07	2.51	1.86	1.59	1.06	0.683	0.461
9	Max. efficiency	%	91	90	90	91	90	91	91	91	90	90	90	90	90	89	89
	Characteristics																
10	Terminal resistance	Ω	0.390	0.536	1.46	2.12	3.17	4.99	7.41	9.24	13.7	19.2	25.8	30.1	45.1	70.2	104
11	Terminal inductance	mH	0.0353	0.0447	0.108	0.199	0.292	0.464	0.676	0.839	1.12	1.67	2.26	2.63	3.81	5.86	8.46
12	Torque constant	mNm / A	10.6	11.9	18.5	25.2	30.4	38.4	46.3	51.6	59.6	72.8	84.7	91.3	110	136	164
13	Speed constant	rpm / V	902	802	515	380	314	249	206	185	160	131	113	105	86.8	70.0	58.2
14	Speed / torque gradient	rpm / mNm	33.2	36.1	40.6	32.0	32.7	32.3	32.9	33.1	36.8	34.5	34.4	34.5	35.6	36.0	37.0
15	Mechanical time constant	ms	4.99	4.84	4.62	4.51	4.49	4.48	4.48	4.47	4.51	4.50	4.50	4.49	4.52	4.53	4.54
16	Rotor inertia	gcm²	14.3	12.8	10.9	13.5	13.1	13.2	13.0	12.9	11.7	12.5	12.5	12.4	12.1	12.0	11.7

Specifications

Thermal data

17	Thermal resistance housing-ambient	15.8 K / W
18	Thermal resistance winding-housing	4.0 K / W
19	Thermal time constant winding	15.8 s
20	Thermal time constant motor	1260 s
21	Ambient temperature	-30 ... +65°C
22	Max. permissible winding temperature	+85°C

Mechanical data (sleeve bearings)

23	Max. permissible speed	11000 rpm
24	Axial play	0.1 - 0.2 mm
25	Radial play	0.012 mm
26	Max. axial load (dynamic)	1.7 N
27	Max. force for press fits (static)	80 N
28	Max. radial loading, 5 mm from flange	5.5 N

Mechanical data (ball bearings)

23	Max. permissible speed	11000 rpm
24	Axial play	0.1 - 0.2 mm
25	Radial play	0.025 mm
26	Max. axial load (dynamic)	5 N
27	Max. force for press fits (static)	75 N
28	Max. radial loading, 5 mm from flange	20.5 N

Other specifications

29	Number of pole pairs	1
30	Number of commutator segments	13
31	Weight of motor	159 g

CLL = Capacitor Long Life

Values listed in the table are nominal.
Explanation of the figures on page 49.

Option
Ball bearings in place of sleeve bearings
Pigtails in place of terminals
Without CLL

Operating Range

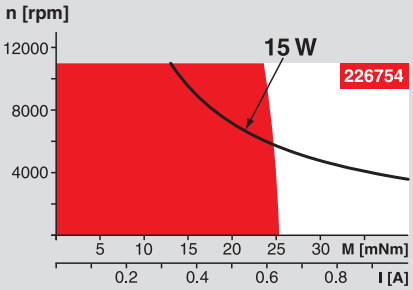

Comments

Continuous operation
In observation of above listed thermal resistance (lines 17 and 18) the maximum permissible winding temperature will be reached during continuous operation at 25°C ambient.
= Thermal limit.

Short term operation
The motor may be briefly overloaded (recurring).

Assigned power rating

maxon Modular System

Overview on page 16 - 21

Planetary Gearhead
∅26 mm
0.5 - 2.0 Nm
Page 227

Planetary Gearhead
∅32 mm
0.75 - 4.5 Nm
Page 230

Planetary Gearhead
∅32 mm
1.0 - 6.0 Nm
Page 233

Spindle Drive
∅32 mm
Page 249 / 250 / 251

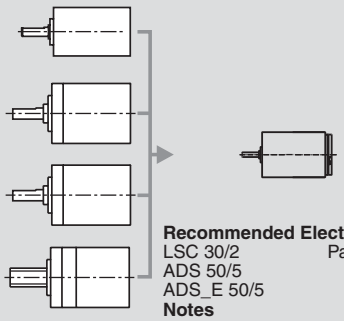

Recommended Electronics:

LSC 30/2	Page 282
ADS 50/5	282
ADS_E 50/5	283
Notes	**18**

EC 22 ∅22 mm, brushless, 40 Watt

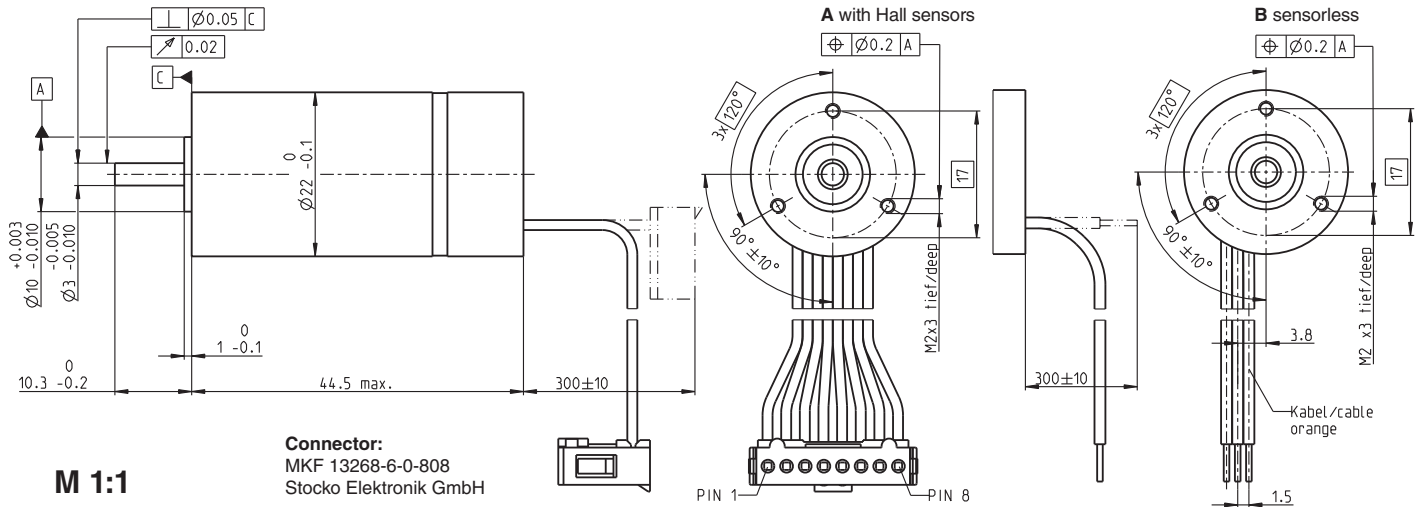

M 1:1

Connector:
MKF 13268-6-0-808
Stocko Elektronik GmbH

Stock program
Standard program
Special program (on request)

Order Number

A with Hall sensors	**386657**	**386658**	386659	**386660**					
B sensorless	**386661**	386662	386663	386664					

Motor Data									
	Values at nominal voltage								
1	Nominal voltage	V	12	24	36	48			
2	No load speed	rpm	30400	35100	31600	34200			
3	No load current	mA	268	166	94.3	79.5			
4	Nominal speed	rpm	27000	31900	28400	31000			
5	Nominal torque (max. continuous torque)	mNm	18.6	19.7	20	19.8			
6	Nominal current (max. continuous current)	A	5.18	3.16	1.92	1.54			
7	Stall torque	mNm	184	243	221	237			
8	Starting current	A	49.1	37.4	20.4	17.7			
9	Max. efficiency	%	86	87	87	87			
	Characteristics								
10	Terminal resistance phase to phase	Ω	0.244	0.641	1.76	2.71			
11	Terminal inductance phase to phase	mH	0.0182	0.0546	0.152	0.231			
12	Torque constant	mNm / A	3.75	6.49	10.8	13.3			
13	Speed constant	rpm / V	2550	1470	882	716			
14	Speed / torque gradient	rpm / mNm	166	145	144	145			
15	Mechanical time constant	ms	4.16	3.64	3.6	3.64			
16	Rotor inertia	gcm²	2.39	2.39	2.39	2.39			

Specifications

Thermal data

17	Thermal resistance housing-ambient	10 K / W
18	Thermal resistance winding-housing	2 K / W
19	Thermal time constant winding	4.85 s
20	Thermal time constant motor	278 s
21	Ambient temperature	-20 ... +100°C
22	Max. permissible winding temperature	+155°C

Mechanical data (preloaded ball bearings)

23	Max. permissible speed		60000 rpm
24	Axial play at axial load	< 5 N	0 mm
		> 5 N	max. 0.14 mm
25	Radial play		preloaded
26	Max. axial load (dynamic)		4 N
27	Max. force for press fits (static)		45 N
	(static, shaft supported)		250 N
28	Max. radial loading, 5 mm from flange		16 N

Other specifications

29	Number of pole pairs	1
30	Number of phases	3
31	Weight of motor	85 g

Values listed in the table are nominal.

Connection A

brown	Motor winding 1	Pin 1
red	Motor winding 2	Pin 2
orange	Motor winding 3	Pin 3
yellow	VHall 3 ... 24 VDC	Pin 4
green	GND	Pin 5
blue	Hall sensor 1	Pin 6
violet	Hall sensor 2	Pin 7
grey	Hall sensor 3	Pin 8

Wiring diagram for Hall sensors see p. 27

Connection B (Cable AWG 24)

brown	Motor winding 1
red	Motor winding 2
orange	Motor winding 3

Operating Range

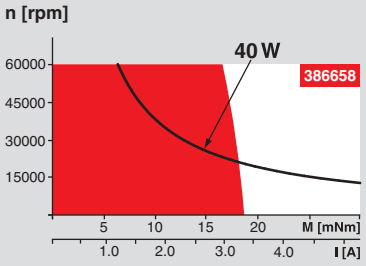

Comments

Continuous operation
In observation of above listed thermal resistance (lines 17 and 18) the maximum permissible winding temperature will be reached during continuous operation at 25°C ambient.
= Thermal limit.

Short term operation
The motor may be briefly overloaded (recurring).

Assigned power rating

maxon Modular System

Overview on page 16 - 21

Planetary Gearhead
∅22 mm
0.5 - 3.4 Nm
Page 223 / 224

Spindle Drive
∅22 mm
Page 247 / 248

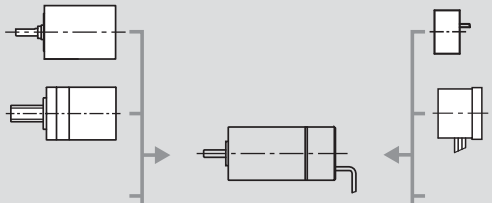

for type A:
Encoder MR
128 / 256 / 512 CPT,
Page 261

for type B:
Resolver
on request

Recommended Electronics:

DECS 50/5	Page 289
DEC 24/3, Module 24/2	290
DEC 50/5, Module 50/5	291
DECV 50/5	297
DES 50/5	298
EPOS2 Module 36/2	304
EPOS2 24/5, EPOS2 50/5	305
EPOS2 P 24/5	308
Notes	**20**

Planetary Gearhead GP 22 HP ∅22 mm, 2.0 - 3.4 Nm

High Power

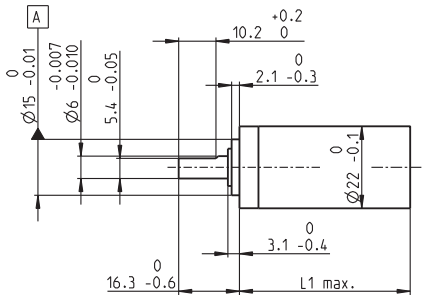

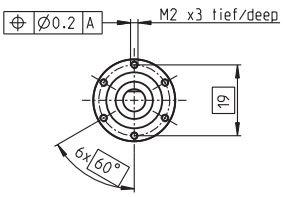

M 1:2

Technical Data	
Planetary Gearhead	straight teeth
Output shaft	stainless steel, hardened
Bearing at output	ball bearing
Radial play, 10 mm from flange	max. 0.2 mm
Axial play	max. 0.2 mm
Max. radial load, 10 mm from flange	70 N
Max. permissible axial load	100 N
Max. permissible force for press fits	100 N
Sense of rotation, drive to output	=
Recommended input speed	< 17'000 rpm
Recommended temperature range	-40 ... +100°C

Stock program
Standard program
Special program (on request)

Gearhead Data (provisorisch)		Order Number									
		370683	370687	370690	370776	370780	370783	370792	370797	370802	370807
1 Reduction		3.8 : 1	14 : 1	20 : 1	53 : 1	76 : 1	104 : 1	198 : 1	316 : 1	410 : 1	590 : 1
2 Reduction absolute		15/4	225/16	81/4	3375/64	1215/16	87723/845	50625/256	2777895/8788	6561/16	59049/100
3 Max. motor shaft diameter	mm	4	4	4	4	4	3.2	4	3.2	4	4
Order Number		370685	370688	370691	370778	370781	370784	370794	370799	370803	370808
1 Reduction		4.4 : 1	16 : 1	24 : 1	62 : 1	84 : 1	109 : 1	231 : 1	333 : 1	455 : 1	690 : 1
2 Reduction absolute		57/13	855/52	1539/65	12825/208	185193/2197	2187/20	192375/832	69255/208	5000211/10985	1121931/1625
3 Max. motor shaft diameter	mm	3.2	3.2	3.2	3.2	3.2	4	3.2	3.2	3.2	3.2
Order Number		370686	370689	370692	370779	370782	370785	370795	370800	370805	370809
1 Reduction		5.4 : 1	19 : 1	29 : 1	72 : 1	89 : 1	128 : 1	270 : 1	370 : 1	479 : 1	850 : 1
2 Reduction absolute		27/5	3249/169	729/25	48735/676	4617/52	41553/325	731025/2704	10556001/28561	124659/260	531441/625
3 Max. motor shaft diameter	mm	2.5	3.2	2.5	3.2	3.2	3.2	3.2	3.2	3.2	2.5
Order Number							370786	370796	370801	370806	
1 Reduction							157 : 1	285 : 1	389 : 1	561 : 1	
2 Reduction absolute							19683/125	18225/64	263169/676	2368521/4225	
3 Max. motor shaft diameter	mm						2.5	4	3.2	3.2	
4 Number of stages		1	2	2	3	3	3	4	4	4	4
5 Max. continuous torque	Nm	2	2.4	2.4	3	3	3	3.4	3.4	3.4	3.4
6 Intermittently permissible torque at gear output	Nm	2.5	3	3	3.5	3.5	3.5	3.8	3.8	3.8	3.8
7 Max. efficiency	%	84	70	70	59	59	59	49	49	49	49
8 Weight	g	51	64	64	78	78	78	91	91	91	91
9 Average backlash no load	°	1.0	1.2	1.2	1.6	1.6	1.6	2.0	2.0	2.0	2.0
10 Mass inertia	gcm²	0.6	0.4	0.4	0.4	0.4	0.4	0.4	0.4	0.4	0.4
11 Gearhead length L1	mm	25.4	32.2	32.2	39.0	39.0	39.0	45.8	45.8	45.8	45.8

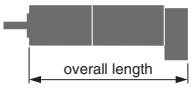

maxon Modular System

+ Motor	Page	+ Sensor / Brake	Page	Overall length [mm] = Motor length + gearhead length + (sensor / brake) + assembly parts									
EC 22, 40 W	149			70.0	76.8	76.8	83.6	83.6	83.6	90.4	90.4	90.4	90.4
EC 22, 40 W	149	MR	261	76.0	82.8	82.8	89.6	89.6	89.6	96.4	96.4	96.4	96.4
EC 22, 100 W	151			88.2	95.0	95.0	101.8	101.8	101.8	108.6	108.6	108.6	108.6
EC 22, 100 W	151	MR	261	94.2	101.0	101.0	107.8	107.8	107.8	114.6	114.6	114.6	114.6
EC-max 22, 12 W	164			57.5	64.3	64.3	71.1	71.1	71.1	77.9	77.9	77.9	77.9
EC-max 22, 12 W	164	MR	261	67.2	74.0	74.0	80.8	80.8	80.8	87.6	87.6	87.6	87.6
EC-max 22, 12 W	164	AB 20	316	93.1	99.9	99.9	106.7	106.7	106.7	113.5	113.5	113.5	113.5
EC-max 22, 25 W	165			74.0	80.8	80.8	87.6	87.6	87.6	94.4	94.4	94.4	94.4
EC-max 22, 25 W	165	MR	261	83.7	90.5	90.5	97.3	97.3	97.3	104.1	104.1	104.1	104.1
EC-max 22, 25 W	165	AB 20	316	109.7	116.5	116.5	123.3	123.3	123.3	130.1	130.1	130.1	130.1
EC-4pole 22	173			74.1	80.9	80.9	87.7	87.7	87.7	94.5	94.5	94.5	94.5
EC-4pole 22	173	HEDL 5540	270	95.6	102.4	102.4	109.2	109.2	109.2	116.0	116.0	116.0	116.0
EC-4pole 22	174			91.5	98.3	98.3	105.1	105.1	105.1	111.9	111.9	111.9	111.9
EC-4pole 22	174	HEDL 5540	270	113.0	119.8	119.8	126.6	126.6	126.6	133.4	133.4	133.4	133.4

Planetary Gearhead GP 32 C ∅32 mm, 1.0 - 6.0 Nm

Ceramic Version

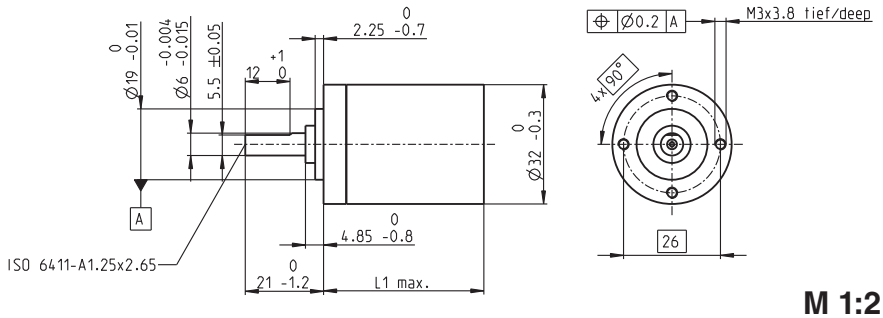

Technical Data

Planetary Gearhead	straight teeth
Output shaft	stainless steel
Shaft diameter as option	8 mm
Bearing at output	ball bearing
Radial play, 5 mm from flange	max. 0.14 mm
Axial play	max. 0.4 mm
Max. radial load, 10 mm from flange	140 N
Max. permissible axial load	120 N
Max. permissible force for press fits	120 N
Sense of rotation, drive to output	=
Recommended input speed	< 8000 rpm
Recommended temperature range	-40 ... +100°C

Option: Low-noise version

Stock program
Standard program
Special program (on request)

			Order Number										
			166930	166933	166938	166939	166944	166949	166954	166959	166962	166967	166972	166977
Gearhead Data														
1	Reduction		3.7 : 1	14 : 1	33 : 1	51 : 1	111 : 1	246 : 1	492 : 1	762 : 1	1181 : 1	1972 : 1	2829 : 1	4380 : 1
2	Reduction absolute		26/7	676/49	529/16	17576/343	13824/125	421824/1715	86112/175	19044/25	10123776/8575	8626176/4375	495144/175	109503/25
3	Max. motor shaft diameter	mm	6	6	3	6	4	4	3	3	4	4	3	3
	Order Number		166931	166934		166940	166945	166950	166955	166960	166963	166968	166973	166978
1	Reduction		4.8 : 1	18 : 1		66 : 1	123 : 1	295 : 1	531 : 1	913 : 1	1414 : 1	2189 : 1	3052 : 1	5247 : 1
2	Reduction absolute		24/5	624/35		16224/245	6877/56	101062/343	331776/625	36501/40	2425488/1715	536406/245	1907712/625	839523/160
3	Max. motor shaft diameter	mm	4	4		4	3	3	4	3	3	3	3	3
	Order Number		166932	166935		166941	166946	166951	166956	166961	166964	166969	166974	166979
1	Reduction		5.8 : 1	21 : 1		79 : 1	132 : 1	318 : 1	589 : 1	1093 : 1	1526 : 1	2362 : 1	3389 : 1	6285 : 1
2	Reduction absolute		23/4	299/14		3887/49	3312/25	389376/1225	20631/35	279841/256	9345024/6125	2066688/875	474513/140	6436343/1024
3	Max. motor shaft diameter	mm	3	3		3	3	4	3	3	4	3	3	3
	Order Number			166936		166942	166947	166952	166957		166965	166970	166975	
1	Reduction			23 : 1		86 : 1	159 : 1	411 : 1	636 : 1		1694 : 1	2548 : 1	3656 : 1	
2	Reduction absolute			576/25		14976/175	1587/10	359424/875	79488/125		1162213/686	7962624/3125	457056/125	
3	Max. motor shaft diameter	mm		4		4	3	4	3		3	4	3	
	Order Number			166937		166943	166948	166953	166958		166966	166971	166976	
1	Reduction			28 : 1		103 : 1	190 : 1	456 : 1	706 : 1		1828 : 1	2623 : 1	4060 : 1	
2	Reduction absolute			138/5		3588/35	12167/64	89401/196	158171/224		2238912/1225	2056223/784	3637933/896	
3	Max. motor shaft diameter	mm		3		3	3	3	3		3	3	3	
4	Number of stages		1	2	2	3	3	4	4	4	5	5	5	5
5	Max. continuous torque	Nm	1	3	3	6	6	6	6	6	6	6	6	6
6	Intermittently permissible torque at gear output	Nm	1.25	3.75	3.75	7.5	7.5	7.5	7.5	7.5	7.5	7.5	7.5	7.5
7	Max. efficiency	%	80	75	75	70	70	60	60	60	50	50	50	50
8	Weight	g	118	162	162	194	194	226	226	226	258	258	258	258
9	Average backlash no load	°	0.7	0.8	0.8	1.0	1.0	1.0	1.0	1.0	1.0	1.0	1.0	1.0
10	Mass inertia	gcm²	1.5	0.8	0.8	0.7	0.7	0.7	0.7	0.7	0.7	0.7	0.7	0.7
11	Gearhead length L1	mm	26.5	36.4	36.4	43.1	43.1	49.8	49.8	49.8	56.5	56.5	56.5	56.5

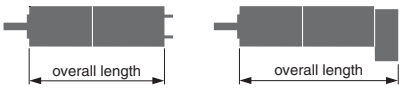

maxon Modular System

+ Motor	Page	+ Sensor / Brake	Page	Overall length [mm] = Motor length + gearhead length + (sensor / brake) + assembly parts											
RE-max 29	131-134			71.3	81.2	81.2	87.9	87.9	94.6	94.6	94.6	101.3	101.3	101.3	101.3
RE-max 29	132/134	MR	262	80.1	90.0	90.0	96.7	96.7	103.4	103.4	103.4	110.1	110.1	110.1	110.1
EC 32, 80 W	154			86.6	96.5	96.5	103.2	103.2	109.9	109.9	109.9	116.6	116.6	116.6	116.6
EC 32, 80 W	154	HED_ 5540	267/269	105.0	114.9	114.9	121.6	121.6	128.3	128.3	128.3	135.0	135.0	135.0	135.0
EC 32, 80 W	154	Res 26	277	106.7	116.6	116.6	123.3	123.3	130.0	130.0	130.0	136.7	136.7	136.7	136.7
EC-max 22, 25 W	165			75.1	85.0	85.0	91.7	91.7	98.4	98.4	98.4	105.1	105.1	105.1	105.1
EC-max 22, 25 W	165	MR	261	84.8	94.7	94.7	101.4	101.4	108.1	108.1	108.1	114.8	114.8	114.8	114.8
EC-max 22, 25 W	165	AB 20	316	111.6	121.5	121.5	128.2	128.2	134.9	134.9	134.9	141.6	141.6	141.6	141.6
EC-max 30, 40 W	166			68.9	78.8	78.8	85.5	85.5	92.2	92.2	92.2	98.9	98.9	98.9	98.9
EC-max 30, 40 W	166	MR	262	81.1	91.0	91.0	97.7	97.7	104.4	104.4	104.4	111.1	111.1	111.1	111.1
EC-max 30, 40 W	166	HEDL 5540	269	89.5	99.4	99.4	106.1	106.1	112.8	112.8	112.8	119.5	119.5	119.5	119.5
EC-max 30, 40 W	166	AB 20	316	104.5	114.4	114.4	121.1	121.1	127.8	127.8	127.8	134.5	134.5	134.5	134.5
EC-max 30, 40 W	166	HEDL 5540 / AB 20	269/316	125.1	135.0	135.0	141.7	141.7	148.4	148.4	148.4	155.1	155.1	155.1	155.1
EC-4pole 22, 90 W	173			75.2	85.1	85.1	91.8	91.8	98.5	98.5	98.5	105.2	105.2	105.2	105.2
EC-4pole 22, 90 W	173	HEDL 5540	270	96.7	106.6	106.6	113.3	113.3	120.0	120.0	120.0	126.7	126.7	126.7	126.7
EC-4pole 22, 120 W	174			92.6	102.5	102.5	109.2	109.2	115.9	115.9	115.9	122.6	122.6	122.6	122.6
EC-4pole 22, 120 W	174	HEDL 5540	270	114.1	124.0	124.0	130.7	130.7	137.4	137.4	137.4	144.1	144.1	144.1	144.1
EC 32 flat, 15 W	188			44.5	54.4	54.4	61.1	61.1	67.8	67.8	67.8	74.5	74.5	74.5	74.5
EC 32 flat IE, IP 00	189			54.6	64.5	64.5	71.2	71.2	77.9	77.9	77.9	84.6	84.6	84.6	84.6
EC 32 flat IE, IP 40	189			56.3	66.2	66.2	72.9	72.9	79.6	79.6	79.6	86.3	86.3	86.3	86.3
EC-i 40, 50 W	190			58.1	68.0	68.0	74.7	74.7	81.4	81.4	81.4	88.1	88.1	88.1	88.1
EC-i 40, 50 W	190	MR	263	73.8	83.7	83.7	90.4	90.4	97.1	97.1	97.1	103.8	103.8	103.8	103.8
EC-i 40, 50 W	190	HEDL 5540	270	81.5	91.4	91.4	98.1	98.1	104.8	104.8	104.8	111.5	111.5	111.5	111.5
EC-i 40, 70 W	191			68.1	78.0	78.0	84.7	84.7	91.4	91.4	91.4	98.1	98.1	98.1	98.1
EC-i 40, 70 W	191	MR	263	83.8	93.7	93.7	100.4	100.4	107.1	107.1	107.1	113.8	113.8	113.8	113.8
EC-i 40, 70 W	191	HEDL 5540	270	91.5	101.4	101.4	108.1	108.1	114.8	114.8	114.8	121.5	121.5	121.5	121.5
MCD EPOS, 60 W	313			150.2	160.1	160.1	166.8	166.8	173.5	173.5	173.5	180.2	180.2	180.2	180.2
MCD EPOS P, 60 W	313			150.2	160.1	160.1	166.8	166.8	173.5	173.5	173.5	180.2	180.2	180.2	180.2

Cell Specification

● Typical Capacity[1)]		7.5 Ah
● Nominal Voltage		3.7 V
● Charge Condition	Max. Current	7.5 A
	Voltage	4.2V ± 0.03 V
● Discharge Condition	Continuous Current	15.0 A
	Peak Current	37.5 A
	Cut-off Voltage	2.7 V
● Cycle Life [@ DOD80%] [2)]		> 800 Cycles
● Operating Temp.	Charge	0 ~ 40 ℃
	Discharge	-20 ~ 60 ℃
● Dimension	Thickness (mm)	7.5 ± 0.2
	Width (mm)	106.0 ± 2.0
	Length (mm)	100.0 ± 2.0
● Weight (g)		155.0 ± 5.0

1) Typical Capacity : 0.5C, 4.2 ~ 2.7V @25^{O}C
2) Voltage Range : 4.15 ~ 3.40V under 1.0C / 1.0C

List of abbreviations

AFO	Ankle-foot orthosis
AK	Ankle-knee
B.W.	Body weight
BWS	Body Weight Support
COM	Center of mass
DOF	Degree of freedom
FEA	Finite element analysis
GC	Gait cycle
GRF	Ground reaction force
HC	Heel contact
IC	Initial contact
ISw	Initial Swing
KH	Knee-hip
LR	Loading response
MSt	Mid-Stance
MSw	Mid-Swing
PSw	Pre-Swing
ROM	Range Of Motion
SEA	Series elastic actuator
TO	Toe-off
TSt	Terminal Stance
TSw	Terminal Swing

List of Figures

List of Tables

Bibliography

[1] *aluSELECT*, http://aluminium.matter.org.uk/aluselect/default.asp.

[2] *Associated Spring SPEC*, http://www.assocspring.co.uk/.

[3] *KHK Stock gears catalog*, volume 7 - Bevel gears, http://www.mecapedia.uji.es/catalogos/engranaje/khk.5.pdf. Kohara Gear Industry Co., Ltd.

[4] *What's "HAL" (Hybrid Assistive Limb®)?*, http://www.cyberdyne.jp/english/robotsuithal/.

[5] *Maxon DC motor and maxon EC motor - Key information*, http://www.maxonmotor.com/medias/sys_master/8797217488926/DC-Das-wichtigste-ueber-maxonmotoren_11_DE-EN___036.pdf?mime=application2011.

[6] *Maxon gear: Technology - short and to the point*, http://www.maxonmotor.com/medias/sys_master/8797220241438/gear-Das-wichtigste-ueber-getriebe_11_DE-EN_030-031.pdf?mime=applicationMay 2011.

[7] D. Aoyagi, W.E. Ichinose, S.J. Harkema, D.J. Reinkensmeyer, and J.E. Bobrow. A robot and control algorithm that can synchronously assist in naturalistic motion during body-weight-supported gait training following neurologic injury. *Neural Systems and Rehabilitation Engineering, IEEE Transactions on*, 15(3):387–400, 2007.

[8] S.K. Banala, S.K. Agrawal, A. Fattah, V. Krishnamoorthy, W.L. Hsu, J. Scholz, and K. Rudolph. Gravity-balancing leg orthosis and its performance evaluation. *Robotics, IEEE Transactions on*, 22(6):1228–1239, 2006.

[9] S.K. Banala, S.K. Agrawal, and J.P. Scholz. Active leg exoskeleton (alex) for gait rehabilitation of motor-impaired patients. *Rehabilitation Robotics*, pages 401–407, 2007.

[10] J.A. Blaya and H. Herr. Adaptive control of a variable-impedance ankle-foot orthosis to assist drop-foot gait. *Neural Systems and Rehabilitation Engineering, IEEE Transactions on*, 12(1):24–31, 2004.

[11] Branko Brackx. Reverse engineering and redesign of a passive below-knee prosthesis prototype. Master's thesis, Vrije Universiteit Brussel, 2010.

[12] RC Browning, JR Modica, R. Kram, and A. Goswami. The effects of adding mass to the legs on the energetics and biomechanics of walking. *Medicine and science in sports and exercise*, 39(3):515, 2007.

[13] M. Cenciarini and A.M. Dollar. Biomechanical considerations in the design of lower limb exoskeletons. 120(140/0):10, 2011.

[14] S.H. Collins. *Dynamic walking principles applied to human gait*. PhD thesis, The University of Michigan, 2008.

[15] H. P. Crowell, A. C. Boynton, and M. Mungiole. Exoskeleton power and torque requirements based on human biomechanics, November 2002.

[16] B. Danneskiold-Samsøe, EM Bartels, PM Bülow, H. Lund, A. Stockmarr, CC Holm, I. Wätjen, M. Appleyard, and H. Bliddal. Isokinetic and isometric muscle strength in a healthy population with special reference to age and gender. *Acta Physiologica*, 197:1–68, 2009.

[17] MP De Looze, HM Toussaint, DA Commissaris, MP Jans, and AJ Sargeant. Relationships between energy expenditure and positive and negative mechanical work in repetitive lifting and lowering. *Journal of Applied Physiology*, 77(1):420, 1994.

[18] P. DeVita and T. Hortobagyi. Age causes a redistribution of joint torques and powers during gait. *Journal of Applied Physiology*, 88(5):1804, 2000.

[19] A.M. Dollar and H. Herr. Lower extremity exoskeletons and active orthoses: Challenges and state-of-the-art. *Robotics, IEEE Transactions on*, 24(1):144–158, 2008.

[20] A. Duschau-Wicke, J. Zitzewitz, L. Lünenburger, and R. Riener. Patient-driven cooperative gait training with the rehabilitation robot lokomat. pages 1616–1619, 2009.

[21] D.P. Ferris, G.S. Sawicki, and M.A. Daley. A physiologist's perspective on robotic exoskeletons for human locomotion. *International journal of HR: humanoid robotics*, 4(3):507, 2007.

[22] T. Fukunaga, K. Kubo, Y. Kawakami, S. Fukashiro, H. Kanehisa, and C.N. Maganaris. In vivo behaviour of human muscle tendon during walking. *Proceedings of the Royal Society of London. Series B: Biological Sciences*, 268(1464):229, 2001.

[23] J. Jansen, B. Richardson, F. Pin, R. Lind, and J. Birdwell. Exoskeleton for soldier enhancement systems feasibility study. Technical report, Oak Ridge National Laboratory, 2000.

[24] H. Kazerooni and R. Steger. The berkeley lower extremity exoskeleton. *Journal of dynamic systems, measurement, and control*, 128:14, 2006.

[25] K. Kong and D. Jeon. Design and control of an exoskeleton for the elderly and patients. *Mechatronics, IEEE/ASME Transactions on*, 11(4):428–432, 2006.

[26] A.D. Kuo. A simple model of bipedal walking predicts the preferred speed–step length relationship. *Journal of Biomechanical Engineering*, 123:264, 2001.

[27] A.D. Kuo. Energetics of actively powered locomotion using the simplest walking model. *Journal of Biomechanical Engineering*, 124:113, 2002.

[28] I.R. Lanza, T.F. Towse, G.E. Caldwell, DM Wigmore, and J.A. Kent-Braun. Effects of age on human muscle torque, velocity, and power in two muscle groups. *Journal of Applied Physiology*, 95(6):2361, 2003.

[29] Q. Li, V. Naing, JA Hoffer, DJ Weber, AD Kuo, and JM Donelan. Biomechanical energy harvesting: Apparatus and method. *Robotics and Automation, 2008. ICRA 2008. IEEE International Conference on*, pages 3672–3677, 2008.

[30] HB Lim, T.P. Luu, KH Hoon, X. Qu, A. Tow, and KH Low. Study of body weight shifting on robotic assisted gait rehabilitation with nature-gaits. In *Intelligent Robots and Systems (IROS), 2011 IEEE/RSJ International Conference on*, pages 4923–4928. IEEE, 2011.

[31] Argo Medical Technologies Ltd., editor. *Rewalk*, http://www.argomedtec.com/index.asp.

[32] J. Martin, A. Pollock, and J. Hettinger. Microprocessor lower limb prosthetics: Review of current state of the art. *JPO: Journal of Prosthetics and Orthotics*, 22(3):183, 2010.

[33] S.J. Mattes, P.E. Martin, and T.D. Royer. Walking symmetry and energy cost in persons with unilateral transtibial amputations: Matching prosthetic and intact limb inertial properties. *Archives of physical medicine and rehabilitation*, 81(5):561–568, 2000.

[34] B.J. McFadyen and D.A. Winter. An integrated biomechanical analysis of normal stair ascent and descent. *Journal of biomechanics*, 21(9):733–744, 1988.

[35] T.A. McMahon, G. Valiant, and E.C. Frederick. Groucho running. *Journal of Applied Physiology*, 62(6):2326, 1987.

[36] D. Muhs, H. Wittel, M. Becker, D. Jannasch, and J. Voßiek. *Roloff/Matek Machineonderdelen*. Sdu Uitgevers, 4th edition edition, 2003.

[37] M. Nordin and V.H. Frankel. *Basic biomechanics of the musculoskeletal system*. Lippincott Williams & Wilkins, 2001.

[38] J.A. Norris, K.P. Granata, M.R. Mitros, E.M. Byrne, and A.P. Marsh. Effect of augmented plantarflexion power on preferred walking speed and economy in young and older adults. *Gait & posture*, 25(4):620–627, 2007.

[39] Ronan O'Rahilly. Basic human anatomy - a regional study of human structure. On the WWW, http://www.dartmouth.edu/ humananatomy/figures/chapter_17/17-6.HTM, 2008.

[40] M.L. Palmer. Sagittal plane characterization of normal human ankle function across a range of walking gait speeds. Master's thesis, Citeseer, 2002.

[41] Jacquelin Perry. *Gait Analysis: Normal and Pathological Function.* SLACK Incorporated, 1992.

[42] TD Royer and PE Martin. Manipulations of leg mass and moment of inertia: effects on energy cost of walking. *Medicine and science in sports and exercise*, 37(4):649, 2005.

[43] A. Silder, B. Heiderscheit, and D.G. Thelen. Active and passive contributions to joint kinetics during walking in older adults. *Journal of biomechanics*, 41(7):1520–1527, 2008.

[44] J.D. Smith and P.E. Martin. Walking patterns change rapidly following asymmetrical lower extremity loading. *Human movement science*, 26(3):412–425, 2007.

[45] A. Valiente. Design of a quasi-passive parallel leg exoskeleton to augment load carrying for walking. Master's thesis, Massachusetts Institute of Technology, 2005.

[46] A. van den Bogert. Exotendons for assistance of human locomotion. *BioMedical Engineering OnLine*, 2(1):17, 2003.

[47] Joop van der Lelij. Understanding the behavior of complex structures under load. On the WWW, http://www2.dupont.com/Plastics/en_US/assets/downloads/design/DCI391.pdf.

[48] W. van Dijk, H. van der Kooij, and E. Hekman. A passive exoskeleton with artificial tendons: Design and experimental evaluation. *Rehabilitation Robotics*, pages 1–6, 2011.

[49] R. Van Ham. *Compliant actuation for biologically inspired bipedal walking robots.* PhD thesis, VUB, 2006.

[50] J.F. Veneman, R. Kruidhof, E.E.G. Hekman, R. Ekkelenkamp, E.H.F. Van Asseldonk, and H. van der Kooij. Design and evaluation of the lopes exoskeleton robot for interactive gait rehabilitation. *Neural Systems and Rehabilitation Engineering, IEEE Transactions on*, 15(3):379–386, 2007.

[51] R. Versluys, P. Beyl, M. Van Damme, A. Desomer, R. Van Ham, and D. Lefeber. Prosthetic feet: State-of-the-art review and the importance of mimicking human ankle-foot biomechanics. *Disability & Rehabilitation: Assistive Technology*, 4(2):65–75, 2009.

[52] M. Vukobratovic, B. Borovac, D. Surla, and D. Stokic. Biped locomotion, scientific fundamentals of robotics 7. 1989.

[53] C.J. Walsh. Biomimetic design of an under-actuated leg exoskeleton for load-carrying augmentation. Master's thesis, MIT, 2006.

[54] C.J. Walsh, K. Endo, and H. Herr. A quasi-passive leg exoskeleton for load-carrying augmentation. *International Journal of Humanoid Robotics*, 4(3):487–506, 2007.

[55] M. Whittle. *Gait analysis: an introduction.* Butterworth Heinemann. Butterworth-Heinemann, 2007.

[56] D.A. Winter. *Biomechanics and motor control of human movement.* John Wiley & Sons, Inc., second edition edition, 1990.

[57] D.A. Winter. *Biomechanics and motor control of human gait.* University of Waterloo Press, second edition edition, 1991.

[58] T. Yakimovich, ED Lemaire, and J. Kofman. Engineering design review of stance-control knee-ankle-foot orthoses. *Journal of rehabilitation research and development*, 46(2):257, 2009.